A NEW EXPERIMENTAL DESIGN AND METHOD FOR IMPROVED DELAYED NEUTRON DATA OF GROUP ABUNDANCES

BY

HEEJUN CHUNG

A DISSERTATION PRESENTED TO THE GRADUATE SCHOOL
OF THE UNIVERSITY OF FLORIDA IN PARTIAL FULFILLMENT
OF THE REQUIREMENTS FOR THE DEGREE OF
DOCTOR OF PHILOSOPHY

UNIVERSITY OF FLORIDA

2014

This doctoral dissertation is dedicated to my wonderful parents,
Jougup Chung and Youngok Kim who have supported me and made all of this possible.
I also dedicate this dissertation to my loving and supportive wife Yereum Yun, and particularly
to my first baby (James Taemin Chung) who is the joy of our lives.

ACKNOWLEDGMENTS

My special thanks go to Professor Kelly A. Jordan, my advisor and the supervisory committee chair, for his guidance and support. Without his strong help, this work would not have been possible.

I would like to thank my supervisory committee members, Professor Wesley E. Bolch, Sedat Goluoglu, and Heather Ray for their guidance, support, and instruction.

I also need to thank my outstanding colleagues at Adelphi Technology Inc. and in my lab, Jason M. Lewis, Lucas M. Rolison, and Ryan P. Kelley, for their support and help on the equipment. It has been my pleasure to work with them.

Finally, I would like to thank all my family members for their consistent support through the many years of my education. I am especially grateful to my older sister, Professor Youngjin Chung, for encouraging me to pursue an advanced degree.

TABLE OF CONTENTS

page

LIST OF TABLES

LIST OF FIGURES

LIST OF ABBREVIATIONS

D-D	Deuterium-Deuterium
D-T	Deuterium-Tritium
UO_2	Uranium Dioxide
NDA	Non-Destructive Assay
PANDA	PAssive Non-Destructive Analysis
HPGe	Hyper-Pure Germanium
MCNP	Monte Carlo N-Particle model (transport code)
SPS	Spark Plasma Sintering
LSF	Least-Square Fit
PPS	Personal Protection System
JEFF	Joint Evaluated Fission and Fusion file
ENDF	Evaluated Nuclear Data File
FWHM	Full Width at Half Maximum

Abstract of Dissertation Presented to the Graduate School
of the University of Florida in Partial Fulfillment of the
Requirements for the Degree of Doctor of Philosophy

A NEW EXPERIMENTAL DESIGN AND METHOD FOR IMPROVED DELAYED NEUTRON DATA OF GROUP ABUNDANCES

By

Heejun Chung

May 2014

Chair: Kelly A. Jordan
Major: Nuclear Engineering Sciences

The nuclear data on the physics of delayed neutrons coming from fission events are of key importance in reactor kinetics and safeguards applications. The accuracy of reactor kinetics calculations, reactor physics validation studies and techniques for non-destructive assay of special nuclear material are all limited by the quality of these data.

The uncertainties on the delayed neutron group abundances of the longest-lived delayed neutron groups are particularly large - up to 13 % for thermal fissions of ^{235}U, 16 % for fast fissions of ^{238}U, and 38 % for fast fissions of ^{239}Pu [1]. There are also several competing data sets with significant variation in values. Recent work indicates that these already large uncertainties are underestimated due to numerical instabilities in the parametric fitting methods [2].

A novel approach to experimentally measure delayed neutron group yields has been proposed by Jordan and Perret [3]. This approach combines gamma-ray scanning and delayed neutron fission rate measurement techniques. With two independent estimates of the same fission rate, a higher uncertainty delayed neutron parameters can be linked to lower uncertainty delayed gamma parameters.

An experimental apparatus implementing these techniques has been designed, optimized, and built. The apparatus consists of a D-D neutron generator, a detector bundle, a sample

handler, and related electronics. Existing neutron generator technology was unsuitable for these measurements. A D-D neutron generator (model DD-109X) was newly designed and installed to run at a maximum intensity of up to $4x10^9$ neutrons per second, with modifications to the accelerator beamline allowing very large solid angle irradiations.

A pelletized UO_2 sample was irradiated by a D-D generator, and delayed neutrons and delayed gamma-rays at 1032 keV from ^{89}Rb from the sample were simultaneously measured. The time was respectively set up 20 min, 170 sec, and 360 sec for irradiation, cooling, and acquisition. The neutron generation yield during the experiment was $1.1x10^9$ neutrons per second at 115 kV.

The relative uncertainty of the longest-lived delayed neutron group for fast fission of ^{238}U using the optimized experimental measurements has been reevaluated and reduced to 8.6 %. This reevaluated uncertainty value is almost a factor of two lower than the Spriggs and Campbell recommended data set (16 % [1]).

The system built has shown considerable potential to reduce the large uncertainties of the longest-lived delayed neutron group abundances. The neutron generator technology has more widespread applications for nuclear security and safeguards. More accurate fission yield measurements can be carried out by comparison of multiple fission rate measurement models. A new prompt neutron measurement technique with a prototype ^4He scintillator detector is proposed as a third experimental technique for future experimental evaluation of nuclear data.

CHAPTER 1
INTRODUCTION

Fission is the process of importance in a nuclear reactor; from fission, energy is generated. Fission reaction rates depend on the kinetic energy and flux of the fissioning neutrons, fuel material composition, and the location in the reactor core. The process of fission drives fuel material composition changes in a reactor core over time, which in turn alters the neutron flux and fission rates. Estimation of fission rates and its relative uncertainty over time and position are the essential core of reactor physics. Several computational methods have been developed to solve the neutron transport equation, which governs neutronics. However, the accuracy of computation is limited by the accuracy and quality of the nuclear data underlying the computational model.

Reactor kinetics, describing the changing of overall fission (power) levels in a reactor, is dependent on a property of how neutrons are produced in time from fission events. Whereas most neutrons are emitted immediately, a small fraction (order of 1 %) is released later. These neutrons are *"delayed"*, and the properties of these delayed neutrons drive the kinetics of the reactor as a whole [4].

Delayed neutrons are emitted from decays of certain fission products. There are more than 100 fission product isotopes that give rise to delayed neutrons, each with their own time constant. For mathematical (and experimental) convenience, these isotopes are collected into a series of groups of similar decay constants and given effective half-lives and abundances for the whole group.

These group constants are experimentally determined from reactor irradiation measurements of fissile isotopes (described in greater detail in Chapter 2). The relative uncertainties of the longest-lived groups are considerably higher than for other groups. These

high uncertainties originate either from the statistical quality of the parametric fitting methods or the quantity of the measurement data sets. Recent work indicates that the high uncertainties might be underestimated due to numerical instabilities in the parametric fitting methods used to estimate these relative group parameters [2].

Another application in which delayed neutrons are important goes to the question of experimental validation of reactor physics parameters and computational models. Gamma scanning techniques have been used for the derivation of fission rates in fresh fuel since the 1960's. However, the accuracy of this technique can suffer from the long-lived delayed gamma precursors or from high background activity in the case of spent (burnt) fuel [5]. In order to overcome this, delayed neutron measurement techniques can be applied as an alternative method of measuring these reactor reaction rates [6]. In both cases, the quality of nuclear data limits the accuracy of measurement.

This dissertation implements a novel technique for measuring delayed neutron group parameters first conceptualized by Jordan and Perret [3]. This method combines the well-established fission rate measurement techniques using delayed gammas and delayed neutrons (*"the combined technique"* in following chapters). Each technique provides an independent estimate of the fission rate in a well-characterized sample. Next, the estimate fission rates via two techniques are set equal since fission rates were estimated from the same fissile sample.

Thus, one can then solve different parameters in the equations used to derive the individual fission rate estimates. Consequently, the high-uncertainty delayed neutron data can be expressed in terms of the low-uncertainty delayed gamma data and hence, the uncertainty on the parameter of interest can be reduced. However, this technique has never been experimentally implemented. Chapter 2 provides a basic introduction and background of previous works in delayed neutron

experiences and data fitting with uncertainty. Six- and eight-group delayed neutron models are explained. In Chapter 3, the combined technique is explained, as well as the theoretical background of the delayed gamma scanning and neutron techniques.

An apparatus has been designed and built to carry out a proof-of-concept experiment for improvement of a targeted parameter, namely the first delayed neutron group abundance of ^{238}U. Chapter 4 introduces the design concepts and the actual experimental apparatuses with a purpose of improvement on the relative uncertainties on the delayed neutron group abundances. Chapter 6 describes UO_2 sample fabrication and the analysis of the material composition (mass ratio) of uranium elements in the fabricated UO_2 samples. Chapter 7 gives the projected results of the relative abundance and its improved uncertainty of the longest-lived delayed neutron group for fast fission of ^{238}U. The sensitivity studies of the relevant parameters in uncertainty calculation were also performed.

In addition to the results associated with the originating motivation described above, two significant new developments were realized while pursuing improved nuclear data measurements: 1) a marked improvement in neutron generator technology; 2) a new fission measurement technique using prompt neutrons and a prototype gas scintillator fast neutron detector.

An accelerator-drive deuterium-deuterium fusion reaction-based neutron generator was built. These systems are specialized, but commercially available. However, the technology was not sufficiently developed to perform the proposed nuclear data measurements. As a part of the work presented in this dissertation, a novel neutron generator design was built in collaboration with Adelphi Technology Inc., a neutron generator manufacturing spinoff from Lawrence Berkeley National Laboratory. The improvements in generator performance from this design –

neutron flux intensity on target – resulted in an order of magnitude increase. The commercial product resulting from this work was awarded an R&D 100 award as one of the 100 most commercially significant research achievements of 2013. Chapter 5 highlights the design, construction, testing, and qualification of the newly designed D-D generator (DD-109X).

In the last offshoot of this main work, the neutron generator has been used to characterize a novel gas scintillator fast neutron detector. Delayed neutron and gamma measurements are used to quantify induced fission rates because there has been no experimental method of differentiating between neutrons produced by a source (in this case a neutron generator), and new fission neutrons induced by the source neutrons. Using delayed emissions, a source can be removed or turned off, and the delayed particles measured. However, with the advent of this new gas scintillator fast neutron detector technology, a technique that differentiates between the energy of neutrons from a neutron generator and fission becomes possible. The implications of this technique and measurements demonstrating the feasibility are presented in Chapter 8.

This work concludes with a summary of the dissertation and recommendations for future work based on the experimental results in Chapter 9.

CHAPTER 2
LITERATURE REVIEW OF DELAYED NEUTRONS

Overview of Delayed Neutrons

When a heavy fissile nucleus undergoes a fission reaction, it breaks apart into various fragment pairs (light nuclei) of unequal mass and energy. An average energy from this fission reaction is about 195 MeV. Most of the energy (about 162 MeV) is carried away by the fragment pairs and the rest (about 33 MeV) produces particles such as neutrinos, prompt neutrons, and photons in the form of gamma-rays [7]. The produced fission fragments are unstable due to unbalanced neutron and proton ratios. In order to adjust these unbalanced ratios, the excited fission fragments undergo several beta-decays until becoming stable. In some cases, the excitation energy of daughter nuclei formed by beta decays (β) is higher than the neutron separation energy S_n, and the daughter nuclei then emit neutrons again sometime after the fission reaction. This decay chain is written as:

$$ {}^{A}_{Z}X_N \xrightarrow{\beta^-} {}_{Z+1}{}^{A}Y_{N-1} \rightarrow {}_{Z+1}{}^{A}Z_{N-2} + n \qquad (2\text{-}1) $$

The fission fragment *X*, undergoing a beta decay, is called as a delayed neutron precursor, the daughter nucleus *Y*, emitting a delayed neutron, is called as a delayed neutron emitter, and the emitted neutron *n* in Equation 2-1 is called as a delayed neutron. The total delay time is mainly governed by the half-life of a precursor nucleus since there is no significant time delay from a daughter nucleus (a delayed neutron emitter). The daughter nucleus emits neutrons nearly immediately after it is formed by beta-decay. If the excitation energy is lower than the neutron separation energy, the daughter nucleus then emits delayed gamma-rays instead of delayed neutrons. The neutron separation energy S_n varies based on the nuclear structure of precursors, and its average value can be calculated in terms of mass distribution or binding energy difference between a precursor (A, N-1) and its daughter nucleus (A, N-2) [8]:

$$\{m({}^{A}_{Z+1}Z_{N-2}) + m(n) - m({}^{A}_{Z+1}Y_{N-1})\} \cdot c^2 = S_n \quad (2\text{-}2)$$

$$BE({}^{A}_{Z+1}Y_{N-1}) - BE({}^{A}_{Z+1}Z_{N-2}) = S_n, \quad (2\text{-}3)$$

where *m(x)* is the mass of *x* element in the unit AMU or kg, *c* is the speed of light in vacuum (2.998×10^8 m/s), and *BE(x)* is the binding energy of *x* element in MeV, typically.

The calculated value through Equation 2-2 has a unit Joule (J=kg·m^2/s^2) but can be converted to MeV since 1 MeV is equal to 1.6×10^{-13} J. The whole decay processes, mentioned above, is described in Figure 2-1.

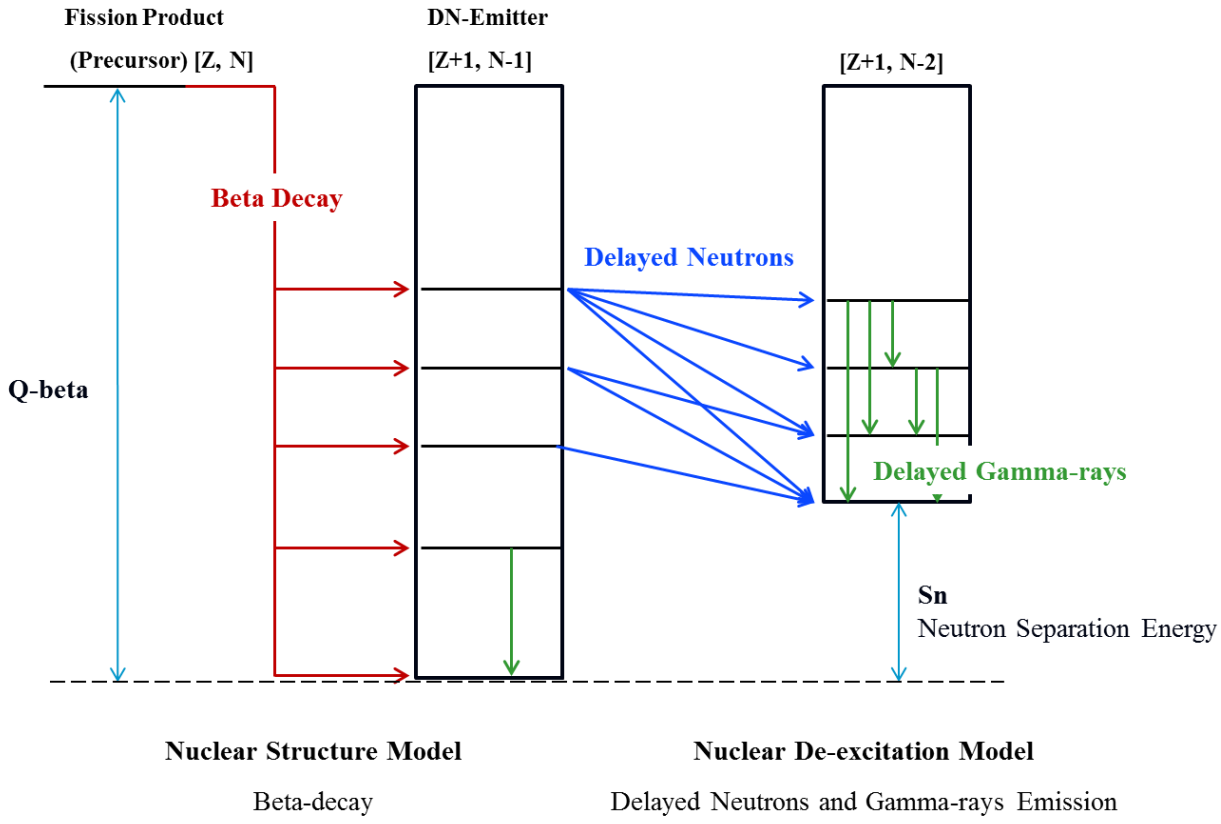

Figure 2-1. Delayed neutron precursors are produced from fission and undergo beta decay, becoming delayed neutron emitters. These emitters de-excite by delayed neutron emission.

From the fission reaction, two different types of neutrons are released. Nearly all of fission neutrons (more than 99%) are released at the instant of fission within the order of 10^{-16} seconds

or smaller. These neutrons are prompt neutrons. Relatively long after fission, a small amount of neutrons (less than 1%) are released through beta decay processes. There neutrons are delayed neutrons.

The average number of neutrons per fission, denoted by υ, varies with the energy of the incident neutron. In the case of thermal fissions, the most fission events are caused by ^{233}U, ^{235}U, ^{239}Pu, and ^{241}Pu since they have large fission cross sections. The observed mean value of the fission cross sections and their average number of neutrons per fission, obtained from the Evaluated Nuclear Data File (ENDF/B-VII.0) standards evaluation, are listed in Table 2-1 [9].

Table 2-1. Thermal fission data from ENDF/B-VII.0 showing the fission cross section and the average number of fission neutrons produced per thermal fission (at 0.0253 eV) for several fissile isotopes.

Isotope	Fission Cross Section (barn)	Average number of fission neutrons (υ)
^{233}U	531.22 ± 0.25 %	2.497 ± 0.14 %
^{235}U	584.33 ± 0.17 %	2.436 ± 0.09 %
^{239}Pu	750.00 ± 0.24 %	2.884 ± 0.16 %
^{241}Pu	1013.96 ± 0.65 %	2.948 ± 0.18 %

The (mean) number of neutrons per fission is typically called the yield. The total fission neutron yield is the sum of prompt and delayed neutron yields

$$\upsilon = \upsilon_P + \upsilon_d, \tag{2-4}$$

where υ_d is the delayed neutron yield, and υ_P is the prompt neutron yield per fission.

The carried energy by these prompt neutrons is varied based on the mass distribution of fission fragments and the energy of the incident particle that induced the fission reaction. The distribution of prompt neutrons at a certain energy level *E* in MeV per fission χ(E) can be represented by Equation 2-5 [4]:

$$\chi(E) = 0.453e^{-1.036 \cdot E} \cdot sinh\sqrt{2.29 \cdot E}. \quad (2\text{-}5)$$

Since χ(E) is a probability density function,

$$\int_0^\infty \chi(E)dE = 1. \quad (2\text{-}6)$$

The prompt neutrons are distributed from 0.1 MeV to 10 MeV. In the case of ^{235}U, the most probable energy of prompt neutrons is about 0.7 MeV, and the average is about 2 MeV [Figure 2-2].

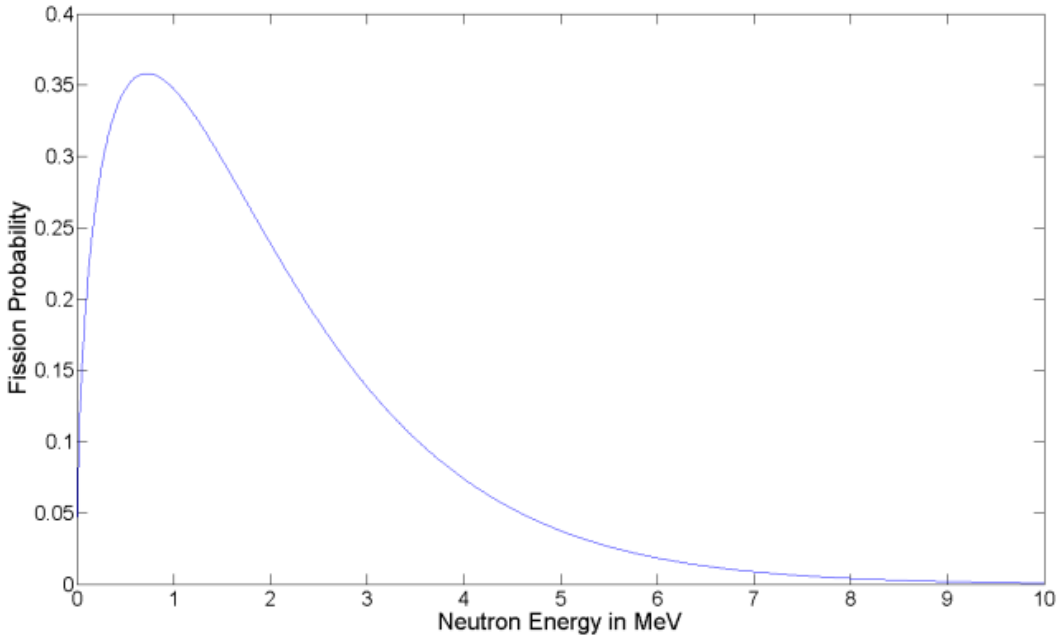

Figure 2-2. The prompt neutron spectrum for thermal fission of ^{235}U. Prompt neutrons are born with energies between 0.1 and 10 MeV, with 0.7 MeV being the most probable energy. The average prompt neutron energy is about 2 MeV.

In addition to the prompt neutrons in fission, delayed neutrons are often emitted by beta decay processes. These delayed neutrons show different physical properties from the properties of prompt neutrons: 1) the fraction of delayed neutrons is typically less than 1 or 2 % per fission; 2) they are released usually within the order of seconds (0.07 to 80 sec) and born at a somewhat

lower energy in the range of a hundred keV (about 250 to 620 keV); and 3) every fissioning isotope has a distinct signature of delayed neutron emission.

The total fraction of delayed neutrons can be denoted by β, called the delayed neutron fraction β [4]:

$$\beta = \frac{\upsilon_d}{\upsilon}. \tag{2-7}$$

This delayed neutron fraction represents the number of emitted delayed neutrons of the total number of fission neutrons per fission. By combining and rearranging above equations [Equation 2-4 and 2-7], equations for the yield of prompt υ_P and delayed υ_d neutrons per fission can be written as:

$$\upsilon_P = \upsilon - \upsilon_d = \upsilon(1 - \beta) \tag{2-8}$$

$$\upsilon_d = \beta \cdot \upsilon. \tag{2-9}$$

The delayed neutron fraction β depends on the energy of the incident neutron and the target fissile or fertile nuclide which is undergoing the fission reaction. A fissile material is composed of nuclides for which fission is possible with neutrons of any energy level, and a fertile material is composed of nuclides for which can be transformed (transmuted) into fissile materials by the bombardment of neutrons [10]. As they eventually induce fission events, they can be described as either fissioning or fission nuclides. The delayed neutron fractions for the major fission nuclides are listed in the Table 2-2 [11].

Table 2-2. The delayed neutron fraction (β) for thermal and fast fission of several fissionable nuclides, showing the fraction of all fission neutrons that are born delayed.

Isotope	Fission Type	Delayed Neutron Fraction β
^{233}U	Thermal	0.00268 ± 0.013 %
^{235}U	Thermal	0.00665 ± 0.021 %
^{238}U	Fast	0.01650 ± 0.086 %
^{239}Pu	Thermal	0.00225 ± 0.011 %

The total fission neutron yield υ must be the sum of prompt and delayed neutron yields per fission, and some references do not really differentiate between the total fission neutron yield υ and the yield of the prompt neutrons υ_P since the delayed neutron yield is quite small. However, this small number of delayed neutrons plays a vital role in many applications, so the total fission neutron yield υ should be expressed by the sum of prompt and delayed neutron yields per fission.

Additionally, the meaning of fraction β is mixed with the meaning of yield υ. Later in this study, the fraction is defined as "the ratio between delayed and all fission neutrons". The yield means "the actual (mean) number of neutrons per fission".

The importance of delayed neutrons in reactor kinetics calculations can be easily understood by comparing properties of the above two fission neutrons, prompt and delayed. Delayed neutrons have significantly longer lifetime, compared to prompt neutrons, and their longer lifetime plays a vital role in the design and control of a nuclear reactor. The longer lifetime of delayed neutrons increases the total neutron lifetime l in a reactor, and consequently leads to a longer reactor period T. A longer reactor period slows the power growth rate in a reactor and enhances the safety of the system.

The total neutron lifetime *l* can be simply defined as the time between the birth of a neutron from fission and its death. A fast neutron is typically moderated (losing its kinetic energy) by the collisions within a moderator such as light water, heavy water, and graphite just after its release from a fission reaction. When it reaches the thermal energy range, it is absorbed and causes another fission reaction to occur. This repeated process is referred as the nuclear chain reaction.

Therefore, the total neutron lifetime can be defined by the sum of times of generation, moderation (slowing-down) and thermalization:

$$Lifetime\ l = Time_{gen} + Time_{mod} + Time_{th}. \quad (2\text{-}10)$$

The generation time is a releasing time of fission neutrons, the moderation time is a slowing-down time into the thermal energy range (about 0.025 eV) of the fission neutrons, and the thermalization time means the average time which the thermalized neutrons diffuse before being lost in some way. The thermalization time can be expressed by the mean diffusion time. The mean diffusion time in various moderators that are widely used in a reactor is listed in Table 2-3 [4].

Table 2-3. Approximate diffusion time for several common moderators, taken from J. R. Lamarsh (Introduction to Nuclear Engineering, 2nd ed., pp. 277, 1983). The uncertainty of these data was not reported.

Moderator	Diffusion Time (sec)
H_2O	2.1×10^{-4}
D_2O	4.3×10^{-2}
Be	3.9×10^{-3}
Graphite	1.7×10^{-2}

The number density of neutrons in a reactor is proportionally changed by the multiplication factor *k*, which accounts for the rate of neutron production from fission reactions and loss

through absorptions within reactor materials and leakage from a reactor. Therefore, the neutron population in each generation is written in terms of the multiplication factor *k*, the ratio of the number of fission neutrons in the next generation (n+1th) divided by the number of fission neutrons in current nth generation [7]:

$$k_{eff} = \frac{N_f(n+1^{th})}{N_f(n^{th})} = f \cdot \eta \cdot \epsilon \cdot \rho \cdot L_F \cdot L_{TH}, \quad (2\text{-}11)$$

where f is the thermal fuel utilization factor, η is the reproduction factor, ϵ is the fast fission factor, ρ is the resonance escape probability, L_F is the fast non-leakage factor, and L_{TH} is the thermal non-leakage factor.

The multiplcation factor can be expressed as the infinite multiplication factor (k_∞), only considering neutron production and absortion ($f \cdot \eta \cdot \epsilon \cdot \rho$), and the effective multiplication factor (k_{eff}) for a finite reactor, regarding the actual reactor size. As shown in Equation 2-11, the effective multiplication factor is written in terms of the infinite multiplication factor (k_∞)and two additional factors (L_F and L_{TH}) that allow for neutron leakage.

When the rate of neutron production and loss between a preceding and current generation is balanced, the effective multiplication factor is 1.0, and the reactor is critical or steady-state at a constant power level. If k_{eff} is bigger than 1.0, the reactor is supercritical, and the reactor power level is rising. Oppositely, k_{eff} is less than 1.0, the reactor is subcritical, and the reactor power level is decreasing [4].

The effective multiplication factor indicates the change of the reactor power level, directly proportional to neutron population. The difference between a value of k_{eff} and 1.0 is called the k-excess, and is represented by δk. This excess value can be positive or negative, and is a useful quantity in reactivity calculations. Reactivity can be defined as the term explaining the reactor power level (operation condition) or showing a margin from the critical point of a reactor (k_{eff} =

1.0), and expressed by ρ (rho). The reactivity ρ is different from the resonance escape probability in Equation 2-11 even though the expression symbol is the same. Reactivity is defined as [4]:

$$\rho = \frac{k_{eff} - 1.0}{k_{eff}} = \frac{\delta k}{k_{eff}}. \tag{2-12}$$

The reactivity ρ is generally expressed in a number or percent, but is also often given in units of dollars ($) or cents (0.01$). The unit of one dollar was derived in order to express the core reactivity in terms of the delayed neutron fraction β. The delayed neutron fraction is an important factor in reactor control and will change as the fuel composition changes throughout the core's life. The unit of the dollar is useful in that it gives a sense of the size of the reactivity change, relative to the delayed neutron fraction. One dollar indicates the reactor is critical and the reactivity is equivalent to the delayed neutron fraction:

$$\$1 = \frac{\rho_0}{\beta}. \tag{2-13}$$

If the dollar value is larger than one dollar, then reactor power increases. Oppositely, the reactor power level decreases when the dollar value is less than one dollar.

From Equation 2-11, the number density of neutrons per $cm^3 \cdot sec$ at time t and at a certain location in a homogeneous reactor can be written as:

$$N_f(t + l) = k_{eff} \cdot N_f(t) \approx N_f(t) + l \cdot \frac{dN_f(t)}{dt}. \tag{2-14}$$

By rearranging Equation 2-14,

$$\frac{dN_f(t)}{dt} \approx \frac{(k_\infty - 1)}{l} \cdot N_f(t). \tag{2-15}$$

Intergrating Equation 2-15,

$$N_f(t) = N_f(t = 0) \cdot e^{\frac{t \cdot l}{(k_\infty - 1)}}. \tag{2-16}$$

Let,

$$T \equiv \frac{l}{(k_\infty - 1)} = \frac{l}{\Delta k}. \tag{2-17}$$

Equation 2-16 can be simply written with the reactor period T [Equation 2-17], defined as the taken time to exponentially increase the relative reactor power level:

$$N_f(t) = N_f(t=0) \cdot e^{\frac{t}{T}}. \quad (2\text{-}18)$$

Without delayed neutrons, the total neutron lifetime l is the same as the prompt neutron lifetime l_P. The average lifetime is only in the order of 10^{-4} seconds, nearly equal to the moderation time, since the generation time is within the order of 10^{-16} seconds or smaller.

Considering a step change in Δk from 1.0 to 1.001 (0.1%) with that short lifetime (the order of 10^{-4} seconds), the reactor period would be 0.1 sec. It means that the number density of neutrons per fission would increase by a factor of e^{10} per sec in Equation 2-18. Therefore, the design and operation of a reactor would be impossible due to the rapid power changes if only prompt neutrons existed.

With delayed neutrons, the total neutron lifetime becomes:

$$l = l_P + l_d. \quad (2\text{-}19)$$

This Equation 2-19 can be weighted by the relative yields of prompt and delayed neutron fractions [Equation 2-8 and 2-9], and rewritten as:

$$l = (1-\beta) \cdot l_P + \beta \cdot l_d \approx 0.084\ sec. \quad (2\text{-}20)$$

The lifetime of delayed neutrons l_d is dominated by the half-life of delayed neutron precursor nuclei (0.07 to 80 sec) so the mean lifetime of delayed neutrons is much longer than one of prompt neutrons. Therefore, Equation 2-20 is governed by the delayed neutron term $\beta \cdot l_d$. In the case of thermal fissions of ^{235}U, the delayed neutron lifetime is about 0.084 sec.

Taking 0.084 sec into the previous calculation, the number density of neutrons per fission would increase by a factor of $e^{0.01}$ per sec. Therefore, it would take about 100 sec to

exponentially increase the number density of fissions per sec, and it makes a reactor designable and controllable [4].

In summary, prompt and delayed neutrons have their own unique physical properties since they originate from different nuclear processes, fission reactions and beta decay processes. The classification of fission neutrons in thermal fissions of ^{235}U is summarized in Table 2-4 [4].

Table 2-4. Several important parameters for prompt and delayed fission neutrons from thermal fission of ^{235}U.

	Fraction	Mean Lifetime	Origination	Average of Energy
Prompt Neutrons	99.35 %	10^{-4} sec	Fission Mechanism	2 MeV
Delayed Neutrons	0.65 %	0.84 sec	Beta Decay Process of Precursors	300 to 600 keV

To have better results in reactor kinetics calculations, more precursors should be considered. It is currently practical to consider more than 270 precursor nuclei, but possibly more precursors may exist [2]. However, their decay schemes, half-lives, and yields are not well known for every precursor. Therefore, delayed neutrons should be separated into groups and numerical fitting methods should also be used for applications.

History of Delayed Neutron Experiences and Data Fitting

Delayed neutrons were first discovered by Robert et al. in 1939. They bombarded a 100g uranium nitrate bottle with a beam of deuterium, and observed neutrons as long as 1.5 min after the bombardment via a boron-lined chamber. Both the target bottle and the chamber were surrounded by paraffin in order to cut off background radiation [12]. After delayed neutrons were discovered, their properties were extensively studied.

The major three components for measuring delayed neutrons are specification (energy and yield) of a neutron source for sample irradiation, a sample transfer system, and a counting (measurement) system or good detector efficiency. Additionally, the best fitted line, providing lower or minimum uncertainties for each data set, should be required in order to apply measured delayed neutron data to reactor kinetic calculations.

Hughes et al. in 1948 measured the periods, yields and energies of the delayed neutrons from ^{235}U using a heavy water reactor at Argonne Laboratory [13]. Early researchers had used the term 'period' to explain the half-life of each delayed neutron group since they grouped delayed neutrons with different irradiation periods. Hughes et al. measured the longest group first with the longest irradiation time period and tried to find other shorter-lived groups by shortening the irradiation period and subtracting the contribution from the previous measured group data. They were only able to measure yields and energies of five longer-lived groups with half-lives of 55.6, 22.0, 4.51, 1.52, and 0.43 sec [Table 2-5] since the sample transfer system, named 'rabbit', was insufficient for the last shortest-lived group with a half-life of 0.05 sec.

Table 2-5. Half-life, energy, and yield of delayed neutrons, measured by D. J. Hughes et al in 1948. The uncertainty for each energy value was improperly estimated and showed the same value (± 60 kV). The shortest-lived group, with the half-life of 0.05 sec, was unable to me measured due to transport time limitations of the rabbit sample transfer system.

Half-life (sec)	Energy (keV)	Relative Yield to Total Neutron Emission (%)
55.6	250	0.025
22.0	560	0.166
4.51	430	0.213
1.52	620	0.241
0.43	420	0.085
0.05	-	0.025

The rabbit system was designed to move a fissile sample from the reactor to the measurement station in less than 5 min, and its minimum transferring time was not reported. Thus, the yield of the shortest-lived group was just assumed by subtracting previous measured data sets [13].

Their experimental achievements in measuring the delayed neutron energy spectra of ^{235}U can be highlighted, but the yield data may be over/under estimated since they ignored the contribution from the shortest-lived group in the calculation of other groups.

The rabbit transferring system is described in Figure 2-3 [13].

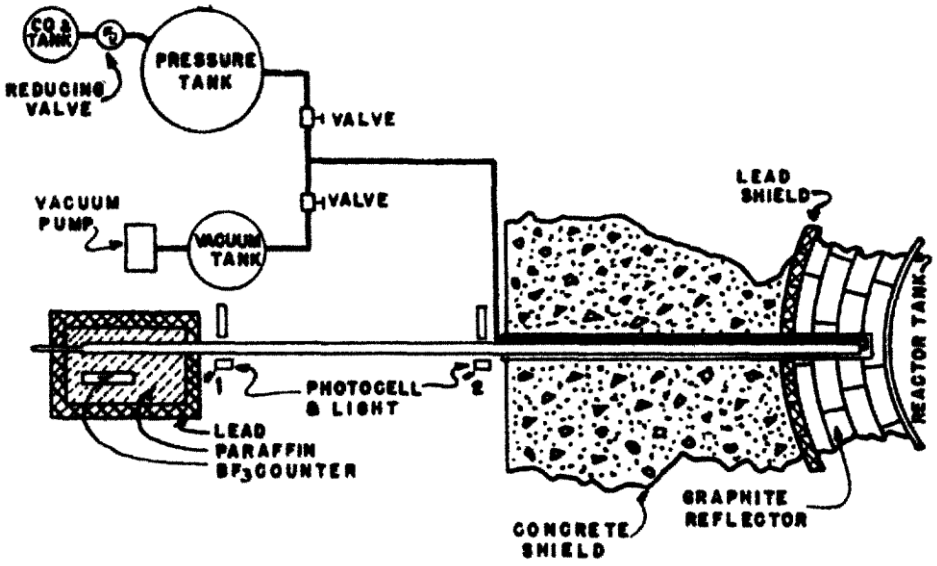

Figure 2-3. The rabbit system, consisting of the rapid transfer tube and associated apparatus at Argonne Laboratory in 1948. The sample was drawn toward the reactor by the vacuum pump, and moved back toward the detector by pressurized gas.

Many improvements on the delayed neutron nuclear data had been made in late 1940's and early 1950's. After that period, the most extensive studies for delayed neutrons were performed at Los Alamos National Laboratory (LANL). The most outstanding result was the six-group model and the eight-group model of delayed neutrons, developed by Keepin et al. [14] and has been commonly used over the past decades.

Six-Group Model of Delayed Neutrons

Keepin et al. in 1957 measured delayed neutrons using the Godiva Reactor, the bare spherical uranium metal critical assembly at Los Alamos Scientific Laboratory, and explained their measurement data with the new six-group model. Through the six-group model, the delayed neutron emission can be described as [14]:

$$n_d(t) = \sum_{i=1}^{6} A_i \cdot e^{-\lambda_i \cdot t}, \tag{2-21}$$

where $n_d(t)$ is the number of delayed neutrons as a function of time t after irradiation, and it can be thought as count rates in the aspect of radiation detection. The index i demotes each delayed neutron group, A_i is the activity of group i, and λ_i is the corresponding decay constant for each i^{th} group.

Since the activity [7] is

$$A_i \equiv \lambda_i \cdot N_i, \tag{2-22}$$

where λ_i is

$$\lambda_i \equiv \frac{ln2}{T_{\frac{1}{2}}}. \tag{2-23}$$

$T_{1/2}$ is the half-life of a precursor, and the number of delayed neutrons N_i in each group can be defined as:

$$N_i \equiv \upsilon_d \cdot a_i, \tag{2-24}$$

where a_i is the group abundance and defined as the ratio between the number of delayed neutrons in each group and all fission delayed neutrons:

$$a_i = \frac{\upsilon_{di}}{\upsilon_d} = \frac{\beta_i}{\beta}. \tag{2-25}$$

Taking all above definitions, Equation 2-21 can be written in terms of group abundances:

$$n_d(t) = \upsilon_d \sum_{i=1}^{6} a_i \cdot \lambda_i \cdot e^{-\lambda_i \cdot t}. \tag{2-26}$$

They measured delayed neutrons from fast and thermal fissions. Six major nuclide samples (^{232}Th, ^{233}U, ^{238}U, ^{239}Pu, and ^{240}Pu) and three nuclides (^{233}U, ^{235}U, and ^{239}Pu) were measured for fast and thermal fissions. For thermal fissions, an 8 inch cubic polyethylene block surrounded by cadmium was placed near the Godiva reactor.

Evaluating delayed neutron emission requires consideration of the precursor saturation. Precursor nuclei are formed in the sample from fission and decay with individual half-lives. The precursors must be built up to equilibrium (saturation). Both "instantaneous" (not long enough for precursors to reach saturation) and "infinite" (long enough for full saturation of the longest lived precursor, about 1 min) conditions were applied [14].

In order to measure delayed neutrons, the BF_3 proportional counter, embedded in a shaped sleeve of boron plastic, was employed. A pneumatic system capable moving a 2-5 g sample in 50 ms was designed and used. The whole experimental apparatus was called Kiva, and is shown in Figure 2-4 [14].

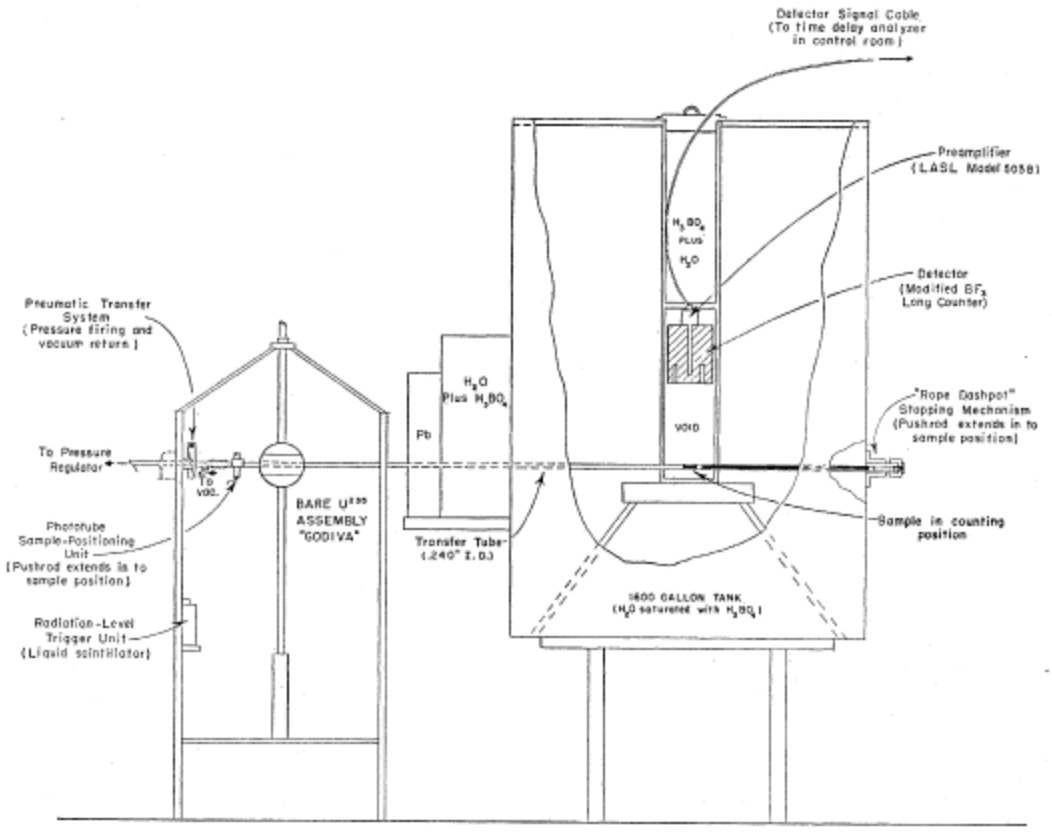

Figure 2-4. The schematic diagram of the delayed neutron experimental system, Kiva at Los Alamos Scientific Laboratory in 1957. A pneumatic system was used to move the sample between the irradiation and measurement positions.

There are many methods available to estimate delayed neutron parameters. Traditionally, a Least-Square Fit (LSF) method is used to describe and fit delayed neutron nuclear data. In the Equation 2-26, the group abundance a_i and decay constant λ_i are free parameters which need to be numerically decided since the count rate and measurement time t are known parameters.

Keepin et al. applied LSF to find the solutions to the group abundance a_i and decay constant λ_i, and finally found that the six-group model was sufficient to fit their experimental data for ^{235}U [14]. Later Keepin used the inverse matrix method with the solution of the weighted LSF to determine probable error of each relative parameter [15]. Keepin's delayed neutron periods (regarding the half-lives of precursors) and relative abundance with uncertainty for fast and thermal fission of ^{235}U is listed in Table 2-6 [14].

Table 2-6. Fast and thermal delayed neutron data from ^{235}U, measured by G. R. Keepin et al in 1957, for each of the six delayed neutron groups.

DN Group	Fast		Thermal	
	Half-life (sec)	Relative Abundance (%)	Half-life (sec)	Relative Abundance (%)
1	54.51 ± 0.94	0.038 ± 0.003	55.72 ± 1.28	0.033 ± 0.003
2	21.84 ± 0.54	0.213 ± 0.005	22.72 ± 0.71	0.219 ± 0.009
3	6.00 ± 0.17	0.188 ± 0.016	6.22 ± 0.23	0.196 ± 0.022
4	2.23 ± 0.06	0.407 ± 0.007	2.30 ± 0.09	0.395 ± 0.011
5	0.496 ± 0.029	0.128 ± 0.008	0.610 ± 0.083	0.115 ± 0.009
6	0.179 ± 0.017	0.026 ± 0.003	0.230 ± 0.025	0.042 ± 0.008

Keepin's six-group model has been shown to be a good approximation for fission estimations in reactor kinetics calculations. However, improved representations (higher-order delayed neutron models) as well as more accurate group abundance data for delayed neutrons have been demanded as more delayed neutron precursors have been discovered following the availability of experimental apparatus. Additionally, it was found that only a dozen or so precursors contributed to 82% of the half-lives for each delayed neutron group, regardless of the nucleus being fission (i.e. U, Pu, and Th) [1]. These two points suggest a model should be made that uses averaged half-lives (using those major precursors) for the groups, for all fissioning isotopes, but at the same time utilize all the known precursors to formulate group abundances for each individual fissioning isotope. This creates a delayed neutron group model that has all fissioning isotopes sharing the group's half-life data but has separate group abundance data for each isotope (as seen in Table 2-6, the following subchapter).

A new, eight-group model was recommended by Spriggs and Campbell in 2002 [1]. This new model was characterized by: 1) the same time set of half-lives of precursors for all

fissioning isotopes, and 2) for fissions induced by neutrons of different energies (thermal-fast-high) [16].

Eight-Group Model of Delayed Neutrons

A new concept for delayed neutron groups, expanding the traditional six-group model to eight-group model, was proposed at an international workshop which was held by the Nuclear Energy Agency's (NEA) working party on delayed neutrons in Russia, 1997. This workshop focused on 1) reviewing the current status of delayed neutron data, and 2) proposing a new model for applications in reactor physics. As a result of the workshop, the eight-group model was initially suggested [1].

This initial eight-group model was modified with the abundance weighted half-lives of precursors, and published in 2002 [1]. The eight-group model for important fissile isotopes is given in Table 2-7.

Table 2-7. Eight-group delayed neutron parameters (relative uncertainties), suggested by G. D. Spriggs and J. M. Campbell in 2002.

DN Group	Half-lives ($T_{1/2}$, sec)	^{235}U (Thermal)	^{238}U (Fast)	^{239}Pu (Thermal)
1	55.6	0.033 (13%)	0.008 (16%)	0.032 (38%)
2	24.5	0.154 (4%)	0.104 (2%)	0.237 (14%)
3	16.3	0.091 (10%)	0.038 (2%)	0.083 (2%)
4	5.21	0.197 (12%)	0.137 (15%)	0.182 (29%)
5	2.37	0.331 (2%)	0.294 (4%)	0.294 (10%)
6	1.04	0.090 (5%)	0.198 (1%)	0.082 (2%)
7	.424	0.081 (2%)	0.128 (10%)	0.072 (43%)
8	.195	0.023 (41%)	0.093 (4%)	0.018 (2%)

The eight-group model was not newly developed. It extended (shifted) Keepin's six-group model by the expansion technique, mathematically expanding the measured six-group parameters into the equivalent eight-group values.

To optimize the two free parameters of the delayed neutron model [Equation 2-26], the group abundance a_i and decay constant λ_i, Spriggs and Campbell suggested the expansion technique for the group abundance a_i and then recommended the fixed (same) half-lives for any fissionable isotopes, based on Piksaikin's abundance-weighted half-lives [1].

Spriggs and Campbell summarized the 245 experimentally measured delayed neutron group parameters for twenty different fission isotopes, calculated the time behavior of the reactor criticality for each isotope based on the Keepin's six group, and evaluated the new eight-group abundances by using the given (conserved) criticality scale for positive reactivities as predicted by the original six-group model. This technique is called the Spriggs' method.

To understand the Spriggs' method, it is necessary to briefly review the point reactor kinetic equation. The rate of change in number of neutrons at certain time and volume is simply considered as the difference between production rate and loss rate.

$$\frac{\partial}{\partial t}N = \ Production\ Rate - Loss\ Rate. \tag{2-27}$$

Production rate in a certain volume is the sum of 1) external source production rate, 2) scattering-in production rate, 3) flow-in production rate, and 4) fission source production rate. Loss rate is the sum of 1) absorption rate, 2) scattering-out rate, and 3) flow-out rate.

Considering each term above, the neutron density at a certain time and volume can be written as [17, 18]:

$$\frac{1}{v(E)}\frac{\partial}{\partial t}\psi(\vec{r},E,\vec{\Omega},t)=\int_0^\infty dE'\int_{4\pi}d\vec{\Omega}'\left[\chi(E)\upsilon\Sigma_f(\vec{r},E')+\Sigma_s(\vec{r},E'\rightarrow E,\vec{\Omega}'\rightarrow\vec{\Omega})\right]\psi(\vec{r},E',\vec{\Omega}',t)+s(\vec{r},E,\vec{\Omega},t)-\vec{\Omega}\cdot\vec{\nabla}\psi(\vec{r},E,\vec{\Omega},t)-\Sigma_t(\vec{r},E)\psi(\vec{r},E,\vec{\Omega},t). \quad (2\text{-}28)$$

This Equation 2-28 is called as time-dependent neutron transport equation or integro-differential form of transport equation. This equation is the microscopic transport equation describing each neutron movement with the angular flux $\psi(r,E,\Omega)$. In fact, this equation is too complicated to directly solve for each neutron. Thus, the macroscopic equation, regarding neutron group movement with flux $\varphi(r,E)$, can be rewritten by some approximations. The approximation methods are explained in Figure 2-5 [18].

Position: (x,y,z) 3 dimension	→	2 dimension	→	1 dimension	→	Point
Energy: Energy-dependent	→	Multi-group	→	Few-group → Two-group	→	One-group
Angle: (θ,φ)	→	P_n method	→	P_1 equation (Diffusion Equation)		
Time: Time-dependent	→	Quasi-static	→	Steady-state		

Figure 2-5. The approximation methods for position, energy, angle, and time in the transport equation

By applying the assumptions for energy and angle, the time-dependent diffusion equation in one-(energy) group, for a non-multiplying homogeneous reactor, without delayed neutrons can be written as [18]:

$$\frac{1}{v}\frac{\partial}{\partial t}\varphi(\vec{r},t)=D\nabla^2\varphi(\vec{r},t)-\Sigma_a\varphi(\vec{r},t)+\upsilon\Sigma_f\varphi(\vec{r},t). \quad (2\text{-}29)$$

where v (vi) is the one-group neutron speed in cm/sec, and it should be identified with the neutron yield υ (nu) in the last term. D is the diffusion coefficient in cm^2/sec and is defined in Equation 2-30, ∇^2 is the Laplacian operator, and Σ_x is the cross-section on the parameter x in cm^2. The cross-section Σ_x can be considered with the flux $\varphi(r,E)$ [Equation 2-32] as a probability that fission or absorption events on the parameter x occur.

The diffusion coefficient is defined as:

$$D \equiv \frac{1}{3\Sigma_{tr}} = \frac{\lambda_{tr}}{3}. \quad (2\text{-}30)$$

Σ_{tr} is the macroscopic transport cross-section, and λ_{tr} is called the transport mean free path. The diffusion length in a medium totally depends on the atomic density of a medium so the diffusion coefficient D can be written in terms of the atomic mass number A [4]:

$$D = \frac{1}{3\sum_s(1-\frac{2}{3A})}. \quad (2\text{-}31)$$

The flux $\varphi(r,E)$ is defined as:

$$\varphi(\vec{r},t) = vn(\vec{r},t). \quad (2\text{-}32)$$

Therefore, Equation 2-29 can be written in terms of number of neutrons:

$$\frac{\partial}{\partial t}n(\vec{r},t) = D\nabla^2 vn(\vec{r},t) - \Sigma_a vn(\vec{r},t) + v\Sigma_f vn(\vec{r},t). \quad (2\text{-}33)$$

In a steady state (the left neutron term is equal to 0 in Equation 2-33) and homogeneous reactor, the Laplacian term ∇^2 can be replaced by the geometrical buckling factor B^2 which is a geometrical quantity measuring neutron leakage and totally depends on the size or shape of a reactor:

$$\nabla^2 vn(\vec{r},t) = -B^2 vn(\vec{r},t). \quad (2\text{-}34)$$

The geometrical bucking factor B^2 is defined as:

$$B^2 = \frac{\frac{1}{k_{eff}}v\Sigma_f - \Sigma_a}{D}. \quad (2\text{-}35)$$

The effective multiplication factor K_{eff} is 1.0 in a steady state (critical), meaning neutron production rate is equal to loss rate.

Therefore, Equation 2-33 becomes:

$$\frac{\partial}{\partial t}n(\vec{r},t) = -DB^2 vn(\vec{r},t) - \Sigma_a vn(\vec{r},t) + v\Sigma_f vn(\vec{r},t). \quad (2\text{-}36)$$

The source term (the last term in Equation 2-36) is now rewritten in terms of prompt and delayed neutron:

$$\upsilon\Sigma_f \nu n(\vec{r},t) = \upsilon(1-\beta)\Sigma_f \nu n(\vec{r},t) + \lambda C(\vec{r},t). \quad (2\text{-}37)$$

C is the precursor concentration showing the ratio between the production rate and decay rate so the delayed neutron term $\lambda C(r,t)$ can be defined by the radioactive-decay law:

$$\frac{\partial}{dt} C(\vec{r},t) = \upsilon\beta\Sigma_f \nu n(\vec{r},t) - \lambda C(\vec{r},t). \quad (2\text{-}38)$$

Considering the prompt and delayed neutron terms, Equation 2-36 becomes:

$$\frac{\partial}{\partial t} n(\vec{r},t) = \upsilon(1-\beta)\Sigma_f \nu n(\vec{r},t) - DB^2 \nu n(\vec{r},t) - \Sigma_a \nu n(\vec{r},t) + \lambda C(\vec{r},t). \quad (2\text{-}39)$$

By factorizing the term $\upsilon\Sigma_f\nu$,

$$\frac{\partial}{\partial t} n(\vec{r},t) = \upsilon\Sigma_f \nu [1-\beta-\frac{DB^2+\Sigma_a}{\upsilon\Sigma_f}] n(\vec{r},t) + \lambda C(\vec{r},t). \quad (2\text{-}40)$$

From Equation 2-35, the effective multiplication factor under a critical is defined as:

$$k_{eff} = \frac{\upsilon\Sigma_f}{DB^2+\Sigma_a}. \quad (2\text{-}41)$$

The definition of the mean neutron generation time in one-goup model Λ in sec:

$$\Lambda = \frac{1}{\upsilon\Sigma_f \nu}. \quad (2\text{-}42)$$

By applying Equation 2-12 (ρ), 2-41 (K_{eff}), and 2-42 (Λ), the time-dependent neutron density with subdelayed neutron groups in a homogeneous and steady state can be simply written as:

$$\frac{\partial n}{\partial t} = \frac{\rho-\beta}{\Lambda} n + \sum_{i=1}^{n} \lambda_i C_i \quad (2\text{-}43)$$

$$\frac{\partial C_i}{\partial t} = \frac{\beta_i}{\Lambda} n - \lambda_i C_i. \quad (2\text{-}44)$$

These equations can be solved by assuming general solutions of the exponential form:

$$n(t) = n_0 e^{wt} \quad (2\text{-}45)$$

$$C(t) = C_0 e^{wt}. \quad (2\text{-}46)$$

The n_0 and C_0, resulting from the initial condition (t=0), are constants and ω is a parameter to be determined. Substituting the solution forms into Equation 2-43 and 2-44, and solving for reactivity, we can get:

$$\rho = \omega\Lambda + \sum_{i=1}^{n} \frac{\omega\beta_i}{\omega+\lambda_i}. \tag{2-47}$$

This Equation 2-47 is known as the inhour equation since the unit of root ω is typically taken as inverse hour. The root ω is also called as the inverse period, and solved by a graphical determination of the roots to the inhour equation [19]. The root ω is the corresponding decay constant for each i^{th} delayed neutron group and describes the time-behavior of the relative neutron density. If there is no reactivity feedback from other factors such as fuel depletion, temperature, pressure, poisons, and control rod movement, the amount of reactivity in a reactor core can be determined by the time change of the neutron population only. Therefore, the reactor power change can be written in terms of only neutron population at certain time period:

$$n(t) = \frac{n}{n_0} = \sum_{i=1}^{n+1} A_j e^{\omega_j t}, \tag{2-48}$$

where

$$A_j = \frac{\rho_\$}{\omega_j(\frac{\Lambda}{\beta}+\sum_{i=1}^{m}\frac{a_i\lambda_i}{(\omega_j+\lambda_i)^2})}. \tag{2-49}$$

$n(t)$ is the relative neutron power, ω_j is j^{th} root of the inhour equation, and A is the amplitude. The amplitude A_j is related to the relative abundance a_i and decay constant λ_i of each delayed neutron group, and also proportional to the system reactivity in dollar unit $\rho_\$$. The system reactivity in dollar unit $\rho_\$$ is easily defined as dividing Equation 2-47 by the effective delayed neutron fraction [Equation 2-13].

In Equation 2-48, the free parameters are originally the amplitude A and root ω of j^{th} transient term. Spriggs inferred these free parameters using the original delayed neutron

parameters. The original parameters can be estimated from the previous order model. For instance, Keepin's six-group is the original model in order to produce parameters for the next higher-group model [1, 20].

This Equation 2-49 states that the root ω of j^{th} transient term for a higher order-model can be solved by a given set of delayed neutron parameters, a given mean neutron generation time, and a value of the root which is inferred from the original delayed neutron model. Spriggs and Campbell notated this inferred root as ω_a, and it was used to obtain the remaining roots ω_j [1]. This step was iterated to form the eight-group model with 20 different transient data sets. In the calculation, the following quantities were conserved: 1) the time-dependent behavior of the system as predicted from the original delayed neutron group model, 2) the reactivity scale for positive periods, and 3) the mean delayed neutron half-life. The conserved mean half-life was evaluated by LANL based on 28 different isotopes and is shown in Table 2-8 [1].

Table 2-8. The dominant precursor and half-life of each of the eight delayed neutron groups, as evaluated by LANL. The uncertainty of half-life was not reported.

DN Group	(Dominant) Precursor	Half-lives ($T_{1/2}$, sec)
1	^{87}Br	55.6
2	^{137}I	24.5
3	^{88}Br	16.3
4	^{89}Br	4.35
5	^{90}Br	1.91
6	^{98}Y	0.548
7	^{95}Rb	0.378
8	^{96}Rb	0.203

Based on the conserved data sets and the Spriggs' method, the initial eight-group model with the above fixed half-lives for any isotopes was constructed. However, this initial model was

revised with Piksaikin's abundance weighted half-lives since it showed lower sum of the squares of the deviation, and was ensured as a better fit. The Piksaikin's abundance weighted half-lives was calculated by:

$$\bar{T} = \sum_{j=1}^{8} T_j a_j. \quad (2\text{-}50)$$

Equation 2-50 gives the final average half-lives of precursors in each group, and the calculated values are presented in Table 2-9 [1, 21].

Table 2-9. Piksaikin's abundance weighted half-lives for eight-group delayed neutron model. This model applied weighting factor to each of the groups to achieve a lower sum of squares of the deviation. The uncertainty of half-life was not reported.

DN Group	(Dominant) Precursor	Half-lives ($T_{1/2}$, sec)	
		Spriggs and Campbell	Piksaikin
1	^{87}Br	55.6	55.6
2	^{137}I	24.5	24.5
3	^{88}Br	16.3	16.3
4	^{89}Br, ^{93}Rb, ^{138}I	4.35	5.21
5	^{94}Rb, ^{139}I, ^{85}As, ^{98m}Y	1.91	2.37
6	^{93}Kr, ^{144}Cs, ^{140}I	0.548	1.04
7	^{95}Rb, ^{91}Br	0.378	0.424
8	^{96}Rb, ^{97}Rb	0.203	0.195

This new eight-group model was constructed by splitting the original Keepin's group number (No.) 2 into two groups and the group No. 6 into two groups. The most featured improvements of this new eight-group model were: 1) recommending more available sets of delayed neutron, 2) investigating new delayed group parameters, regarding an explicit function of incident neutron energies: thermal, fast, and high, 3) suggesting the same half-lives of precursors for any fissionable isotopes [16].

Different models such as a seven- or thirteen-model have been suggested by many other studies but they have not been supported since the eight-group model shows better prediction in the reactivity calculation than a lower-order group model, and a higher-order group model also suffers from assigning shorter-lived delayed neutrons in the frame of milliseconds.

Even though the eight-group model shows better prediction, some numerical solutions or other group models have to be studied further to find better numerical solutions to explain the delayed neutron emission and to reduce its associated uncertainties.

Uncertainty on Six and Eight-Group Model of Delayed Neutrons

As shown in Table 2-7, the uncertainties on delayed neutron nuclear data are particularly large. These high uncertainties can fundamentally originate either from the statistical quality of the chosen fitting methods or the quantity of the measurement data sets.

The measured data sets can be precisely provided by the well-designed experimental apparatus, but their final solution and relative uncertainty (standard derivation) can be different due to the fitting methods. According to Wang and Reece in 2008, the reported parameters in many studies interestingly fit their individual measured delayed neutron data well even though the experimental data are significantly different [2].

As mentioned, the LSF method has been commonly used to describe and fit delayed neutron nuclear data. The LSF is a common mathematical method to find a best-fit line or curve by minimizing the sum of the squares of the offsets (distance from the experimental value to the expected value). However, the coefficients, the shape of the fitted curve, and the relative error via LSF can be dramatically changed by adding a few more data points or considering the quantity of the measured data points, so the validation study of coefficients and the error analysis of each parameter have to be performed [22].

The analytical goodness of the LSF method between the measured data set and the fitted group parameters is expressed by the sum of squared residual, notated by the capital *S*. The residual *e* is the quantity showing the difference between an observed (measured) response *y* and a predicted response *y´* by the fitting equation.

$$S = \sum e^2 = \sum (y_i - y_i')^2. \tag{2-51}$$

The subscript *i* indicates the order of observation. The predicted response *y´* can be defined as:

$$y_i' = f(x_i, \beta) + \varepsilon_i, \tag{2-52}$$

where ε_i is the error in the i^{th} observation, and β is the unknown parameter of the least-squares line. Equation 2-52 can be simply rewritten for the linear model by denoting β_0 as the intercept and β_1 as the slope of the least-squares line.

$$y_i' = \beta_0 + \beta_1 x_i + \varepsilon_i. \tag{2-53}$$

The linear least-squares fitting technique is the simplest applied form of linear regression and directly provides a solution by the best fitting straight line. Unlike the linear model, the non-linear model is complicated and its solution can not be directly provided. Generally, the possible solution can be provided by iteratively applying the linear least-squares model until unknown parameters in the function f [Equation 2-52] is converged to the form of linear [23, 24].

In Equation 2-53, the error ε_i creates uncertainty in the estimates β_0 and β_1. It means that an observed (measured) response *y* is the same with a predicted response *y´* if there is no error. If the error has small magnitude, and then the difference between an observed (measured) response *y* and a predicted response *y´* is also small. In the same manner, the large error leads to the big difference [23].

Most fitting methods, including linear or non-linear LSF methods, use one common assumption which each data point is equally precisely provided (measured). It means that each error ε_i has the same variance and is normally distributed, but it is undeniably unavailable in real experiences. Therefore, many researchers use the weight function to provide more precise fitting line or curve and its relative uncertainty. The common model of the weight LSF is:

$$\sum \frac{1}{w_i}(y_i - y_i')^2, \tag{2-54}$$

where *w* is a weighting factor and known constant.

Applying this factor, data points with low variance (precisely measured) will be given higher weights and points with higher variance (non-precisely measured) are given lower weights. The major advantage of this weight technique is that the better analytical goodness of the LSF method between the measured data set and the fitted group parameters can be obtained since the prediction line can be significantly shifted to match the data with weights. However, it has to be remembered that this weight technique must be performed with the precisely known constants. Otherwise, the final predicted model will be totally distorted.

This weighted least-squares model was used to judge the goodness of the fitted six-group parameters, the group abundance a_i and decay constant λ_i, by Keepin [15, 25]:

$$S = \sum \frac{1}{C_i}(C_i - f(x_n, T_i))^2. \tag{2-55}$$

C_i represents the observed counts at the time interval T_i, *x* is the unknown parameters in the time-dependent function *f*, and the indices *i* and *n* are respectively represented as time interval corresponding to half-lives of precursors in the six-group model and data points.

The variable *x* is can be defined by:

$$x = (a_1, \dots, a_n, \lambda_1, \dots, \lambda_n). \tag{2-56}$$

Keepin used two different irradiation conditions, named “instant” and “infinite”. For each condition, two different probability density functions were separately written.

For the instant condition,

$$f(x_n, T_i) = PT_i \sum a_n \lambda_n e^{-\lambda_n T_i}. \quad (2\text{-}57)$$

For the infinite condition,

$$f(x_n, T_i) = PT_i \sum a_n e^{-\lambda_n T_i}. \quad (2\text{-}58)$$

P is a proportional constant depending on the reactor power level, the fissile sample properties, and detector efficiency.

As mentioned, the non-linear LSF can be solved by iterative processes. For this iteration, the initial estimations (seeds) have to be decided. Traditionally, the Matrix Inverse method, Levenberg-Marquardt method, and Quasi-Newton method have been widely used for this problem [23]. However, it is not clear which method is precise. Later the validation study for these numerical algorithms was performed by Wang and Reece in 2011 [2].

They compared three different methods, Matrix Inverse with singular value decomposition, Levenberg-Marquardt, and Quasi-Newton, with different regularization techniques in order to estimate the parameter values. It was resulted that the Levenberg-Marquardt method produced the most acceptable values, but also pointed out that the fitted delayed neutron decay parameters are very flexible even though they are calculated based on the perfect data sets [2].

To calculate uncertainties on the new eight-group model, Spriggs and Campbell firstly conserved and expanded Keepin’s uncertainty. However, the final result with the conserved data from the expansion technique was unrealistically small. They thus calculated the relative uncertainty on the group abundance (free parameter) corresponding to the variance of the reactivity (measured parameter). The variance of the reactivity is also calculated by the original

delayed neutron model. The half-life sets were assumed as perfect values since they suggested the fixed specific numbers for them. The error propagation for the new eight-group model was [1]:

$$\sigma_\rho^2 = \sum_{j=1}^{m} \left(\frac{\partial \rho}{\partial a_j}\right)^2 \sigma_{a_j}^2, \tag{2-59}$$

where

$$\frac{\partial \rho}{\partial a_j} = \frac{\omega}{(\omega+\lambda_i)}. \tag{2-60}$$

After expanding the delayed neutron group model, the validation study was performed using experimental data for ^{237}Np. The relative group abundance and its uncertainty were calculated by the six- and eight-group models, and the results were compared. In this study, the eight-group model showed that the relative abundances are showing a good agreement with the six-group model, and uncertainties were also accepted as realistic data since the uncertainty of the reactivity scale was smaller in the eight-group model than in the six-group model [1].

Even though the relative uncertainties in the eight-group model were considered to be acceptable, the relative uncertainties on the delayed neutron group abundances of the longest-lived delayed neutron groups are particularly large - up to 13% for thermal fissions of ^{235}U, 16% for fast fissions of ^{238}U, and 38% for fast fissions of ^{239}Pu. These high uncertainties hinder the accurate estimation of fission rates in a fissile sample.

CHAPTER 3
NUMERICAL METHODOLOGIES

The derivations in this chapter assume the following experimental process: A sample of fissile material (a single isotope) is irradiated with neutrons during irradiation time t_i. After the irradiation, the sample is transported to the measurement position; this time between the end of irradiation and beginning of measurement is the cooling time t_c. After the cooling time, the radiation signatures from the sample are measured with suitable detectors during the acquisition time t_a [Figure 3-1].

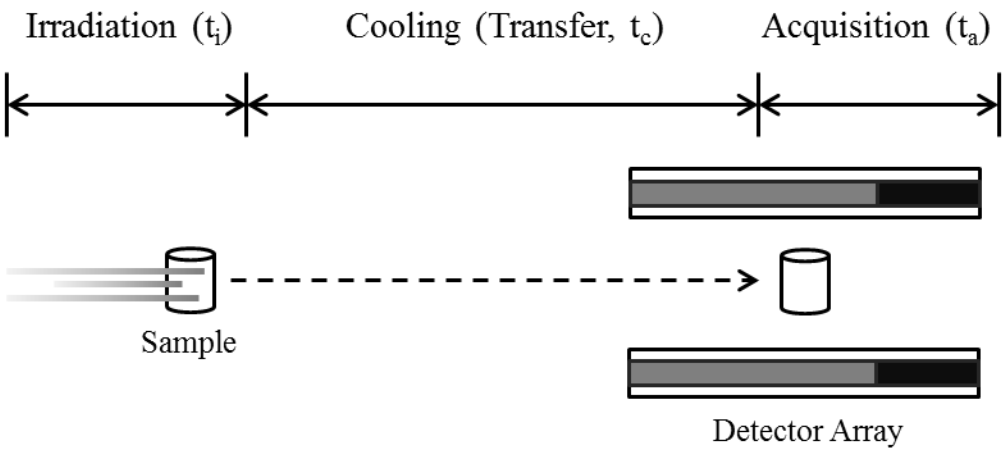

Figure 3-1. A schematic of the experimental process used for this study. A fissile sample is irradiated for time T_i, transferred and allowed to cool for a time T_c, and then measured for time T_a.

Detector Count Rates as a Function of Fission Yields

In a fissile sample undergoing fission, the delayed neutron yield is related to the number density of precursor nuclei produced during the irradiation. The number density of the precursor nuclei ($\frac{dN_{FP}}{dt}$) produced can be written as:

$$\frac{dN_{FP}}{dt} = Y_{FP} \cdot \sigma_F \cdot \varphi \cdot N - \lambda \cdot N_{FP}. \quad (3\text{-}1)$$

Or in terms of the fission rate F, as:

$$\frac{dN_{FP}}{dt} = Y_{FP} \cdot F - \lambda \cdot N_{FP}, \quad (3\text{-}2)$$

where N_{FP} is the number density of precursor nuclei, F ($=\sigma_F \cdot \varphi \cdot N$) is the fission rate, λ is the decay constant of precursor nuclei, and Y_{FP} is the cumulative yield (hence, the average number of precursor nuclei of a certain kind, coming from one fission reaction).

By integrating Equation 3-2 with the initial condition $N_{FP} = 0$ (at t=0), the equation for the number density of precursor nuclei produced at the end of irradiation for time t_i is:

$$N_{FP} = Y_{FP} \cdot \frac{F}{\lambda} \cdot (1 - e^{-\lambda \cdot t_i}). \quad (3\text{-}3)$$

After the irradiation, the sample is transferred to the measurement station. The number density of precursor nuclei at the end of cooling time ($t=t_i+t_c$):

$$N_{FP} = Y_{FP} \cdot \frac{F}{\lambda} \cdot (1 - e^{-\lambda \cdot t_i}) \cdot e^{-\lambda \cdot t_c}. \quad (3\text{-}4)$$

The change in the number density of precursor nuclei between the beginning and the end of the acquisition time gives the total number of precursors per unit volume that decayed during this time and, hence, can be measured. This can be written as:

$$N_{FP} = Y_{FP} \cdot \frac{F}{\lambda} \cdot (1 - e^{-\lambda \cdot t_i}) \cdot e^{-\lambda \cdot t_c} \cdot (1 - e^{-\lambda \cdot t_a}). \quad (3\text{-}5)$$

By defining $T = \frac{1}{\lambda}(1 - e^{-\lambda \cdot t_i}) \cdot e^{-\lambda \cdot t_c} \cdot (1 - e^{-\lambda \cdot t_a})$, Equation 3-5 is simplified to:

$$N_{FP} = Y_{FP} \cdot F \cdot T. \quad (3\text{-}6)$$

The total counts (C_{FP}) for delayed neutrons or delayed gamma-rays from the precursor density depend on the detector efficiency (ε) and the attenuation coefficient (μ), and are generally written as:

$$C_{FP} = Y_{FP} \cdot F \cdot T \cdot \varepsilon \cdot \mu. \quad (3\text{-}7)$$

The counts for delayed neutrons and gamma-rays from precursors depend on the incident neutron flux, target nucleus density, sample size, detector efficiency, solid angle, and beam attenuation.

Delayed Gamma Fission Rate Measurement Technique (Gamma Scanning)

The derivation of the delayed gamma fission rate measurement technique (called as "*the delayed gamma technique"* in later chapters) starts from Equation 3-7. A fissile sample is irradiated by a neutron generator, and delayed gamma rays (gamma lines) from fission products are emitted with energies characteristic of the decaying isotopes. If the fission yields of the isotopes are known, the fission rate during the irradiation is calculated and related to the measured signal (M_γ) via [5]:

$$M_\gamma = F \cdot \alpha_\gamma = F \cdot \varepsilon_\gamma \cdot \mu_\gamma \cdot b_\gamma \cdot \sum_k T_{\gamma_k} \cdot A_{\gamma_k}, \tag{3-8}$$

where α_γ is the proportionality factor accounting for physical and geometrical properties of the detection setup, ε_γ is the detector efficiency, μ_γ is the attenuation coefficient, b_γ is the gamma-ray intensity, and $T_{\gamma k}$ accounts for the build-up and decay of the gamma-ray emitting isotope during irradiation, cooling and acquisition time (analogous to the definition of T in Equation 3-6). $A_{\gamma k}$ is the fission yield of the isotopes in the decay chain with relevant half-lives (meaning that the half-lives are long enough not to completely decay during cooling time and short enough not to remain unchanged over cooling and acquisition time). The index k denotes the different isotopes at each state in the decay chain leading to the emission of the gamma-ray of interest.

To obtain low uncertainty fission rate estimates from the delayed gamma technique the analyzed gamma-ray lines must have certain properties. The criteria for a gamma line to be useful for the analysis are: 1) good peak statistics (and therefore large cumulative fission yields, large beta-gamma branching ratio, low background), 2) suitable half-lives of all relevant isotopes

in the investigated decay chain, 3) small uncertainties on the nuclear data, and 4) isolation of the peak in the spectrum.

The decay chains of the delayed gamma precursors can be quite complex, depending on the half-lives and the decay modes involved. For the present experimental setup, however, the considered gamma lines come from decay chains that can be described by a combination of three states: the gamma ray emitter itself, its isomeric state, and its parent. According to the definitions above and its simple decay process, the most promising isotope for this study is ^{89}Rb. Its decay scheme is shown in Figure 3-2.

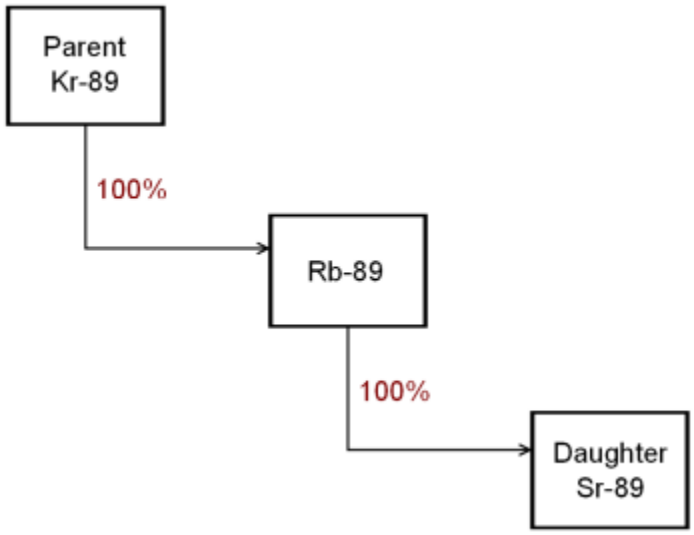

Figure 3-2. The 1032 keV gamma line from the decay of ^{89}Rb was chosen for this study based on its larger yield, low nuclear data uncertainty, and the ability to isolate the peak in the gamma spectrum.

Equations 3-9 to 3-11 are the general decay schemes considering the parent (p), the fission product of interest (FP), and its isomeric state (m) with relevant half-lives (λ_P, λ_{FP}, and λ_m) and branching ratios (q_P and q_m). The Y_{ind} and Y_{cum} terms are the independent and cumulative effective fission yields. If multiple fissile isotopes are present in the sample, their fission yields are summed [5].

$$A_P = \frac{q_P \cdot \lambda_{FP}}{\lambda_{FP} - \lambda_P} \cdot Y_{cum,P}. \quad (3\text{-}9)$$

$$A_m = \frac{q_m \cdot \lambda_{FP}}{\lambda_{FP} - \lambda_m} \cdot Y_{cum,m}. \quad (3\text{-}10)$$

$$A_{FP} = Y_{ind,FP} + \frac{q_P \cdot \lambda_P}{\lambda_P - \lambda_{FP}} \cdot Y_{cum,P} + \frac{q_m \cdot \lambda_m}{\lambda_m - \lambda_{FP}} \cdot Y_{cum,m}. \quad (3\text{-}11)$$

Some parents of the fission products do not decay to the isomeric state but only to the ground state of the fission product like the chosen isotope ^{89}Rb. Thus, Equation 3-9 and 3-11 were considered for the saturation and decay of ^{89}Rb with the time corresponding term $T_{\gamma k}$ in Equation 3-8.

The counts under the selected peaks are integrated, which gives the measured counts (M_γ) in Equation 3-8. By dividing the counts by the proportionality factor, the fission rate of the sample during the irradiation can be derived.

Delayed Neutron Fission Rate Measurement Technique

A delayed neutron fission rate measurement technique (called as *"the delayed neutron technique"* in later chapters) was developed by Jordan and Perret [6] to measure induced fission rates in spent fuel for reactor physics validation studies. If a neutron generator irradiates the sample, and a detector bundle measures the delayed neutrons, the fission rate during the irradiation can be calculated and related to the measured signal (M_n):

$$M_n = F \cdot \alpha_n = F \cdot \sum_i \sum_j T_{n_j} \cdot D_j \cdot S_{n_{i,j}}, \quad (3\text{-}12)$$

where α_n is the proportionality factor, T_{nj} accounts for the build-up and decay of the delayed neutron emitting isotopes during irradiation, cooling and acquisition time (analogous to $T_{\gamma j}$ in the gamma scanning technique), D_j is the correction factor for the solid angle and attenuation corrections, and $S_{ni,j}$ is the normalized group-wise delayed neutron source. The indices *i* and *j* denote the fissioning isotope *i* and delayed neutron group *j*.

The term of the normalized group-wise delayed neutron source $S_{n_{i,j}}$ is given by:

$$S_{n_{i,j}} = \frac{f_i}{F} \cdot \upsilon_{d_i} \cdot \alpha_{d_{i,j}}. \quad (3\text{-}13)$$

The term f_i indicates fission rates from each isotope, and υ_d and α_d account for delayed neutron yields and relative abundances, respectively [6]. The fission rate of the sample at the time of the irradiation can be derived in the same manner as the gamma scanning technique above.

Combining Fission Rate Measurement Techniques to Derive Improved Nuclear Data Parameters

The above two techniques each provide an estimate of the total fission rate in a fissile sample. The total counts of both techniques are proportional to the actual fission rate in each fissile or fertile element. The difference is the proportionality constant between them. If the same sample is irradiated under the same condition, the fission term *F* in Equation 3-8 (the delayed gamma technique) and Equation 3-12 (the delayed neutron technique) can be theoretically set equal, shown in Equation 3-14 [3].

$$\frac{M_n}{M_\gamma} = \frac{\alpha_\gamma}{\alpha_n}. \quad (3\text{-}14)$$

Therefore, the high-uncertainty delayed neutron nuclear data can be expressed (via the two fission rate estimates) as a function of the low-uncertainty delayed gamma nuclear data [Figure 3-3].

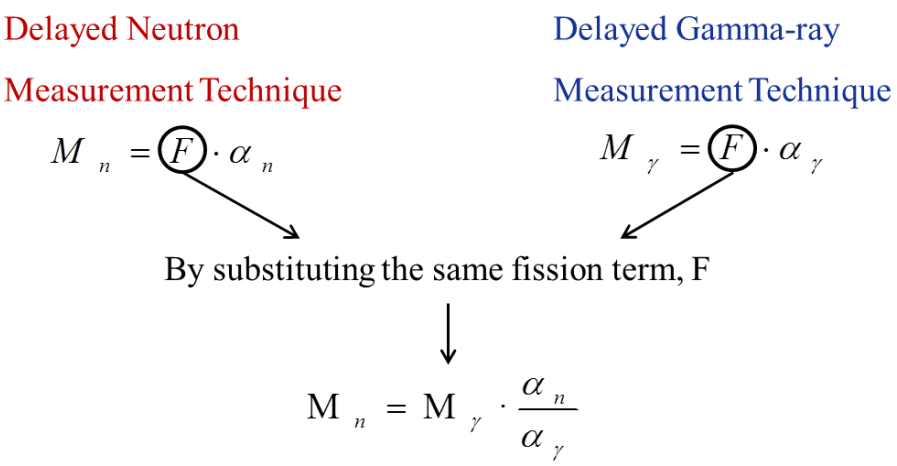

Figure 3-3. Diagram showing how the delayed neutron and gamma techniques were combined based on a proportional constant.

Considering all relative factors, Equation 3-14 becomes:

$$M_n = \frac{\varepsilon_\gamma \cdot \mu_\gamma \cdot b_\gamma \cdot \sum_k T_{\gamma_k} \cdot A_{\gamma_k}}{\sum_i \sum_j T_{n_j} \cdot D_j \cdot S_{n_{i,j}}}. \quad (3\text{-}15)$$

According to Jordan and Perret, the uncertainties on the first longest-lived delayed neutron group can thereby be reduced significantly by a factor of three or four through this combined technique [3].

Uncertainty Calculation for Longest-lived Delayed Neutron Group

As mentioned, the relative uncertainty of the longest-lived delayed neutron group is particularly large. The main reasons of these high uncertainties are: 1) the number of delayed neutrons emitted by the longest-lived group (decay of ^{87}Br) is smaller than for the other delayed neutron groups, and 2) Keepin et al. had the limitation of the data acquisition (330 sec) so which led poor statistics [3]. The expanded eight-group model also showed the problem of the poor statistics since the half-life sets were recalculated, actually recreated, with the assumption that the uncertainty on the reactivity scale was constant. The expanded model was not evaluated based on the measurement data of the delayed neutron parameters, but just reasonably and

mathematically expanded. In fact, Spriggs and Campbell pointed out that the uncertainty values on the expanded relative abundances might not be physically [1, 3].

More statistically meaningful (precise) delayed neutron group parameters can be evaluated by the precise measurements and procedures. For that, an experimental apparatus for high accuracy simultaneous measurements for delayed gamma-rays and neutrons has been designed, optimized, and built. Based on the obtained data sets, uncertainties on the delayed neutron nuclear data were consequently reduced by the combined technique in this study. The experimental setups are explained in the next chapter, and the derivation of uncertainty equation from the combined technique is explained in this subchapter. Before going further, the concepts of error or uncertainty analysis are explained.

Radiation measurement is not a deterministic process; it is instead probabilistic since the emission of atomic or nuclear radiation obeys the rules of quantum theory, based on the probability of an atomic or nuclear reaction. The mean (average) number of particles can be determined within a certain error of the true value [26]. The error refers to the difference between a measured value and the true value. It can be separated into two parts, the systematic error and the random error. The systematic error is often called a bias. Therefore, the measured value can be written as:

$$Measured\ value = true\ value + systematic\ error + random\ error. \quad (3\text{-}16)$$

Systematic errors in experimental observations usually come from the measuring instrument, physical changes in the environment, and measuring technique. The systematic error in experimental observations does not deviate upon repeated measurements under the same experimental conditions. However, it is difficult to determine the exact causes of these

systematic errors and therefore can not be separated and quantified from the total error in a measured value (both systematic and random error).

The random error in experimental measurements comes from statistical fluctuations and varies every time. The cause of occurrence for these types of error can never be determined but can be evaluated through statistical analysis. The random error can be reduced by averaging over a large number of observations [21]. Table 3-1 shows the difference between two types of errors in the experiment.

Table 3-1. A summary of the errors introduced by the experimental process, grouped by systematic and random errors.

Types of Errors	Reasons (causes of errors)
Systematic Error	Measuring instruments (un-calibrated devices)
	Environmental conditions (physical changes with temperature, humidity, airflow, and etc.)
	Measurement techniques/methods
Random Error	Statistical fluctuations

Neglecting systematic error, the standard deviation σ of the mean value μ represents the size of the random error:

$$\mu \pm \sigma. \tag{3-17}$$

The standard deviation σ decreases with larger sample sizes. The Central Limit Theorem (CLT) states that if the sample size (typically denoted by n) from a population is large enough, then the distribution of the sample mean is approximately normal, no matter what population the sample was drawn from [23]:

$$\bar{X} \sim N(\mu, \frac{\sigma^2}{n}). \tag{3-18}$$

The more accurate result can be drawn as the sample size increases since the sample mean will approach the expected value of the population mean μ with the sample variance being approximately equal to the expected value of the population variance σ^2 divided by each sample's size n [23].

Generally, the CLT provides a reasonable approximation when the sample size is larger than 30. However, the statistical result becomes more accurate as the sample size grows larger. This statement is well-explained by Figure 3-4.

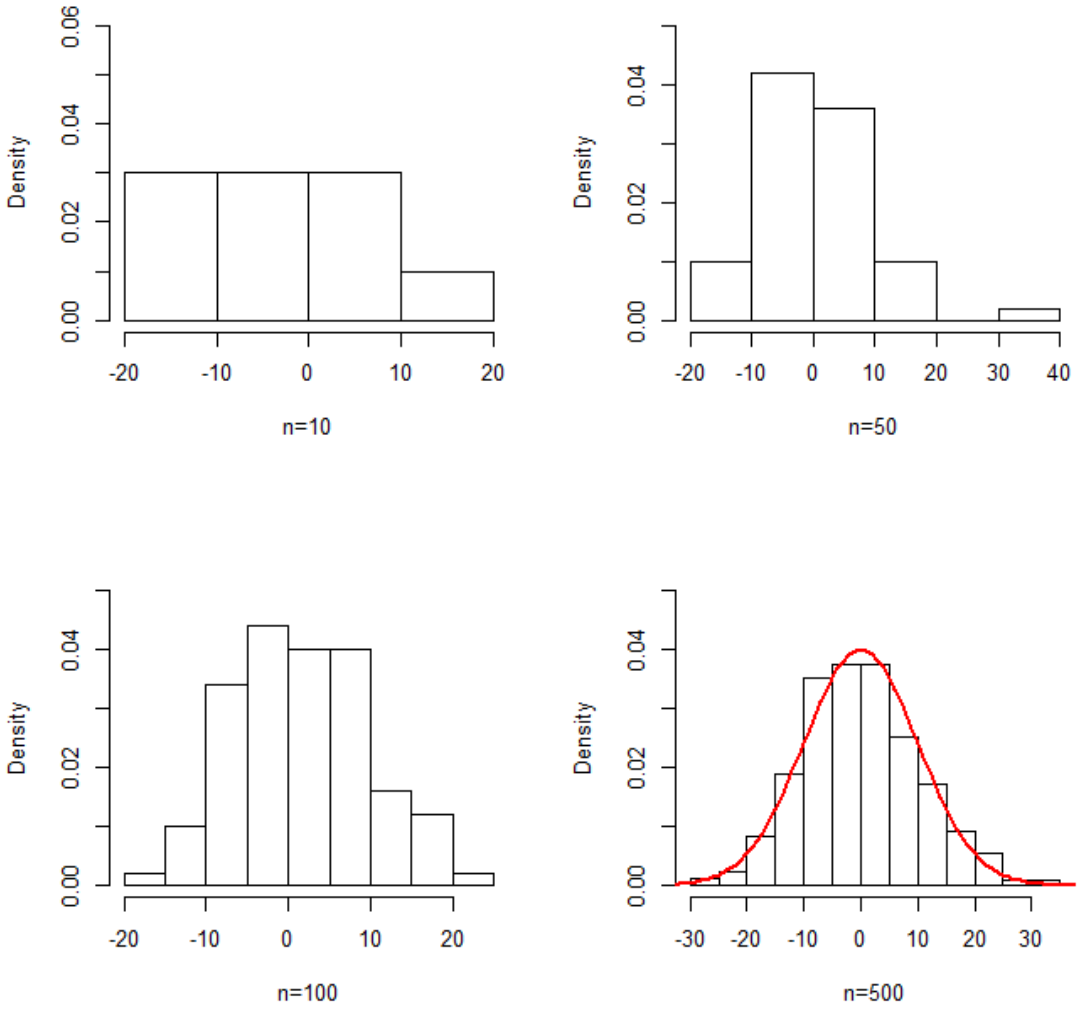

Figure 3-4. The illustration of Central Limit Theorem (n = sample size), showing that a statistical result becomes more accurate as the sample size increases.

The standard deviation can be expressed in terms of absolute and relative uncertainty. The absolute uncertainty is the amount of physical uncertainty in a measurement, has the same unit with the measured object as the quantity, and is expressed in the standard form:

$$\mu \pm \Delta\mu. \tag{3-19}$$

The relative uncertainty indicates how good a measurement is relative to the size of the measured object, is commonly expressed as fraction or percent, has no units, and takes the standard form as:

$$\mu \pm \frac{\Delta\mu}{\mu}. \tag{3-20}$$

This study aims to reduce the relative uncertainty of the longest-lived delayed neutron group so the both expressions, the uncertainty and relative uncertainty, mean only the relative uncertainty.

Additionally, the systematic error and the random error are used to show the accuracy and precision of a measurement. The width of the distribution describes the precision of the measurement, and the distance from the true value to the mean value μ expresses the accuracy of the measurement. These concepts in radiation measuring process are well-explained by N. Tsoulfanidis, and shows in Figure 3-5 [26].

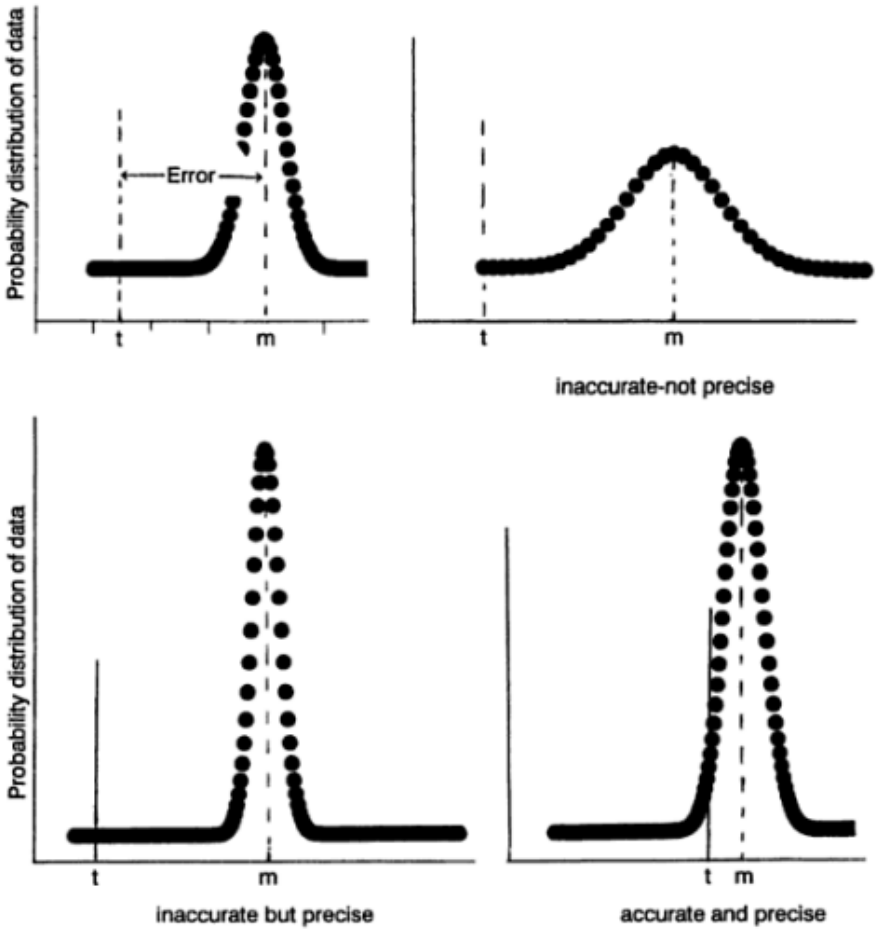

Figure 3-5. Several data sets describing the accuracy and precision of a measurement. The mean value of the measurement data is shown by "m", and the true value is shown by "t".

In Figure 3-5, *t* and *m* separately mean the true value and measured value.

With only one parameter, the standard deviation of its mean value is just the square root of the mean. However, more than two parameters, each with their individual uncertainties, have to be considered in radiation detection. For instance, the total counts for delayed neutrons (M_n) are resulted from other parameters such as the time setup, the correction factor for the solid angle and attenuation corrections, and the normalized group-wise delayed neutron source [Equation 3-12]. Therefore, each parameter and its uncertainty should be combined to come up with the final result of an experiment, $M_n \pm \sigma$. The general formula to estimate the standard deviation for any parameter u is given [23, 27]:

$$\delta_u^2 = (\frac{\partial \mathrm{u}}{\partial \mathrm{a}})^2\, \delta_a^2 + (\frac{\partial \mathrm{u}}{\partial \mathrm{b}})^2\, \delta_{\mathrm{b}}^2 + \cdots + (\frac{\partial \mathrm{u}}{\partial \mathrm{z}})^2\, \delta_{\mathrm{z}}^2 . \quad (3\text{-}21)$$

Equation 3-21 is called as the multivariate propagation of error formula or simply the error propagation equation. It is only valid when each parameter is independent from each other.

The delayed neutron signal M_n in the Equation 3-12 is a sum over all delayed neutron groups from all fissioning isotopes. The cooling time t_c is the interval between the end of the irradiation and the beginning of the measurement. After a minute of cooling, the shorter-lived delayed neutron groups have decayed so that their contributions to the total delayed neutron signal is negligible. Figure 3-6 shows the contributions of the three longest-lived delayed neutron groups to the total signal.

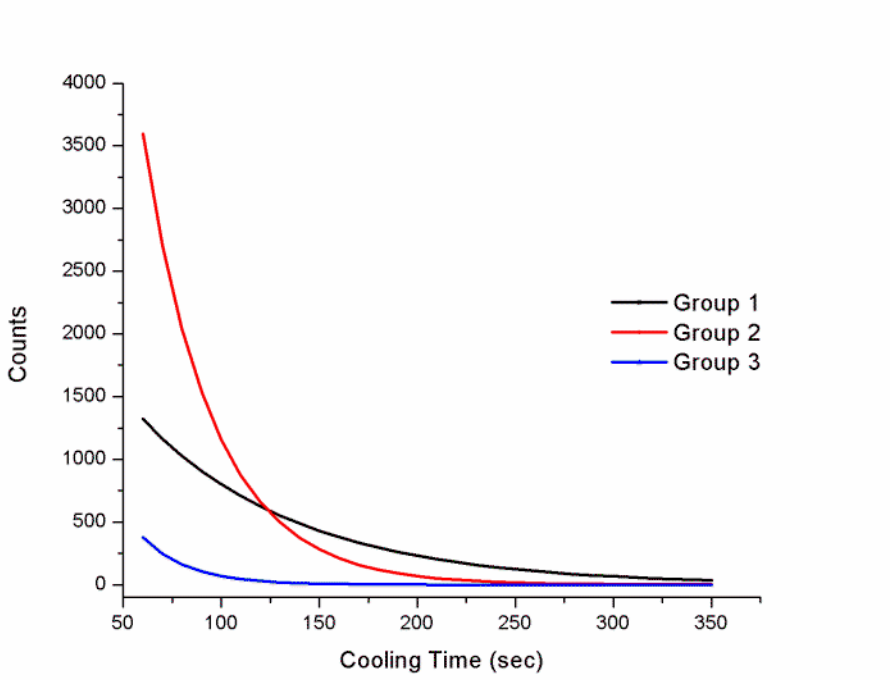

Figure 3-6. Total counts of three longer-lived delayed neutron groups versus the cooling time, showing that the contribution of the higher groups drops as cooling time increases due to decay.

The fraction of neutrons coming from the third group is below 0.55% after a cooling time of 180 sec. If one waits long enough, Equation 3-12 can be rewritten in terms of the first and second group (two longest-lived groups, half-lives of 55.6 s and 24.5 s) only:

$$M_n = F\nu_{di}D_1T_1\alpha_{i1} + F\nu_{di}D_2T_2\alpha_{i2}. \tag{3-22}$$

As described before, the fission rate in Equation 3-21 can be substituted by *F* in the gamma-ray equation [Equation 3-8] by using the simultaneous measurement system with the same fissile sample. This leads to an expression of the relative abundance of the longest-lived delayed neutron group (α_{i1}) from a fission isotope *i* as a function of the measured delayed neutron counts, the measured delayed gamma counts and the abundance of the second delayed neutron group:

$$\alpha_{i1} = \frac{M_n \cdot \mu_\gamma \cdot \varepsilon_\gamma \cdot b_\gamma \cdot T_{\gamma_k} \cdot A_{\gamma_k}}{M_\gamma \cdot \nu_{di} \cdot T_{n1} \cdot D_1} - \alpha_{i2}\frac{T_{n2} \cdot D_2}{T_{n1} \cdot D_1}. \tag{3-23}$$

$$\text{Let } S \equiv \mu_\gamma \cdot \varepsilon_\gamma \cdot b_\gamma \cdot T_{\gamma_k} \cdot A_{\gamma_k}. \tag{3-24}$$

By applying the error propagation equation [Equation 3-21], the relative uncertainty of the longest-lived delayed neutron group is given by:

$$\sigma^2_{\alpha i1} = \left\{1 + \frac{\alpha_{i2}}{\alpha_{i1}}\left(\frac{T_{n2}D_2}{T_{n1}D_1}\right)\right\}^2 \left(\sigma^2_{\mathrm{M_n}} + \sigma^2_S + \sigma^2_{M_\gamma} + \sigma^2_{\nu_{\mathrm{di}}}\right) + \left(\frac{\alpha_{i2}}{\alpha_{i1}}\frac{T_{n2}D_2}{T_{n1}D_1}\right)^2 \sigma^2_{\alpha_{i2}}. \tag{3-25}$$

where σ_x is the relative uncertainty on the parameter *x*, and the Equation 3-25 is called *"the uncertainty equation"* in following chapters.

CHAPTER 4
EXPERIMENTAL DESIGNS AND SETUPS

This chapter presents the design, optimization, and installation of a new experimental apparatus with capability of producing high accuracy measurements for delayed gamma-rays and neutrons. The apparatus consists of a D-D neutron generator, a detector bundle, a sample handler, and related electronics.

The objective of the experimental design is to 1) maximize the fission rate in the sample, 2) optimize the transfer time of the sample from the irradiation position to the measurement station and 3) maximize the efficiency of both the neutron and the gamma detection system. Each of these objectives is discussed in detail in the following subsections. The system optimization was carried out using various Monte Carlo models (MCNP [28]) in conjunction with the nuclear data library, named Joint Evaluated Fission and Fusion file version 3.1 (JEFF-3.1) [29].

The design concept is a fissionable sample, roughly the size of a fuel pellet, irradiated by a D-D neutron generator, which emits neutrons of 2.45 MeV. The sample may contain ^{235}U, ^{238}U, ^{239}Pu or ^{232}Th. The irradiation is initially set up to last 15 min, long enough for the delayed neutron and gamma precursors to saturate. A pneumatic sample handler rotates the sample during the irradiation to achieve a homogeneous fission rate in the sample, and then transfers the sample from the irradiation position to the measurement position. Delayed neutrons and gamma-rays are measured simultaneously by an array of neutron detectors and a gamma detector, respectively [Figure 4-9].

Maximizing Fission Rates in a Sample

The strength of the delayed neutron and the delayed gamma source in the sample is proportional to the induced fission rates. After precursor isotopes are saturated, longer irradiation

does not increase source intensity since the production rate of precursors achieves equilibrium with the decay process. The source strength can be increased by high incoming neutron flux, induced fission reaction, or large mass (size) of a fissile target. The fraction of fissions that emit delayed neutrons is small (in the order of 1 %). Hence, a high fission rate in the sample is needed to obtain low statistical uncertainties.

In order to increase the incoming flux and thus the fission rate on the target, a neutron generator and a sample were surrounded by different thickness metal reflectors (lead and tungsten) in the MCNP simulation for potential implementation. The dimensions of the sample were equivalent to a fuel pellet (diameter: 0.82 cm, height: 0.99 cm). The simulated geometry is shown in Figure 4-1.

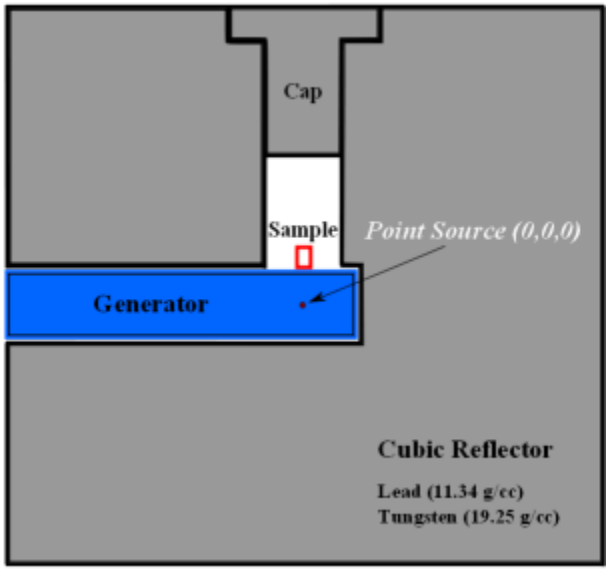

Figure 4-1. MCNP simulation geometry showing the neutron generator (blue) output as appoint source. The sample (red) was placed 2 cm away and was surrounded by a metal reflector (grey) in order to increase the neutron flux incident on the sample.

The generator was placed at the center of the cubic reflector. The sample was placed on top of the generator, 2 cm away from the source point.

Figure 4-2 shows the calculated fission rates in the above setup, using a UO_2 sample, for different reflector thicknesses. Reflectors beyond 30 cm provide minimal additional fission. Lead increases the fission rate 20 % more than tungsten, therefore, a 30 cm thick lead reflector was chosen. This increases the total fission rate in a UO_2 sample by 27 %.

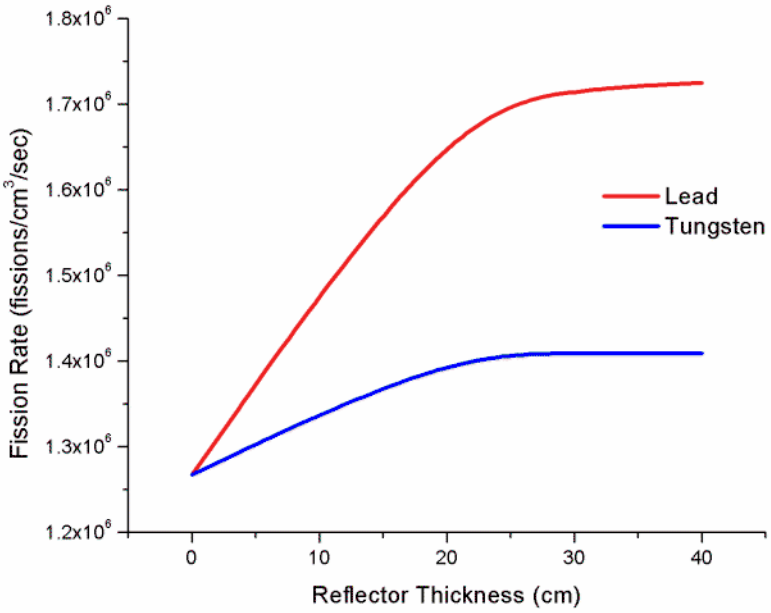

Figure 4-2. Fission rate from a UO_2 sample as a function of reflector thickness for lead and tungsten reflectors. A 30 cm lead reflector was chosen based on the 27 % increase in fission rate.

Fission rates for various samples placed 2 cm away from the generator target with the lead reflector are summarized in Table 4-1.

Table 4-1. Fission rate from a UO_2 sample with different enrichment was estimated via MCNP simulation [fissions/cm^3/sec].

Sample	^{235}U	^{238}U
UO_2 (Enriched, 3.5 w/o)	7.75×10^4	8.21×10^5
UO_2 (Natural Uranium)	3.30×10^4	1.71×10^6
UO_2 (Depleted Uranium)	8.94×10^3	1.72×10^6

This study focuses on the validation of the combined method and improvement of the high uncertainty of the longest-lived delayed neutron group yield of ^{238}U. Therefore, the fission rate from a depleted uranium dioxide (UO_2) sample was selected due to its higher content of ^{238}U and will be used for the further discussions in this paper. The chosen depleted uranium dioxide (UO_2) sample will be simply mentioned a UO_2 sample in later chapters.

Detector Bundle Design

The most important factor to consider for the delayed neutron measurement system is how to effectively detect a small amount of neutrons. The expected delayed neutron emissions from the sample will be on the order of a few hundred counts per second at the end of the irradiation and rapidly decaying thereafter. The energy distribution of delayed neutrons is weakly dependent on the fissile material. However, all delayed neutron groups have low average energy of emission on the order of a few hundred keV [13]. The detector bundle design was optimized to achieve high efficiency for delayed neutron detection. Two possible concepts of detector bundles are shown in Figure 4-3.

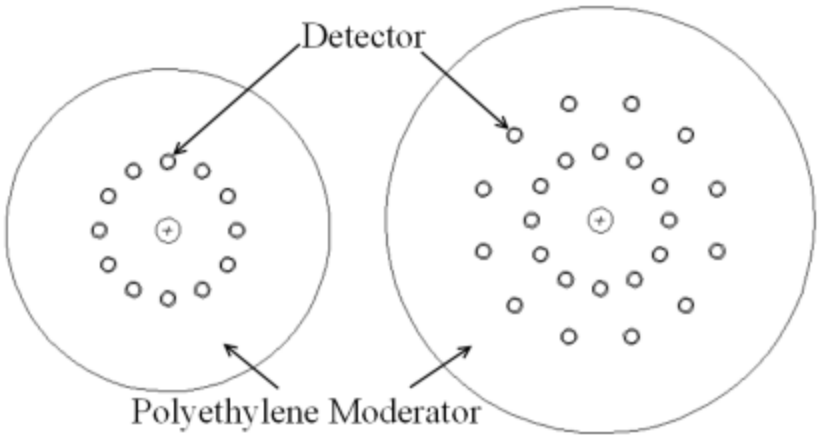

Figure 4-3. The cross sectional view of the two different detector bundle designs, one and two layers. ^{3}He and BF_3 tubes detectors were considered and compared.

^{3}He and BF_3 tubes are commonly used to indirectly detect neutrons through absorption reactions, (n, p) and (n, α) respectively [27]. The reactions in each detector are written as:

$$^{3}He + n \rightarrow H(p) + {}^{3}H \qquad Q = 765\ keV \tag{4-1}$$

$$^{10}B + n \rightarrow {}^{4}He(\alpha) + {}^{7}Li \qquad Q = 2.78\ MeV. \tag{4-2}$$

^{3}He and BF_3 detector tubes of 1 inch diameter were used to form bundles of one and two layers, embedded in a cylindrical block of polyethylene. One and two layer bundles were designed with twelve and twenty four detectors, respectively. In order to maximize the count rates, the detector layers have been placed at different positions in polyethylene cylinders of various diameters and in various configurations. Figure 4-4 shows the results, describing bundle efficiencies as a function of the distance between the bundle center and the detectors in a cylindrical block of polyethylene of 13.54 cm thickness.

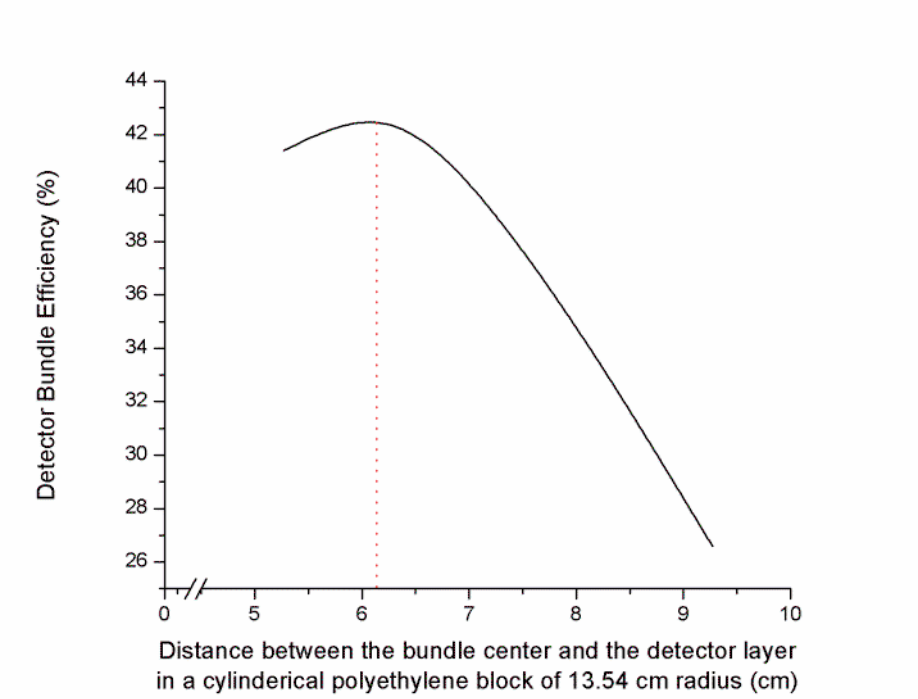

Figure 4-4. The detector bundle efficiencies as a function of layer positions in the cylindrical block of polyethylene of 13.54 cm radius. Efficiency was maximized at 6.17 cm from the center of the bundle.

MCNP calculations have shown that for a one-layer bundle in a 13.54 cm cylinder of polyethylene the ideal detector positions are at about 6.17 cm radius from the center. For a two-layer detector in a polyethylene cylinder of 19.08 cm radius, the ideal detector positions are at about 6.17 cm and 11.81 cm from the center.

To calculate the detector efficiency of the designs above, the pellet size sample was placed at the axial center of the detector bundle. The fission rate distribution, calculated during the previous steps, was used as delayed neutron source distribution inside sample. The results of the simulations for both types of detectors and for one and two layers of tubes (at the optimized distance from the sample) are shown in Table 4-2.

Table 4-2. Absolute efficiency for detector bundles in one and two layer geometries. The ^{3}He detector was about twice as efficiency as the BF_3 in identical geometries.

Tube Type	Pressure, Diameter	Absolute Efficiency
^{3}He, 1 layer	4 atm, 1 inch	42.3%
^{3}He, 2 layers	4 atm, 1 inch	51.7%
BF_3, 1 layer	0.724 atm, 1inch	16.6%
BF_3, 2 layers	0.724 atm, 1inch	21.2%

The absolute efficiency of ^{3}He tube detectors was more than twice as high as that of BF_3 (for identical geometries). The addition of a second layer of tubes increased the overall efficiency of the detector by less than 10 % and 5 % for detectors with ^{3}He tubes and BF_3 tubes, respectively. Based on these results and operational cost-effectiveness, the one single-layer detector design, composed of ^{3}He tubes with a 1 inch diameter, was chosen for the delayed neutron measurements.

Another important factor of this measurement system that it is designed to simultaneously measure delayed neutrons and delayed gamma-rays from the irradiated sample, so the above detector bundle design has to be modified. Instead of a full circle with twelve ^{3}He tubes, a partial circle with seven tubes was used. The remaining space is necessary to accommodate the gamma detector.

A germanium detector (a HPGe) for the delayed gamma-rays was considered due to its high energy resolution. The energy resolution of a detector means the ability of a detector to identify gamma lines which are close together with slightly different energy, and can be defined as the Full Width at Half Maximum (FWHM) of the photo peak at certain energy [Figure 4-5].

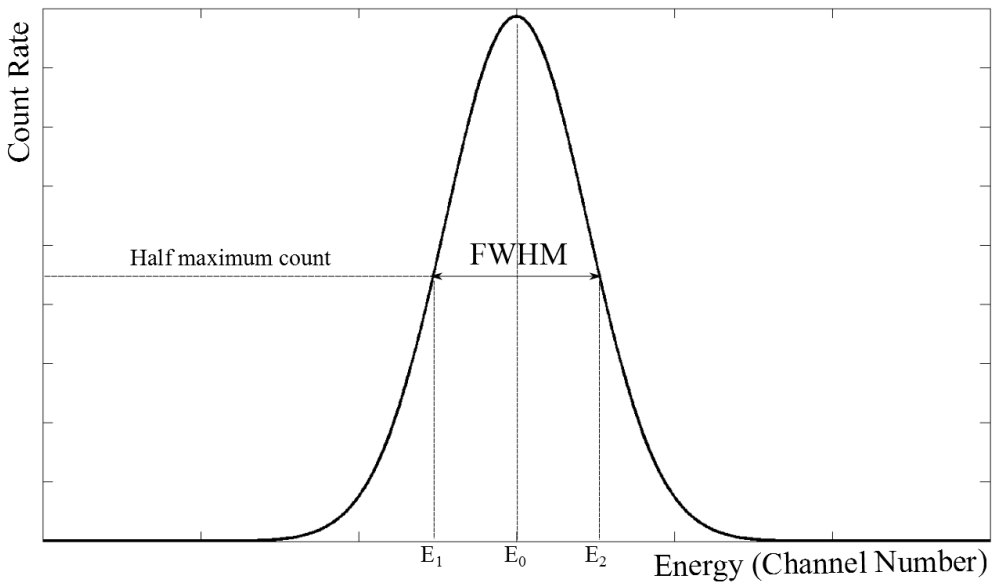

Figure 4-5. Showing the method for determining the Full Width at Half Maximum (FWHM). The detector energy resolution can be calculated by the ratio, FWHM/E_0, and is a standard measure of detector performance.

As shown in Figure 4-5, the FWHM is the difference between E_2 and E_1, the value of energy in the full width at half maximum of the photo peak. The energy value is typically expressed by the number of channels on the gamma-ray spectroscopy program. The energy resolution R_0 is written as the ratio of the full width at half maximum of a given energy peak to the peak height [27]:

$$R_0(E_0) = \frac{\Delta E}{E_0} = \frac{E_2 - E_1}{E_0} = \frac{FWHM}{E_0}. \quad (4\text{-}3)$$

Typically, two types of gamma-ray detectors are commonly used in gamma-ray spectroscopy, a high purity germanium (HPGe) detector and sodium iodide (NaI) detector. A germanium detector generally provides better energy resolution than a NaI detector as shown in Figure 4-6 [30].

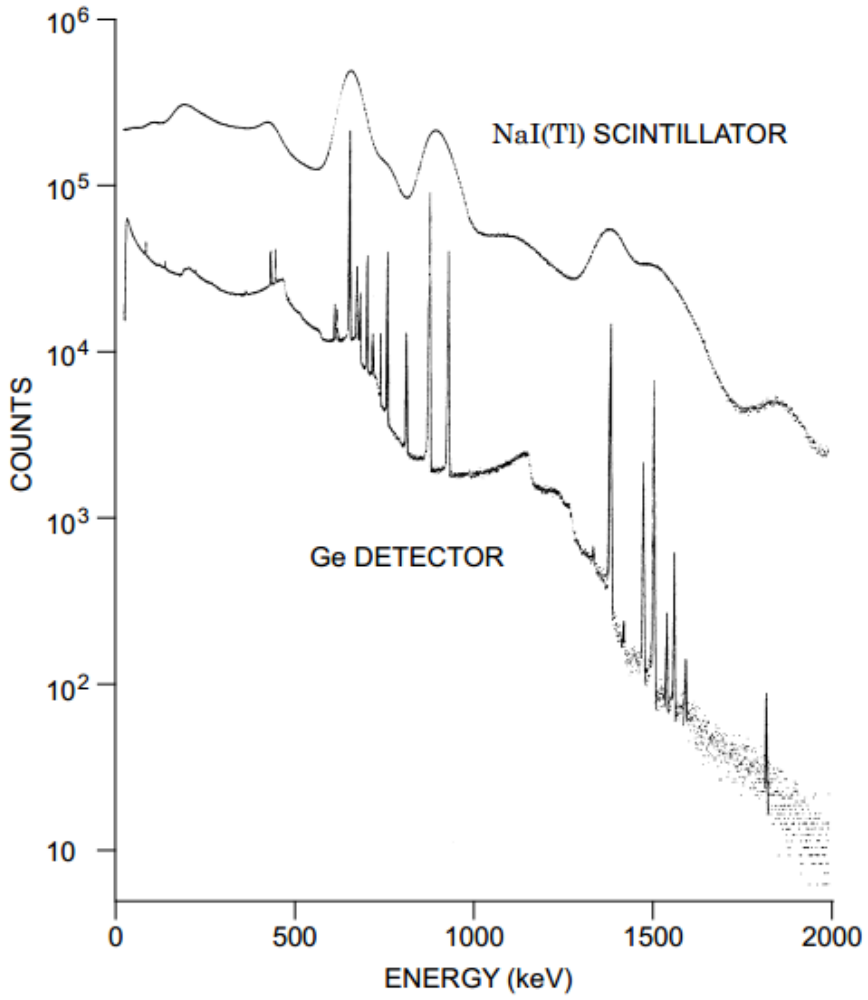

Figure 4-6. An NaI detector has a higher absolute efficiency, and therefore higher count rates, while the Ge(Li) detector offers much better energy resolution.

As mentioned in Chapter 3, the good peak statistics and isolation of the peak in the spectrum are important to obtain better fission rate estimates with low uncertainty from the gamma scanning technique. The obtained fission estimates are directly linked to and used for the improvement of the high uncertainty on delayed neutron data. Therefore, a HPGe detector was employed in the bundle design.

The dimensions of the HPGe detector, used in simulation, are listed in Table 4-3. Cross section views of the detector arrangement are shown in Figure 4-7.

Table 4-3. Dimensions of a HPGe detector, used for MCNP simulation.

Description	Dimension (mm)
Germanium Crystal Diameter	65
Germanium Crystal Length	70
Crystal Center-hole Diameter	9.2
Crystal Center-hole Depth	61.6

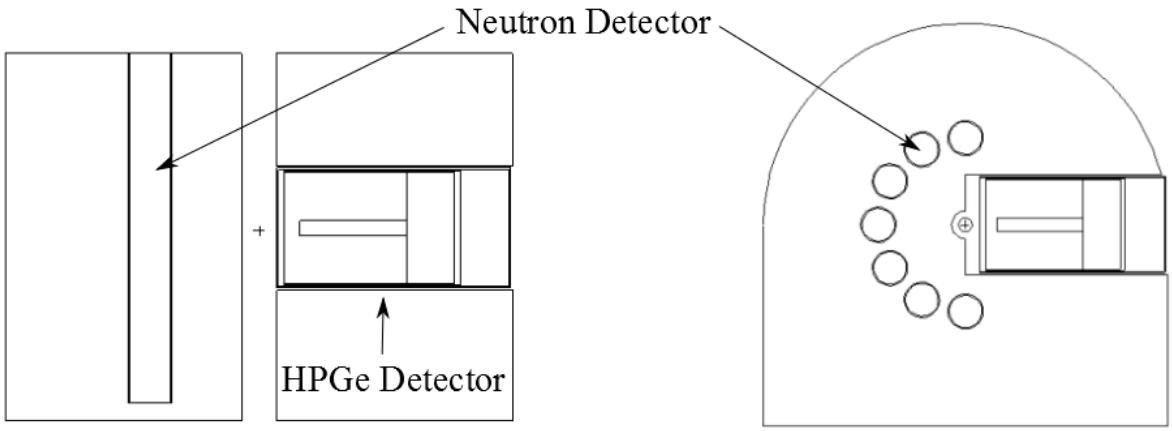

Figure 4-7. The side and cross sectional views (left-XY and right-YZ) of the detector bundle with a HPGe detector.

The altered neutron detection system has a calculated detection efficiency of 23.7%.

Detector Bundle Setup

Based on the above designs and simulated results, the actual detector bundle was built. The bundle is consisted of a HPGe (PopTop 32-TN30642A, ORTEC) gamma detector and seven ^{3}He neutron detector tubes (4atm, LND 252284).

Each neutron tube has the pulse processing electronic modules, built by Precision Data Technology (PDT), attached to its top. The PDT modules are fully featured by their minimized (compact) size, and are composed of two different modules, 10A-MHV and 20A-MHV.

The PDT 10A-MHV contains the pre-amplifier, amplifier, and discriminator in one module. The PDT 20A-MHV has the same electronics as the PDT 10A-MHV but with a high

voltage supplier (HVS). The PDT 20A module generates its own internal high voltage, and this HV can be used to bias each PDT 10A module. The ^{3}He tubes are daisy-chained together by the PDT modules, and work as a single counter [Figure 4-8].

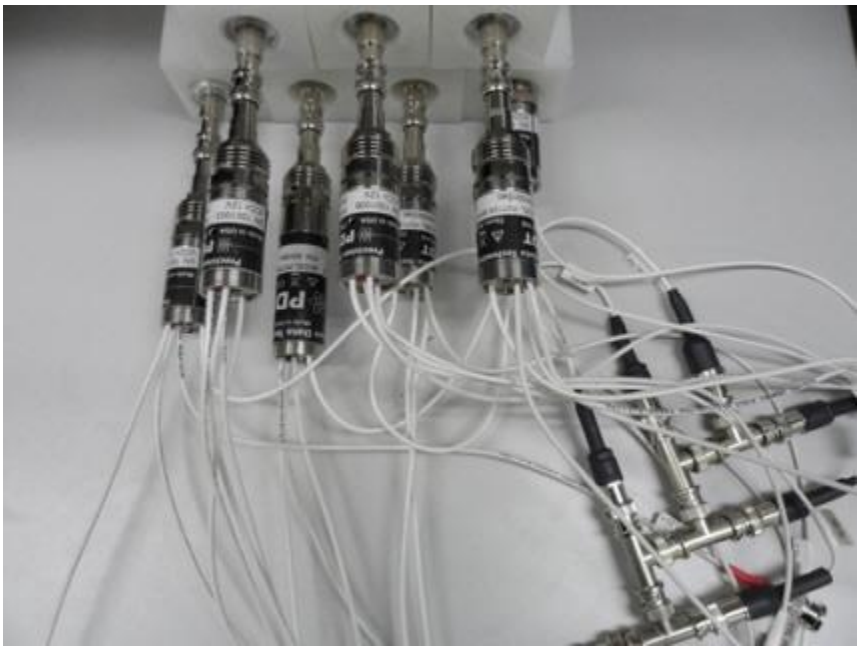

Figure 4-8. The chained ^{3}He neutron detector bundle with electronics, PDT 10A and 20A MHV modules built by Precision Data Technology. These daisy-chained detectors can work as a single counter (Photo: Author, Heejun Chung).

The daisy-chained tubes are connected to nuclear instrumentation modules (NIM) on the measurement workstation in order to count delayed neutrons. The modules consist of a quad counter and timer (Ortec 974), a single channel analyzer (Canberra 2030), and a pulser (Ortec 480) to test modules. A high voltage supply is not required since high voltage can be directly supplied to the PDT 20A module from a DC power supplier (Extech 382200). DC +12 V can generate a proper high voltage (about 1.25 kV) to operate the chained ^{3}He tubes.

The HPGe is connected to a digital spectrum analyzer (DSA 1000, Canberra), and the measured spectra are analyzed by a gamma analysis software (Genie 2000, Canberra). This gamma measurement system was adjusted and calibrated by a certificated Eu-Am source. After

calibration, the gamma line of ^{137}Cs peak at 661.7 keV was determined to be within 3 keV and the FWHM value was about less than 0.85. This measured values met the calibration criteria according to the manual of the gamma analysis software [31].

A new polyethylene block housing was designed to conveniently hold the detectors, since a detector could be placed into any hole. The (n, p) reaction in a ^{3}He neutron detector tube [Equation 4-1] is significantly high for thermal neutrons (5400 barns at 0.025 eV) so polyethylene (moderator) thickness should be modified based on the target neutron energy. The previous design was well made to detect delayed neutrons but suffered from the change in its configuration.

This new design is fundamentally the same with the previous design, but its shape was changed from half cylindrical to box, and twenty six detector holes are placed to easily change neutron detector configuration [Figure 4-9].

Figure 4-9. The cross sectional view of the detector bundle, employing a HPGe gamma-ray detector and seven ^{3}He neutron detector tubes, as shown by the bolded holes.

The detector bundle, when seven detectors are placed at number (No.) 36, 38, 40, 42, 44, 46, and 48 in Figure 4-9, has a calculated efficiency of 15.2 % via MCNP.

A Sample Handler Design and Setup

The design objective of the sample handler is to transfer an irradiated sample from the irradiation position near the neutron source to the measuring position in less than 250 ms in order to maximize the available delayed neutrons for measurement. Additionally, the system must rotate the sample to achieve a homogeneous irradiation. A pneumatic pick-and-pull actuator and a LabView based control system are used. The pick-and-pull actuator consists of a rod attached to a pneumatic piston, which allows for 12 inches of linear motion, combined with a second pneumatic piston, which allows for independent rotation of the linear rod. Hall sensors are attached at both ends of each piston to provide position indication as well as a flow restriction valve on the rotation piston to allow for adjustment of the rotation speed.

Air at 100 psi is used to operate the actuator and is controlled by two dual solenoid operated four-way valves. Each valve controls one of the pistons and allows the air supply to be sent to one side of the piston while venting the other side, which causes the piston to move. The air is supplied via a pressure regulator from a standard air compressor. The four-way valves, as well as the Hall sensors, are connected to a computer using a LabView sixteen channel digital input, digital output card. Additionally, a digital pressure signal is also supplied to the LabView card.

A LabView Virtual instrument (VI) is used to display the piston positions, indicate pressure, and control the four-way valves to operate the system [Figure 4-10]. This VI also has the capability to record accurate timing of the motion of the actuator. The sample handler is shown in Figure 4-11, and Figure 4-12 shows the movement of the pick-and-pull actuator with a sample in the actual experimental system.

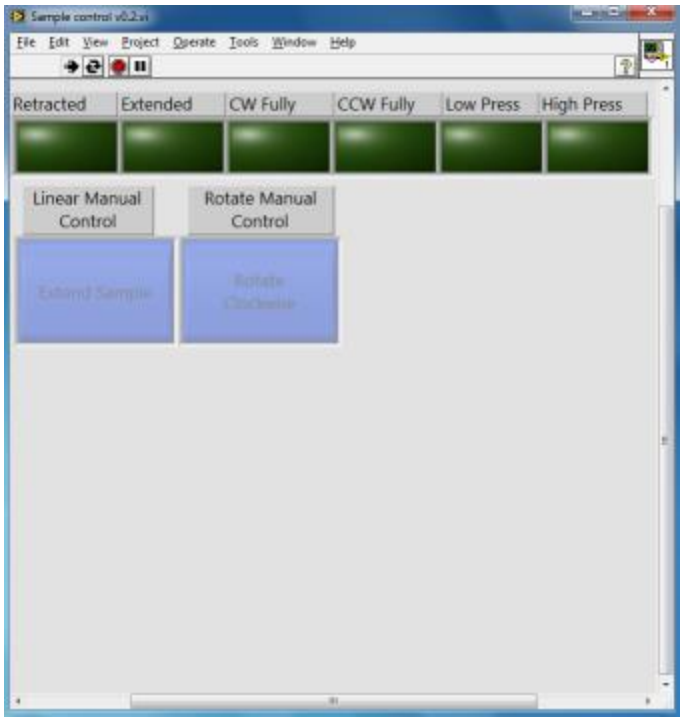

Figure 4-10. The user interface for a pneumatic sample handler, written by a LabView Virtual instrument (VI).

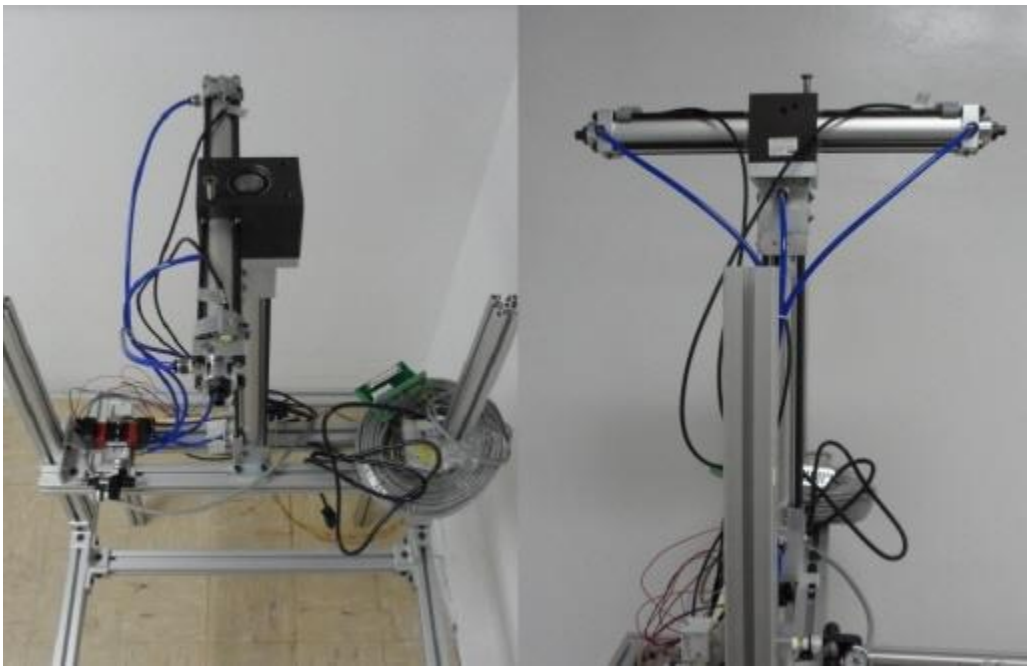

Figure 4-11. Front and side views of the sample handler. This allows the sample to be transferred in less than 250 ms and rotated during irradiation and acquisition times to ensure homogeneity (Photo: Author, Heejun Chung).

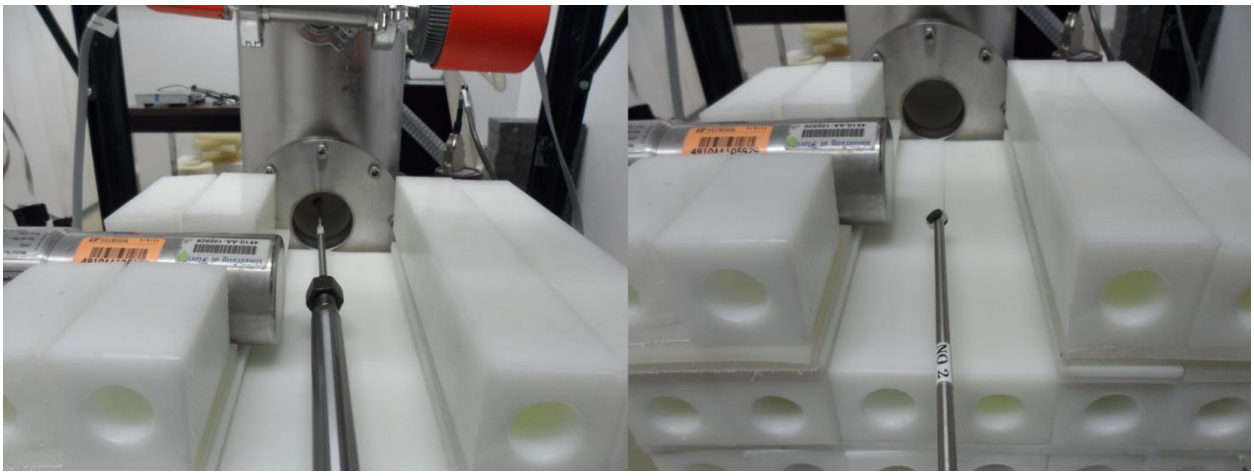

Figure 4-12. The left photo shows the sample inserted into the neutron generator port for irradiation. The right photo shows the sample withdrawn to be counted (Photo: Author, Heejun Chung).

Integral System Design and Setup

An integral design of the experimental system is shown in Figure 4-13, including a D-D neutron generator inside the lead reflector, the pneumatic sample handler, the neutron detector bundle, including a HPGe detector with the Dewar to cool the germanium crystal. The sample handler extends its arm through the lead reflector to the surface of the neutron generator. For the measurement position, the sample handler retreats the arm through the reflector to the center of the detection system. The sample handler is operated by air pressure and is optimized for fast transfer time between irradiation and measurement location, considering shorter-lived delayed neutron groups. Additionally, the sample holder will be able to rotate the sample, which allows a more homogeneous irradiation and detection. The short transfer time is one of the main advantages of doing these experiments with a neutron generator instead of with a nuclear reactor.

In the detector bundle design, seven daisy-chained ^{3}He tubes for the delayed neutrons and a germanium detector (a PopTop HPGe) for the delayed gamma-rays were considered due to its high energy resolution.

Summarizing, the most important features of the detection system being built, are 1) simultaneous measurement for delayed neutrons and gamma-rays, 2) rapid transfer of the sample from the irradiation position to the measurement station, 3) zero or low background unlike in a reactor system, and 4) flexible irradiation time which can easily be controlled.

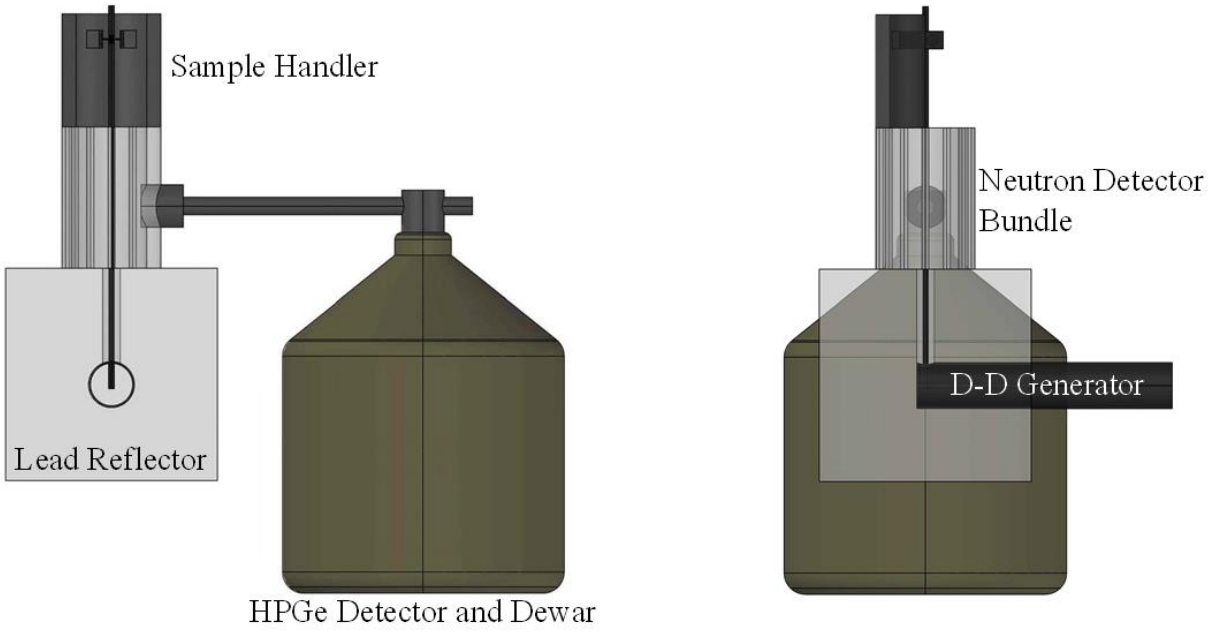

Figure 4-13. Front and side views of the measurement geometry and neutron generator.

CHAPTER 5
NEUTRON GENERATOR DESIGN, CONSTRUCTION, TESTING, AND QUALIFICATION

The new D-D neutron generator, developed in collaboration with Adelphi Technology Inc., is highlighted in this chapter.

This new design allows a sample to be place very close to the emitting neutron target. Previously, a sample was required to be placed at a large distance from the neutron source so the actual flux of fast neutrons to the sample was relatively small. A minimum source-to-sample distance in the new design provides a high flux of fast neutrons to the sample, and the reaction rate in the sample therefore increases.

University of Florida and Adelphi Technology Inc. have received the 2013 R&D 100 award (known as the Oscars of Innovation) for their development of this neutron generator, the model DD-109X.

Neutron Sources

An external neutron source is necessary to induce a nuclear fission reaction. Neutrons can be obtained from nuclear disintegrations or reactions. Neutron sources, widely used, are:

1) Spontaneous fission source

The nuclear binding energy per nucleon decreases as the atomic mass number increases [7]. Some transuranic heavy nuclides are naturally split into two nearly equal mass fragments and emit some fast neutrons. This nuclear process is known as a spontaneous fission reaction and is a type of radioactive decay. The most common spontaneous fission neutron source is ^{252}Cf with a half-life of about 2.65 years.

2) (α, n) reaction source

This type of neutron source is a compound of two different materials, an alpha emitter and a target nuclide. An energetic alpha (α) particle emitted from alpha emitters such as ^{210}Po, ^{226}Ra,

^{239}Pu, or ^{241}Am breaks through the Coulomb barrier of a target nuclide and is absorbed. The Coulomb barrier is the barrier produced by the electrical repulsion, and the energetic alpha (α) particle must overcome this barrier in order to get close enough to the target nucleus in order to undergo an absorption reaction. Since the Coulomb barrier increases with the atomic number, a light element such as ^{7}Li, ^{9}Be, ^{10}B, and ^{19}F is used as a target in order to minimize Coulomb force repulsion between the alpha particle and the target nucleus [32]. The (α, n) reaction in the case of ^{236}Pu and ^{9}Be can be written as:

$$^{9}_{4}Be + \alpha \rightarrow {}^{12}_{6}C + n \qquad E_n = 4.5\ MeV. \tag{5-1}$$

Some available (α, n) reaction sources are also listed in Table 5-1.

Table 5-1. Characteristics of some alpha particle and neutron reaction sources (α, n), including the average energy and half-life.

α emitter	E_α (MeV)	Half-life	Target	E_n (MeV)
^{241}Am	5.4	458 y	Be	4
^{226}Ra	4.5	1620 y	Be	3.6
^{210}Po	5.3	138 d	Be	4.3

3) (γ, n) photoneutron source

Some nuclei emit neutrons when the energy of incident gamma-rays is greater than the binding energy of a neutron in the nuclei. The neutron binding energy is typically higher than 6 MeV. Only two nuclei, ^{9}Be and ^{2}H, are practically available due to their lower binding energy (below 4 MeV):

$$^{9}_{4}Be + \gamma \rightarrow {}^{8}_{4}Be + n \qquad Q = -1.666\ MeV \tag{5-2}$$

$$^{2}_{1}H + \gamma \rightarrow {}^{1}_{1}H + n \qquad Q = -2.226\ MeV. \tag{5-3}$$

These reactions are endothermic (Q value is negative). It means that a photon of at least 1.67 and 2.23 MeV is respectively required to liberate a neutron from beryllium and deuterium

[33]. Through this type of a neutron source, mono-energetic neutrons can be obtained from the selected mono-energetic photons. This is a unique feature of this type of neutron source but some applications are occasionally limited by the presence of high gamma-ray backgrounds.

Some available (γ, n) photoneutron sources are listed in Table 5-2.

Table 5-2. Characteristics of (γ, n) photoneutron sources, including the average energy of each incident and produced particle.

Source	Half-life	E_γ (MeV)	E_n (MeV)
$^{24}Na + {}^{9}Be$	15 h	2.754	0.967
$^{24}Na + {}^{2}H$ (D)	15 h	2.754	0.263
$^{28}Al + {}^{9}Be$	2.24 min	1.779	0.101
$^{38}Cl + {}^{9}Be$	37.3 min	2.168	0.446

The spectrum of bremsstrahlung photons of high energy and intensity from accelerators such as a linear particle accelerator (Linac) can be used as a source to induce the (γ, n) photoneutron nuclear reaction, but this method can not generate mono-energetic neutrons since the energy spectrum of bremsstrahlung photons is continuous.

4) Spallation neutron source

A spallation reaction is a process in which a light projectile such as a proton, neutron, or any light nucleus with high kinetic energy interacts with a heavy nucleus such as a lead (Pb) or tungsten (W). From this process, "*spalled*" neutrons are released from the heavy nucleus [34].

The neutrons produced in spallation reactions can be characterized by their energy, spatial distributions, and multiplicity. The neutron multiplicity is the number of neutrons produced per one beam particle [35]. This technique is advantageous because of higher neutron production rate, but the equipment necessary to accelerate the projectile particle to such high speeds makes this method extremely costly.

5) Nuclear reactor

A nuclear reactor can be considered a continuous neutron source. Neutrons are produced by the fission chain reaction; neutrons are emitted by fissioning nuclei repeatedly inducing fissions in other fissile or fertile materials [4]. A nuclear reactor is mainly based on the fission reaction of ^{235}U to yield two fission fragments and about 2.47 neutrons per fission at 2 MeV kinetic energies. For instance,

$$^{235}_{92}U + n \rightarrow {}^{141}_{56}Ba + {}^{92}_{36}Kr + 2.47\, n \qquad E_n \cong 2\ MeV. \tag{5-4}$$

A nuclear reactor is commonly used, but this source is frequently inappropriate for some medical or research applications which require neutrons of a specific energy or rate without interferences from the distribution of background radiations. In addition, the accessibility to those sources is also always limited by safety issues.

6) Fusion reaction neutron source

There are two important nuclear reactions in which energy is released: fission and fusion reactions. As explained before, nuclear fission is the splitting of a heavy nuclide into two lighter nuclides. On the other hand, a fusion reaction involves two light nuclides fusing into one larger nuclide, and this process also results in the release of neutrons.

Based on the fusion reaction, accelerator-based neutron sources have been developed and widely used for medical and research applications. The operating concept of an accelerator-based neutron source is normally that the charged projectile particles or ions are accelerated by the strong electromagnetic force. The target materials are bombarded by these energetic projectile particles or ions, and nearly mono-energetic neutrons are consequently produced from nuclear reactions.

The widely used accelerator-based source is a fusion-based neutron generator, based on deuterium–deuterium (D-D) or deuterium−tritium (D-T) nuclear reactions. A D-D neutron generator produces fast neutrons of 2.45 MeV and a D-T neutron generator produces 14.1 MeV neutrons [Equation 5-5 and 5-6], but due to the differences in solid angle and applied voltages, it is also possible to see a range of produced neutron energies:

$$D + D \rightarrow n + {}^{3}He \qquad E_n = 2.45\ MeV \tag{5-5}$$

$$D + T \rightarrow n + {}^{4}He \qquad E_n = 14.1\ MeV. \tag{5-6}$$

A neutron generator is usually required for active NDA techniques. The NDA technique was initially developed to investigate nuclear fuel materials without any perturbations in their physical or chemical states. It was started from the proposition that the physical properties of the emitted radiation by spontaneous or nuclear reactions are unique to the isotope(s) of interest, and the radiation intensity can be related to the mass and content of the fissile isotopes.

The NDA techniques are characterized as passive or active interrogation methods. The passive interrogation method measures radiation from the spontaneous decay process of the nuclear material, and the active interrogation method measures radiation induced by an external source [36].

The current NDA techniques, deriving their signals predominantly from the induced fission from Uranium (U) and Plutonium (Pu) isotopes, were reviewed by S. J. Tobin et al., and are listed in Table 5-3 [37].

Table 5-3. Current NDA techniques, organized by active and passive interrogation methods. Active interrogation requires the sample irradiation by an external neutron source.

Type	Technique	Description
Active	Californium Interrogation with Prompt Neutron (CIPN)	A relatively low-cost and light-weight instrument. Fission chambers for neutron measurement are combined with an active interrogation source (^{252}Cf)
	Delayed Gamma (DG)	Measuring delayed gamma-rays emitted from the decay process of fission products. Preliminary data on the delayed gamma decay
	Delayed Neutron (DG)	Same as DG, except for delayed neutrons
	Differential Die-Away (DDA)	Measuring the induced fast fission neutrons between generator pulses. The number of detected neutrons between pulses is proportional to the mass of fissile material.
Passive	Passive Neutron Albedo Reactivity (PNAR)	Measurement of time correlated neutrons from a spent fuel assembly with/without a Cadmium (Cd) layer surrounding the nuclear fuel assembly

To draw better conclusions from the active NDA technique, an important factor to consider is the neutron yield since it is directly related to the induced fission rate. Typically, a D-T generator has higher yields than a D-D generator, roughly twice as high since the fusion cross section of a D-T reaction is larger than a D-D reaction [38]. The cross sections for the primary fusion reactions are shown in Figure 5-1 [8].

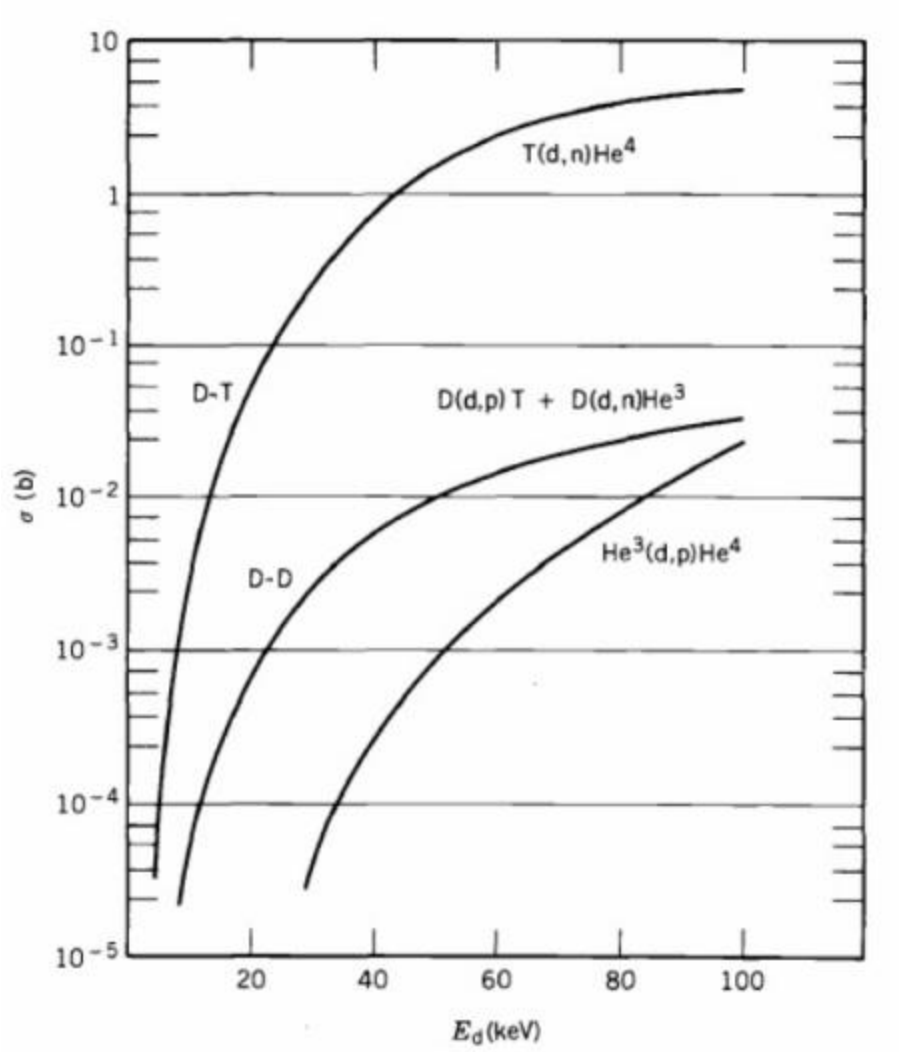

Figure 5-1. The cross sections for the primary fusion reactions, showing that a D-T reaction has the highest cross section, and therefore provides the higher neutron production yield.

For a better fission estimation, a D-T neutron generator would be chosen due to its higher fusion cross section. However, tritium gas is radioactive so its possession or use is always limited by safety and nuclear regulatory concerns.

Neutron Generator Design

In the early stages of the project, a new experimental design and method for improved delayed neutron data, a Kaman A-711 D-T generator was considered as a neutron source. The Kaman A-711 generator is a miniature sealed-tube type accelerator that produces 14.1 MeV

neutrons from the collision of a mixed beam of deuterium and tritium ions with a deuterium-tritium loaded target. It had a maximum intensity of $0.5x10^{11}$ neutrons per second and the capability of rapid startup and shutdown for non-repetitive pulses below 1 sec duration [39].

The generator intensity and capability of a pulsed and continuous working (CW) operation mode made it to be a suitable neutron source for this study. However, the generator tube in the head was no longer viable, the cooling unit needed to be replaced, and the power supply tank no longer met the current American Society of Mechanical Engineers (ASME) regulatory requirements.

In addition, fast neutrons of 14.1 MeV emitted from a D-T generator have to be thermalized for this study since 14.1 MeV neutrons were classified as high energy in the eight-group model. As mentioned in Chapter 2, Spriggs and Campbell used three neutron energies: thermal, fast, and high [1]. For the fast neutron experiments with the Kaman A-711 D-T generator, a moderator is supposed to be designed and installed around the generator head but due to the previous experimental setups, there was not enough space to do so.

Considering the high cost of refurbishment and inconvenience in redesigning other experimental devices for delayed gamma-ray and neutron measurements from fast fission, a new D-D generator was designed and developed with Adelphi Technology Inc.

The generator design concepts focused on 1) high neutron intensity, 2) minimized distance from the source to a fissile sample, 3) operation in both pulsed and continuous working (CW) modes, 4) compactness of the whole system, and 5) easy access to the source.

The signal strength of the delayed neutrons from the two longest-lived groups highly depends on the fission density (the number of fission events per sec) in a fissile sample since other parameters in Equation 3-13 are almost fixed (constant).

Based on the delayed neutron group abundance in the eight-group model, the required generator intensity was calculated [Figure 5-2].

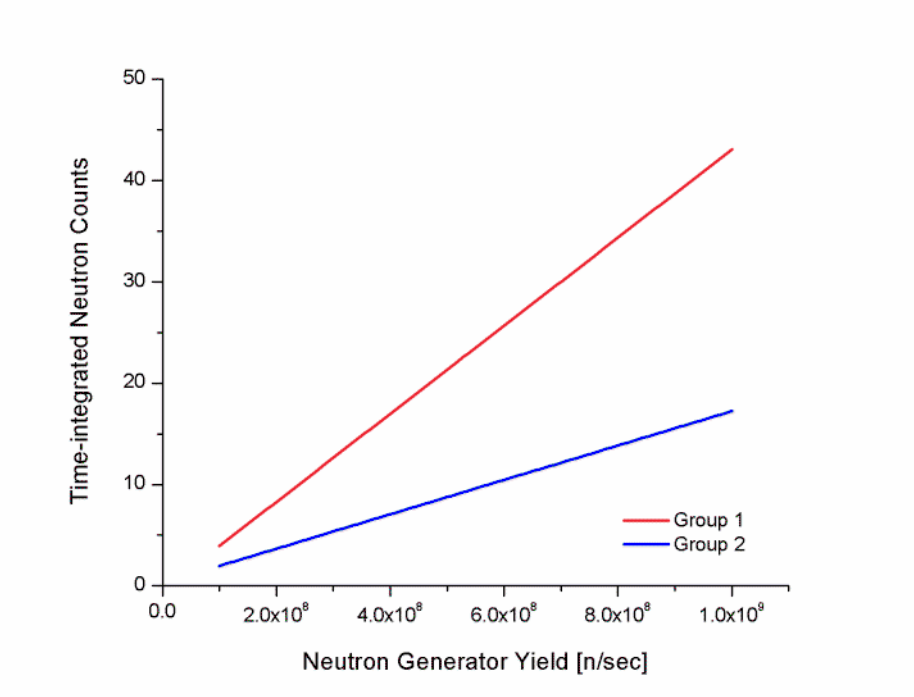

Figure 5-2. Time-integrated neutron counts for the two longest-lived groups of ^{238}U, which was used to determine the minimum required neutron production yield from a D-D neutron generator.

The initial time setups for irradiation, cooling, and acquisition were each 180 sec. The sample was placed next to a generator, and the detector efficiency was assumed to be 20%. According to Figure 5-2, the minimum required neutron yield must be higher than 2.0×10^8 neutrons per sec.

Obviously, the accuracy of delayed neutron parameters increases with higher neutron flux intensity from a generator, so a neutron production yield of 4.0×10^9 neutrons per sec was initially planned. This initial goal was higher than any other current commercial products that use a D-D fusion reaction.

Another way to increase the fission rate is to minimize the distance from the source to a sample. Typically, a sample had to be placed relatively far away from the generator, and the

actual neutron flux incident on the sample was small. In order to utilize the high intensity of a generator, a generator head was designed to be able to inject a sample close to the source.

The purpose of this study is to design experiments to improve delayed neutron group yields and abundances. It is not limited to only the longest-lived delayed neutron group. The other group parameters will be analyzed based on the same experimental system. Thus, a generator should be operated in pulsed and CW modes since the saturation time of other shorter-lived groups is small.

The compact design of a generator is highly sought after by many medical and nuclear applications due to its relative portability and convenience. The compact design refers to not only the generator itself but also all the associated electronic equipment. Since the size of the Kaman A-711 D-T generator was a problem, it was important to try and minimize the whole system while maintaining a higher neutron yield.

The final consideration in the design was easy access to a source. The generator head is typically sealed so it is difficult to maintain and repair. Adelphi Technology Inc. developed the open vaccum system, allowing disassembly for maintenance or re-configuration of the system without being returned to the company. The generator head uses a serviceable stainless steel housing with conflate copper-gasket seals that can be easily removed, permitting most of the components in the generator head to be easily maintained and replaced.

The initial design of the generator head, describing the neutron production, was shown in Figure 5-3.

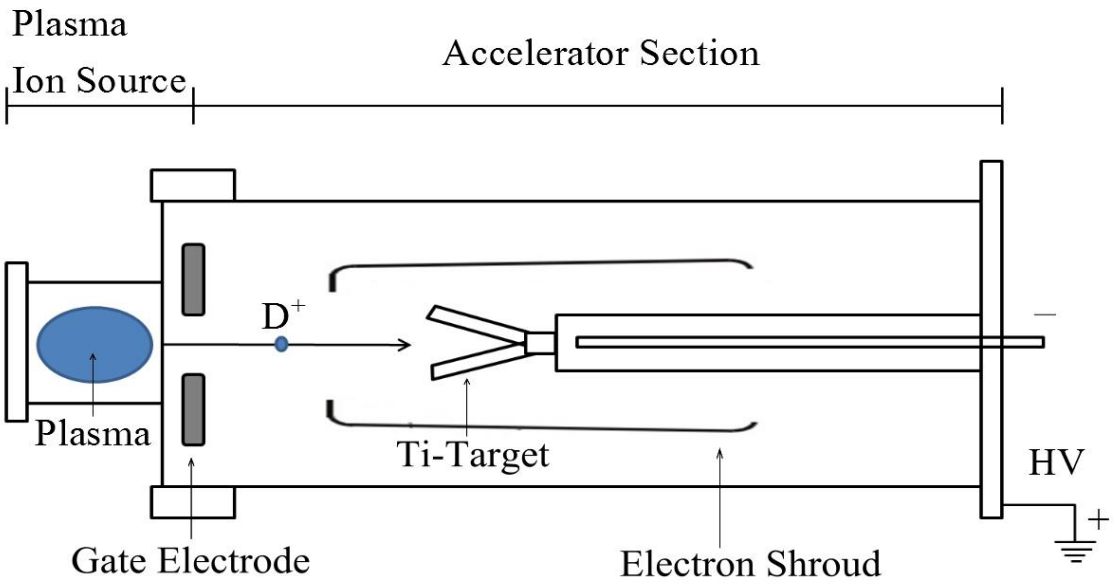

Figure 5-3. The initial design of the generator head and simple working process of neutron production. Deuterium ions are accelerated into the negatively-biased titanium target, these ions are captured by the target, and then react with the next incoming deuterium ions.

The basic process of neutron production is that the plasma ion source supplies deuterium ions which are accelerated across a high electric potential to a negatively-biased titanium target. The energized ions hit the titanium target and are captured by the target lattice, and the next incoming deuterium ions collide (react) with the captured ions, resulting in a D-D fusion reaction.

D-D Neutron Generator Construction and Testing

Based on the design concepts, the D-D generator (DD-109X) has been built and tested with Adelphi Technology Inc. It was designed to achieve the maximum output of 4.0×10^9 neutrons per sec, using up to 30 mA of beam current and 125 kV of acceleration voltage. The final design was almost the same as the initial design [Figure 5-3] but two sample ports were designed into the housing of the generator to allow multiple sample experiments at the same time and a minimum distance from the source to a sample [Figure 5-4].

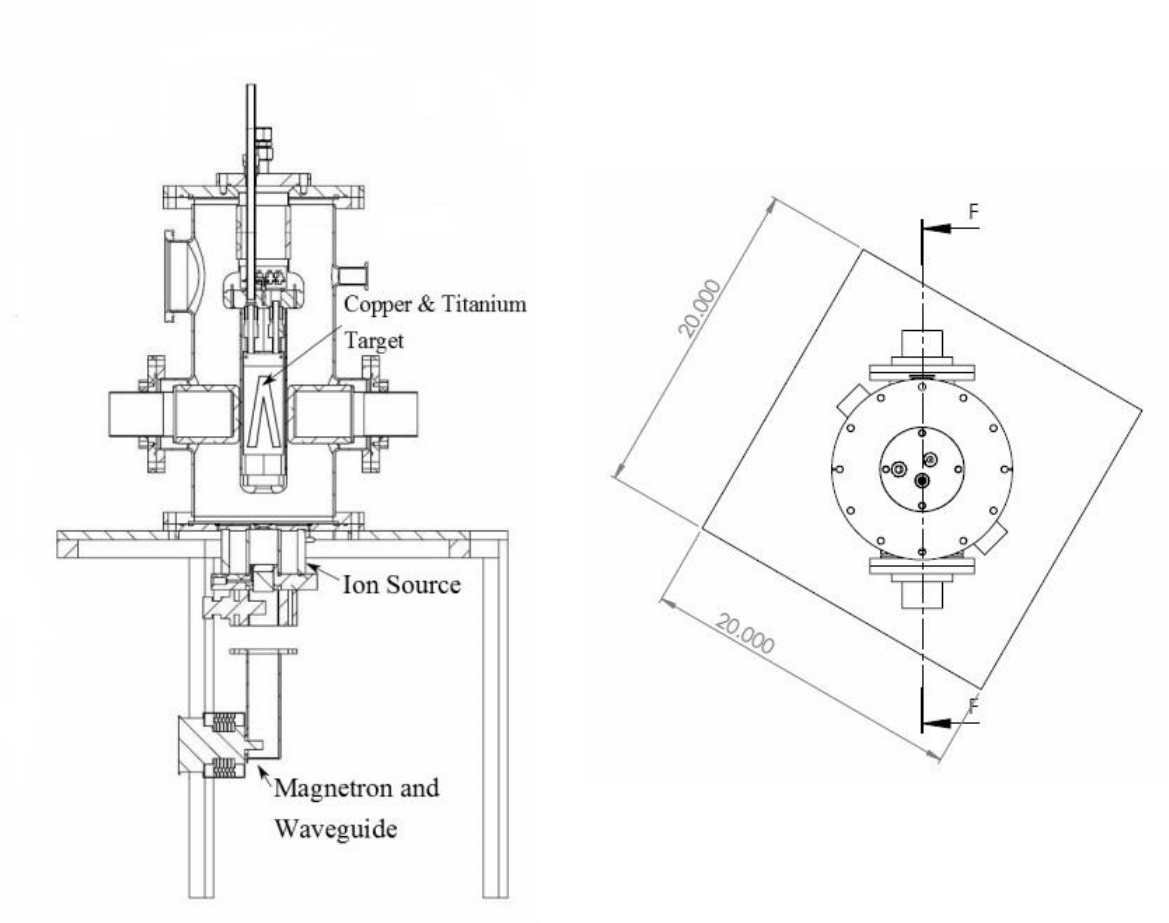

Figure 5-4. The cross sectional view of the DD 109X neutron generator. This generator is featured by its sample irradiation holes since the sample can be close to the neutron source.

The full neutron generator system consists of three main parts: the generator body, a cooling unit, and a power rack. The entire system is controlled by a computer program.

1) Generator body

The generator body is composed of a generator head, a microwave-driven plasma source, a deuterium gas supply, a turbo-molecular high vacuum pump which was designed to reach up to $1.0x10^{-6}$ mbar, and a pre-vacuum pump.

2) Cooling unit

The generator produces nearly 4 kW of heat during operation so sufficient fluorinert, an electrically insulating and ideal for use in many single phase heat transfer applications, is

required. Fluorinert liquid (3M FC-3283) was used and its level is continuously monitored by a personal protection system (PPS) since over time the fluid can evaporate.

3) Power rack

The power rack consists of a high voltage power supply running up to 125 kV (maximum), and the main control panel to control all the subsystems of the generator body. The high voltage power supply can be separated into two parts, Glassman PK and EK series. The PK and EK series respectively control high voltage and current on the generator head and a microwave-driven plasma source.

The actual experimental system, employing the generator system, detector bundle, and sample handler, was built and is shown in Figure 5-5.

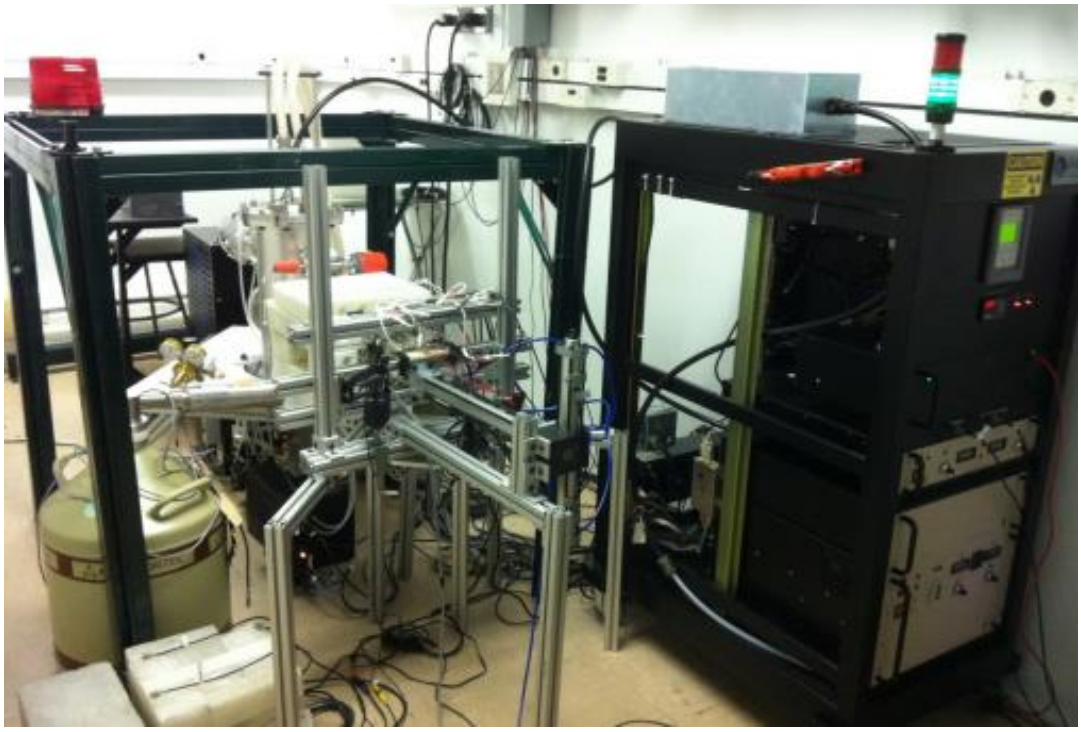

Figure 5-5. The actual whole experimental system, employing the D-D generator, the simultaneous measurement system, and the sample handler (Photo: Author, Heejun Chung).

To ensure human safety from the 2.45 MeV fast neutrons that are generated, the generator becomes disabled when any interlock switches are open. These safety features are controlled by the PPS. The PPS consists of three built-in interlock systems to prevent failures from a fluorinert cooler, a magnetron, and a high voltage supplier bin. Additionally, three highly visible multi-tiered warning devices were installed, along with an emergency kill switch to immediately de-energize the entire system by personnel in the room.

The generator was placed in a secured room, surrounded by 2 foot concrete walls. High density polyethylene blocks, 2.5 inches thick and 60 inches long, were attached to the inner wall. This secured room is called the generator room in following chapters.

Two warning devices with sound are placed in the generator room for radiation workers, and one warning light, in conjunction with an electromagnetic door lock, was installed in the hall way for the public. These warning devices are controlled by the PPS and a controller.

The main control room is located next to the generator room. This room was designed to monitor the generator room in real time and to control the entire experimental setup, the DD-109X neutron generator, the sample handler, and the detector bundle.

To operate the generator, the user interface of the DD-109X was written to control high voltage and current limit on the accelerator and on the magnetron in kV and mA, generator running time in sec, and deuterium gas flow rate in sccm (standard cubic centimeters per minute). The user interface is shown in Figure 5-6.

Figure 5-6. The user interface to control voltage, current, time, and gas flow rate of the neutron generator.

The control room is monitored by two Bonner ball detectors (Model No. 12-4 count ratemeter, LUDLUM). The measured radiation dose in the room was 1 mrem/hr, and below 0.6 mrem/hr around all other side walls. Detailed information of the measured radiation dose is available in Appendix B. To ensure safety and also to check operating conditions in the generator room, four digital high resolution cameras were employed for monitoring and recording. The installed entire control system is shown in Figure 5-7.

Figure 5-7. The whole control system. Monitor in upper-left controls the sample handler, the monitor in upper-right is employed for monitoring and recording the neutron generator, the monitor in lower-left controls the HPGe, and the monitor in lower-right controls the neutron generator (Photo: Author, Heejun Chung).

The above safety features and measured values meet regulatory requirements given in the Code of Federal Regulation Title 10 Part 20 (10CFR20) and part IV of Florida Administrative Code. The state registration (license) number is JR 22505000.

To consistently produce neutrons in the system, the delivered deuterium gas is ionized when appropriate gas pressure and microwave coupling are achieved in the microwave-driven plasma source. The microwave-driven plasma source can consistently deliver deuterium ions and also does not produce metallization inside the vacuum envelope.

When inappropriate microwave coupling is resulted, the metal in the ion source can be sputtered by the energized ions. The sputtered metal is then deposited on the inner surface of the plasma ion source wall. If this sputtering phenomenon occurs continuously for some time, it

results in a fully metalized inner surface of the plasma ion source [40]. This phenomenon is known as the metallization, and it finally leads to tube (system) failure.

The microwave-driven plasma source consists of a magnetron (LG 2M213 Series, 2.54 GHz), the mass flow controller to supply appropriate gas pressure, and related electronics. The employed magnetron and electronics in the mounting box are shown in Figure 5-8.

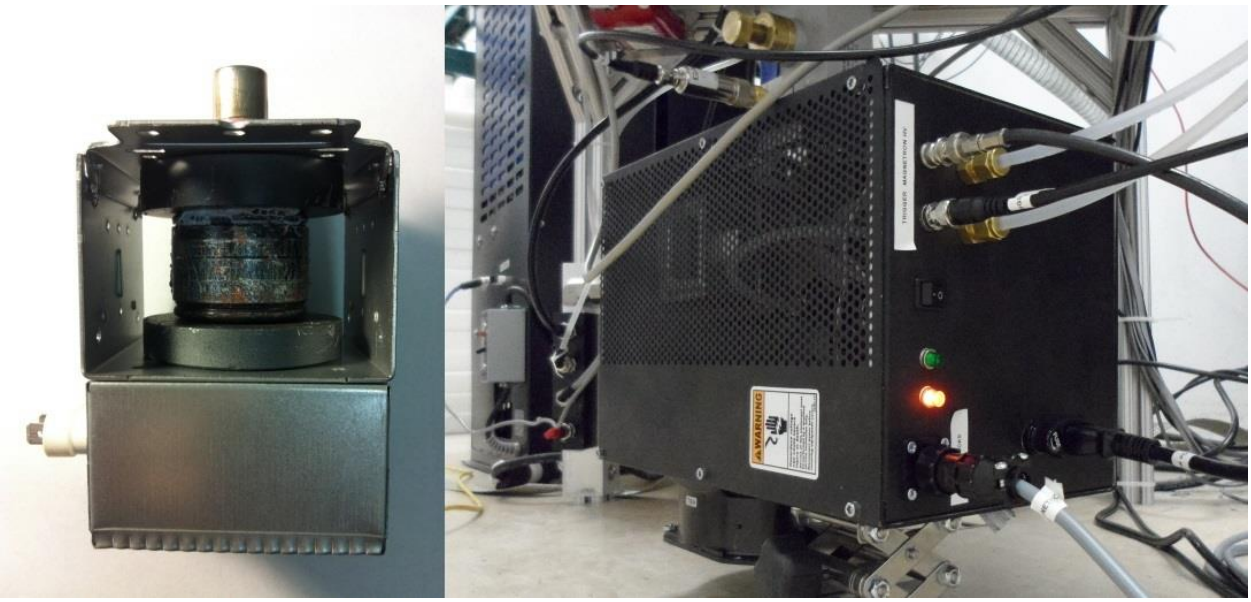

Figure 5-8. The magnetron and electronics in the mounting box, employed for the DD-109X neutron generator (Photo: Author, Heejun Chung).

The deuterium ions are extracted from the plasma, energized to about 100-125 kV, and accelerated toward a titanium target by the high voltage supply. The energized deuterium ions hit the titanium target and are captured by the target lattice, and the next incoming ions collide (react) with the captured ions. Since the ratio between the captured and incoming ions is not balanced, the neutron generation yield is unstable in early stages. However, after some time (about 50-60 min), the amount of the captured and reacted deuterium ions on the titanium layers are in equilibrium. The neutron generation yield from the D-D generator becomes stable with 5-10 % variation, and reached the designed neutron yield in early testing.

D-D Neutron Generator Qualification

Accurate calculation of the neutron generation yield from the D-D generator is most important since the number of counted delayed neutrons and gamma-rays is increased only by the high incoming flux or the sample properties, such as the amount or composition of fission material. To evaluate neutron yield from the generator, Adelphi Technology Inc. performed the activation foil technique with other electronic neutron gauges. They then found response functions from neutron yield to dose rates on a bonner ball neutron detector, and built a neutron yield equation:

$$Neutron\ Yield\ [neutrons/sec] = \frac{mRem}{120} \times r^2 \times 10^8, \quad (5\text{-}7)$$

where *mRem* is the dose rate from a Bonner ball neutron detector, and *r* is the distance from the generator to the bonner ball neutron detector.

However, the calculated yield via Equation 5-7 was mismatched to count rates of delayed neutrons and gamma-rays. Lower number of delayed neutrons and gamma-rays were measured than expected count rates, academically calculated. Thus, one ^{3}He detector which is embedded in a block of polyethylene was placed 1.65 m away from the generator in order to monitor the yield in real time. The neutron yield then can be calculated via:

$$Neutron\ Yield = \frac{Number\ of\ Counts}{(Absorption\ Rate \times Detector\ Volume)}. \quad (5\text{-}8)$$

The absorption rate was calculated via MCNP [Figure 5-9] and the whole detector volume is known. The correlation between the neutron yield and number of counts is shown in Figure 5-10.

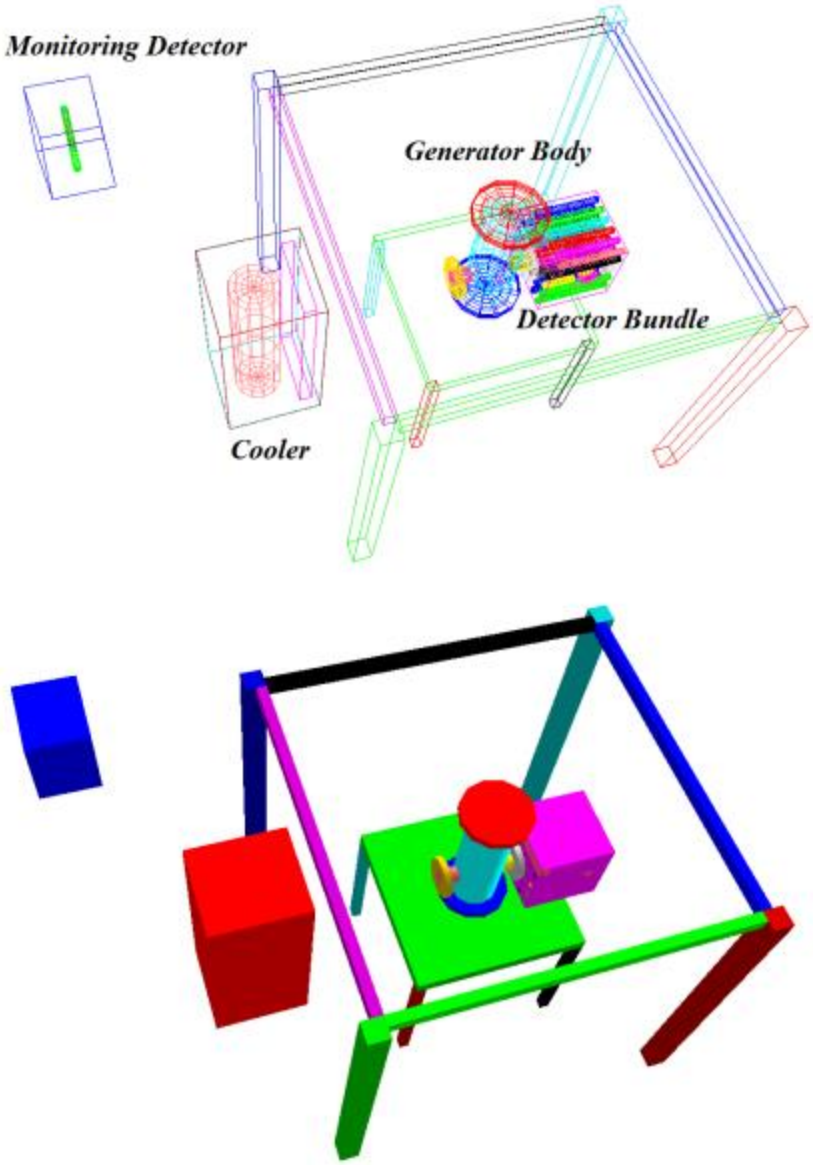

Figure 5-9. The simulation geometry of the actual experimental system, drawn by Moritz Geometry Tool [41]. The monitoring detector is used to measure the real-time neutron production yield from the neutron generator, and the detector bundle is used to count delayed neutrons from the sample after irradiation.

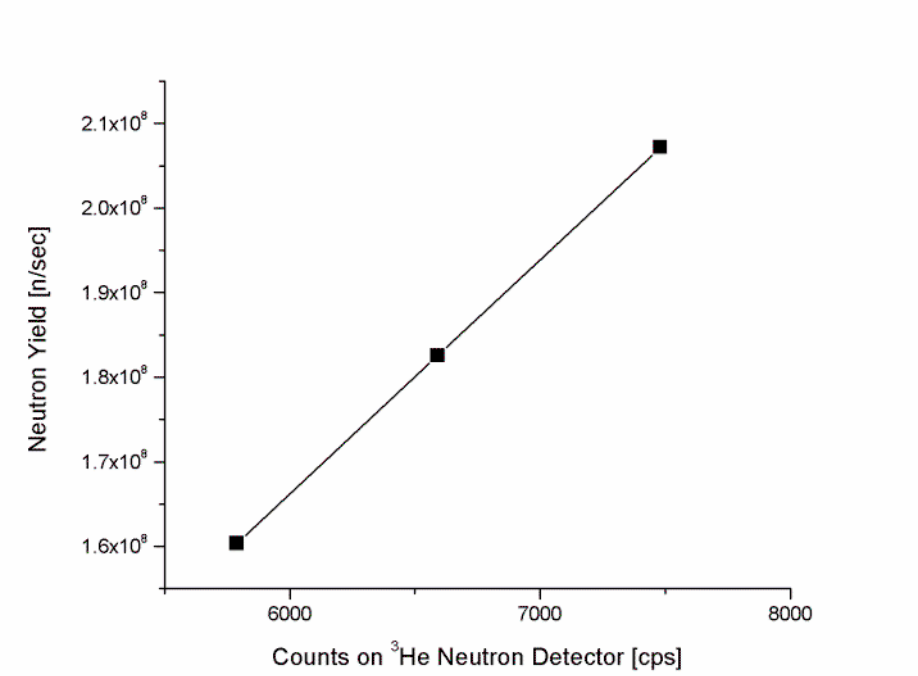

Figure 5-10. The correlation between neutron yield from the D-D generator and number of counts on a ^{3}He monitoring detector (linear fitting).

The neutron yield from the D-D generator gradually increases and becomes stable over time since the high voltage supply and metallic parts are unstably biased from 100 kV to 125 kV in the beginning. The imbalanced amount of captured and reacted deuterium ions on the titanium layers also causes the lower neutron yield at the beginning.

Additionally, the unstably biased parts lead many number of arcing. The rate of arcing in the initial stage is high, and it usually occurs between two ceramic jars and a metal body, or the ceramic part of the high voltage supplier. Melted or scratched parts can also produce arcing in the system since they can create shape points in the high voltage regions. To reduce these high rates of arcing, the system should be conditioned using high voltage and lower current limits, such as 70 kV and 0.05 mA. The applied voltage should then be gradually increased up to the designed experimental levels. The current limit should decrease as voltage increases.

Huge amounts of sparking can damage some parts of the system, so the parts suspected to cause the arcing were inspected after running the generator for about 100 hours. As expected, evidences of arcing were found in these locations, including the ceramic jar and metal body [Figure 5-11 to 5-13]. The scratched and fuliginous parts were cleaned and polished.

Figure 5-11. The scratched target head of the DD-109X neutron generator as a result of arcing inside the neutron generator (Photo: Author, Heejun Chung).

Figure 5-12. The scratched and fuliginous metal body and ceramic jar (Photo: Author, Heejun Chung).

Figure 5-13. The scratched metal body which was placed next to the ceramic jar (Photo: Author, Heejun Chung).

CHAPTER 6
SAMPLE FABRICATION AND COMPOSITION ANALYSIS

Different research approaches can lead to different definitions of a well-defined sample. People who focus on material properties may be interested in microstructure in terms of grain size, porosity distribution, or stoichiometry of a sample. However, for research based on NDA analysis like this study, a well-defined sample means that the density and material composition (mass ratio) of fissile elements in the sample are clearly defined.

Many methods to analyze the isotopic composition of an uranium sample, composed of ^{234}U, ^{235}U, and ^{238}U have been developed and reviewed. From the early 1950's, the mass-spectrometry [42], alpha-spectrometry [43], gamma-spectrometry [44, 45], and photographic spectral [46] techniques have been developed and used for measuring the mass ratios, also known as the signature isotopic ratio, for each type of uranium sample.

Some advanced techniques have been developed by combining earlier methods such as the chromatographic separation technique [47], which is derived from the mass-spectrometric and thermal-ionization mass-spectrometry techniques, as well as mass-spectrometry with ionization in inductively coupled plasma (ICP-MS) techniques [48].

As mentioned, many techniques are currently available, but gamma-spectrometry was chosen for this research since it has been well-validated for so long.

Sample Fabrication

The pelletized samples of depleted uranium dioxide (UO_2) were fabricated by the conventional powder process method (conventional method) [49] and the spark plasma sintering method (SPS) [50]. An example of samples fabricated by each of these methods is in Figure 6-1, and their microstructure pictures are also shown in Figure 6-2, on a scale of hundreds of microns.

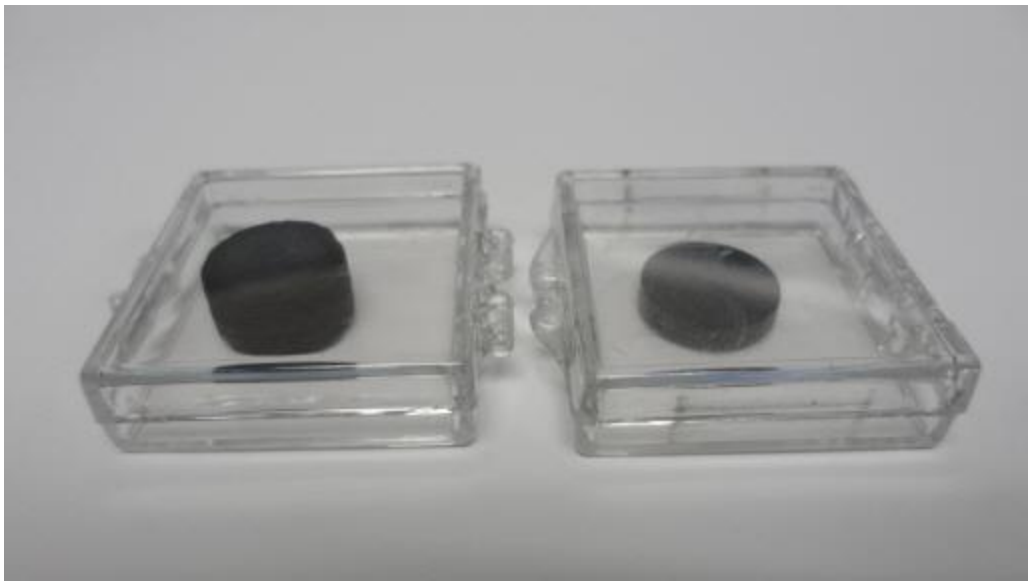

Figure 6-1. UO_2 samples fabricated by the conventional method (left) and the spark plasma sintering method (right) (Photo: Author, Heejun Chung).

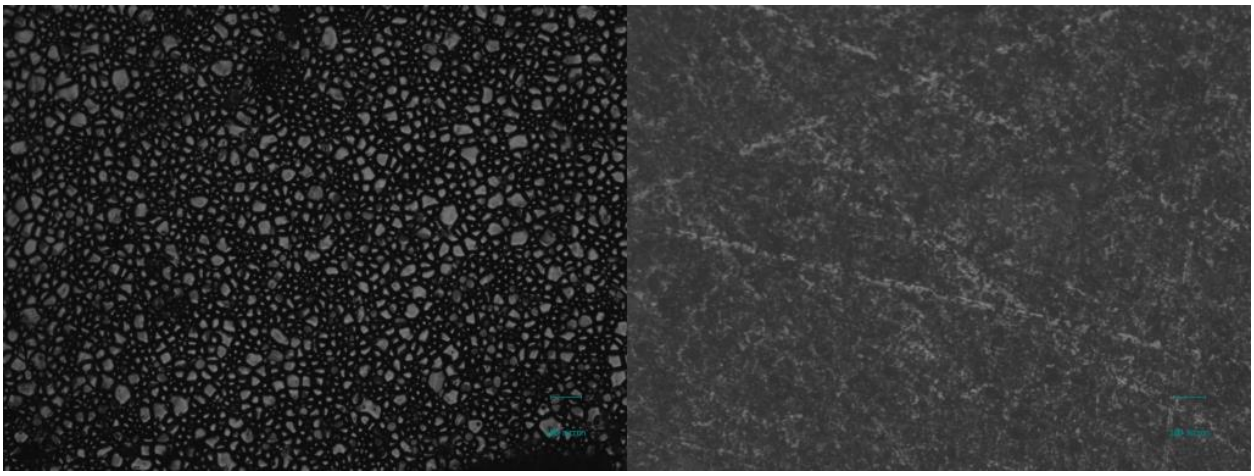

Figure 6-2. Microstructure of UO_2 sample fabricated by the conventional method (left) and the spark plasma sintering method (right).

The conventional powder process method is widely used in nuclear reactors. In the conventional method, UO_2 powder was pressed into green body pellets after milling and then sintered at 1600°C in an aluminum tube furnace for 5 hours with a high purity argon and hydrogen gas atmosphere. The gas flow rate was 2 liter/min during the sintering process. The total duration of this work is about 12 hours.

SPS is a newly developed sintering process, using a microscopic electric discharge between the particles under high pressure. The SPS fabrication process is very similar to the conventional method, but has a much shorter sintering time typically lasting only a few minutes. Using the SPS system, UO_2 powder was sintered at 1600°C for only 5 min.

In principle, the pellet sintered by the SPS process shows small grain size, reduced chemical formation, higher density, and enhanced interfacial contact compared to the pellet fabricated by the conventional powder process [51].

By employing both the conventional method and SPS processes, four UO_2 pellets were finally fabricated. Each pellet density was measured by the Archimedean Immersion Method:

$$Density = \frac{M_{P/air} \cdot \rho_{water}}{M_{P/air} - M_{P/water}}, \quad (6\text{-}1)$$

where $M_{P/air}$ is the mass of a pellet in air, $M_{P/water}$ is the mass in water, and ρ_{water} is density of water (10.242 g/cm^3). The measured pellet properties are shown in Table 6-1.

Table 6-1. UO_2 pellet fabrication methods and properties of the four UO_2 pellets fabricated and used in this study.

No.	Fabrication	Height [cm]	Diameter [cm]	Density [g/cm^3]
1	SPS	0.654	1.224	10.24
2	Conventional	0.888	1.088	9.698
3	Conventional	0.906	0.998	10.74
4	SPS	0.627	1.242	10.48

For this research improving delayed neutron group abundance data for each isotope, determining the isotopic composition of a fabricated UO_2 sample is important in order to know the fission rates from each isotope, indicated by the term f_i in Equation 3-14.

The passive nondestructive analysis (PANDA) for gamma-rays is widely used to determine the uranium isotopic composition ratio ($^{235}U/^{238}U$). The PANDA for gamma-rays is sub-

classified into total photon counting, spectroscopy, and imaging methods [36]. The passive gamma-ray signatures from ^{235}U and ^{238}U are listed in Table 6-2.

Table 6-2. The passive gamma-ray signatures from ^{235}U and ^{238}U.

Isotope	Gamma-ray Energy [keV]	Intensity [%]
^{235}U	143.8	10.95
	185.7	57.10
^{238}U	766.4	0.319
In equilibrium with ^{234m}Pa	1001.0	0.835

The gamma-ray spectroscopy method was employed to determine the isotopic ratio of the fabricated UO_2 samples.

Gamma-ray Spectroscopy Method

The gamma-ray spectroscopy method using a HPGe detector (GEM 30185-P, EG&G ORTEC) in a lead shield was used for the analysis of the activity ratio of ^{235}U and ^{238}U in the fabricated samples. The target gamma lines are 185.7 keV for ^{235}U and 1001.0 keV for ^{234m}Pa, a daughter nuclide of ^{238}U.

The number of counts (C) can be converted to the activity values by:

$$A = \frac{C}{BR \cdot \varepsilon \cdot t}, \tag{6-2}$$

where BR is the branching ratio or the gamma-ray emission rate (intensity), ε is the detector efficiency, and t is counting time (24 hours for this analysis).

From the calculated activity ratio, the enrichment values of the pellets were decided. The enrichment value can be calculated by [44]:

$$Log(wt\%\ 235U) = 1.065 - 0.7317 \cdot \log\left(\frac{A_{U8}}{A_{U5}}\right) - 0.129 \cdot \log\left(\frac{A_{U8}}{A_{U5}}\right), \tag{6-3}$$

where A_{U8} is activity of ^{238}U and A_{U5} is activity of ^{235}U in Bq.

The Equation 6-3 can be rewritten in terms of the count rate:

$$Log(wt\%\ 235U) = 1.065 - 0.7317 \cdot \log\left(\frac{CR_{U8} \cdot 0.572}{CR_{U5} \cdot 0.00837}\right) - 0.129 \cdot \log\left(\frac{CR_{U8} \cdot 0.572}{CR_{U5} \cdot 0.00837}\right). \quad (6\text{-}4)$$

With the same conditions for both measurements, the detector efficiency term ε and the counting time term t are canceled in Equation 6-4.

^{238}U can be precisely estimated by the photopeak at 1001.0 keV since there are no overlapped photopeaks at that energy range, within 3σ. However, the photopeak at 185.7 keV for ^{235}U suffers from interference from the 186.1 keV gamma line of ^{226}Ra, and this interference must be considered before conducting further analysis. According to Ebaid in 2009, the interference between 185.7 keV (57.1%) from ^{235}U and 186.1 keV (3.5%) from ^{226}Ra can be removed by a simple equation [45]:

$$CR_{U5} = 0.417 \cdot CR_T, \quad (6\text{-}5)$$

where CR_T is the total count rate in the photopeak at 185.7 keV.

With the subtracted count rate at 185.7 keV for ^{235}U and the total count rate at 1001.0 keV for ^{238}U, the enrichment value can be calculated through Equation 6-4 and 6-5. The enrichment values for four fabricated samples are listed in Table 6-3.

Table 6-3. Enrichment values for the UO_2 pelletized samples. These values were calculated through the gamma-spectrometry method.

No.	^{235}U	^{238}U
1	0.00096	0.99904
2	0.00094	0.99906
3	0.00244	0.99756
4	0.00282	0.99718

The samples No. 1 and 2 have lower ^{235}U content since two different powders were used to make the samples. The powder for samples No. 1 and 2 was supplied by SPI-Chem Chemicals and another powder for samples No. 3 and 4 was obtained from Areva, Hanford, WA. They showed different purity levels during the milling process, with the powder from SPI-Chem Chemicals being the least pure, as shown in Figure 6-3.

Figure 6-3. Impurities from depleted uranium powder, supplied by SPI-Chem Chemicals (Photo: Author, Heejun Chung).

Other Possible Samples

In a sample, one of the most important factors in inducing more fission events and eventually producing a larger number of delayed neutrons and gamma-rays is the sample size. The fabricated UO_2 samples in the previous subchapter were well made and defined, but it was impossible to increase their size due to the limitation of the size of the sintering supplies and equipment.

For that reason, a natural uranium slug was prepared and its physical characteristics were measured. The slug was distributed to sixty five universities in the U.S.A. by Westinghouse

Savannah River Company for use in subcritical assemblies for R&D and educational aids in nuclear engineering programs. The University of Florida received Mark I slugs (solid slugs) and Mark IV slugs (hollow slugs), but the Mark IV slugs were returned and only the Mark I slugs are currently kept. The Mark I slugs contain natural uranium (0.0054 % ^{234}U, 0.7204 % ^{235}U, and 99.2742 % ^{238}U) clad in cylindrical shaped aluminum [Figure 6-4]. The measured weight of each slug is 1931.4 g. The other measured and reported specifications of the Mark I slug are shown in Table 6-4 [52].

Figure 6-4. The Mark I solid slug. The slug contains natural uranium, surrounded by aluminum cladding (Photo: Author, Heejun Chung).

Table 6-4. Measured and reported specifications of the Mark I slug.

Description	Dimension (cm) and Volume (cm^3)
Slug Radius	1.350
Slug Length	21.273
Slug Volume	121.709
Natural Fuel Slug Radius, Clad in Aluminum	1.254
Natural Fuel Slug Length, Clad in Aluminum	21.081
Natural Fuel Slug Volume, Clad in Aluminum	104.144

The exact specifications of this slug are important to derive or simulate accurate delayed neutron parameters, as discussed in later chapters. The slug will be used to validate the results of this study, which aims to reduce the uncertainties of the longest-lived delayed neutron group for ^{238}U. However, due to its bigger size and heavier weight, the experimental setups should be slightly modified.

Another possible sample is a ThO_2 pellet. The pelletized samples of thorium dioxide (ThO_2) were fabricated by the conventional method [Figure 6-5].

Figure 6-5. ThO_2 samples fabricated by the conventional method (Photo: Author, Heejun Chung).

These were fabricated in almost the same manner as the UO_2 pellet, except slightly modified based on the reference [53]. Thorium powder was pressed into the green body pellets after milling and then sintered at 1550°C in an aluminum tube furnace for 10 hours with a high purity argon and hydrogen gas atmosphere. The gas flow rate was exactly the same as a UO_2 pellet. The total duration of this sintering process is about 18 hours.

Unlike the reference, the two fabricated ThO_2 pellets in Figure 6-5 showed the different conditions of the surface with cracks and two color layers (black and light brown). From the point of view of those focused on material properties, these pellets have failed structures. However, they can be successfully used for NDA research like this study since their density and material composition can be clearly identified.

CHAPTER 7
PARAMETRIC UNCERTAINTY ANALYSIS OF THE DELAYED NEUTRON MEASUREMENT

With regards to the designed setup and the combined technique, a new evaluation of the relative abundance and uncertainty of the longest-lived delayed neutron group for fast fissions of ^{238}U were calculated. The calculated result (based on Equation 3-9, 10, 11 and 23 with the optimized time setups) showed almost same value with the recommended value (0.008) in the eight-group model. The parameters used in the calculation are listed in Table 7-1 [29].

Table 7-1. Parameter values for the relative uncertainty calculation

Parameters	Value	Reference
$\varepsilon_\gamma \cdot \mu_\gamma$	0.002	MCNP and Experiment Results
$Y_{cum,\ Kr\text{-}89}$	$0.03008 \pm 7.841\text{x}10^{-4}$	JEFF-3.1 Nuclear Library
q_P	1	JEFF-3.1 Nuclear Library
$T_{1/2,\ Kr\text{-}89}$	189 ± 2.4 sec	JEFF-3.1 Nuclear Library
$b_{\gamma,\ Rb\text{-}89}$	0.636 ± 0.011	JEFF-3.1 Nuclear Library
$Y_{cum,\ Rb\text{-}89}$	$0.030349 \pm 7.895\text{x}10^{-4}$	JEFF-3.1 Nuclear Library
$Y_{ind,\ Rb\text{-}89}$	$2.6848\text{x}10^{-4} \pm 9.5198\text{x}10^{-5}$	JEFF-3.1 Nuclear Library
$T_{1/2,\ Rb\text{-}89}$	924 ± 12 sec	JEFF-3.1 Nuclear Library
D_j	0.152	MCNP Results

The gamma-ray detector efficiency was evaluated with a ^{60}Co standard source, emitting two gamma rays at 1.173 and 1.333 MeV. These energies are close to the promised gamma line of ^{89}Rb at 1.032 MeV.

The uncertainty equation [Equation 3-25] can be written for only the 1st and 2nd groups of ^{238}U:

$$\sigma_{\alpha 81}^2 = \left\{1 + \frac{\alpha_{82}}{\alpha_{81}}\left(\frac{T_{n2}}{T_{n1}}\right)\right\}^2 \left(\sigma_{\mathrm{M_n}}^2 + \sigma_{\mathrm{S}}^2 + \sigma_{M_\gamma}^2 + \sigma_{\mathrm{\nu_{d8}}}^2 \right) + \left(\frac{\alpha_{82}}{\alpha_{81}}\frac{T_{n2}}{T_{n1}}\right)^2 \sigma_{\alpha_{82}}^2. \qquad (7\text{-}1)$$

As mentioned in the previous subchapter, the terms D_1 and D_2 were canceled out due to the same experimental geometry in Equation 7-1. The parameters with non-negligible contributions are the time term *T*, the gamma-ray summation term *S*, and the delayed neutron yield term υ_{di}.

Parametric Studies for Uncertainty Calculation

In the following subsections the parameters with non-negligible contributions to the uncertainty of the delayed neutron group yields are studied in detail. The objective is to optimize the experimental parameters in order to maximally reduce the uncertainty.

Irradiation, Cooling, and Acquisition Time, *T*

In the uncertainty calculation [Equation 7-1], the most sensitive factor is the time ratio T_{n2}/T_{n1}. By previous definition, the time dependent term *T* can be written as:

$$T = \frac{1}{\lambda} \cdot (1 - e^{-\lambda \cdot t_i}) \cdot e^{-\lambda \cdot t_c} \cdot (1 - e^{-\lambda \cdot t_a}). \qquad (7\text{-}2)$$

It strongly depends on the half-lives of the delayed neutron precursors and the chosen irradiation, cooling, and acquisition times. The decay constants are fixed nuclear data parameters. To reduce the total uncertainty, the irradiation, cooling and acquisition times must be optimized. Table 7-2 shows the delayed neutron precursor half-lives and the inverse decay constants ($1/\lambda_j$) in the eight-group model [1].

Table 7-2. Half-life and inverse decay constant of each delayed neutron group.

DN Group	Half-lives (sec)	$1/\lambda_j$ (sec)
1	55.6	80
2	24.5	35.3
3	16.3	23.5
4	5.21	7.53
5	2.37	3.4
6	1.04	1.5
7	.424	0.6
8	.195	0.3

To maximize the delayed neutron count rate, the sample must be irradiated long enough so that the delayed precursors can saturate. Thus, the irradiation time should be long enough relative to half-life of the longest-lived group. For the current simulation, an irradiation time of 180 sec is chosen, which leads to a saturation of the precursors of the first delayed neutron group of 89 %. Similarly, the acquisition time should be chosen long enough to capture as many delayed neutrons as possible. This is particularly important for the longer-lived groups, since later in the measurement process the ratio of delayed neutrons coming from the longer-lived groups increases, reducing uncertainties.

If irradiation and acquisition times are long enough, the corresponding terms are close to 1.0 in Equation 7-2. This equation can therefore be simplified to:

$$T = \frac{1}{\lambda} \cdot e^{-\lambda \cdot t_c}. \tag{7-3}$$

The uncertainty of the longest-lived group can be reduced due to increasing the cooling time, since the contributions from other groups are cut off by their short half-lives. However, a long cooling time also results in fewer delayed neutrons being counted, which therefore increases

measurement uncertainty. Thus, the optimal cooling time minimizes the contributions to the delayed neutron signal from the shorter-lived groups without sacrificing the signal of the longest-lived delayed neutron group.

The relative uncertainty of the longest-lived delayed neutron group for fast fission of ^{238}U was assessed, based on MCNP simulations and the system configurations described above. The estimated fission rate from a depleted uranium sample was chosen to simulate the total counts (as a function of time) during the acquisition time (180 sec). In accordance with the optimization of the detection system described in Chapter 4, the detector efficiency was set to 20 % for the delayed neutron as well as the delayed gamma detection system. The nuclear data were taken from the JEFF-3.1 library [29]. The correlation between cooling time and the relative uncertainty of the longest-lived group is shown in Figure 7-1.

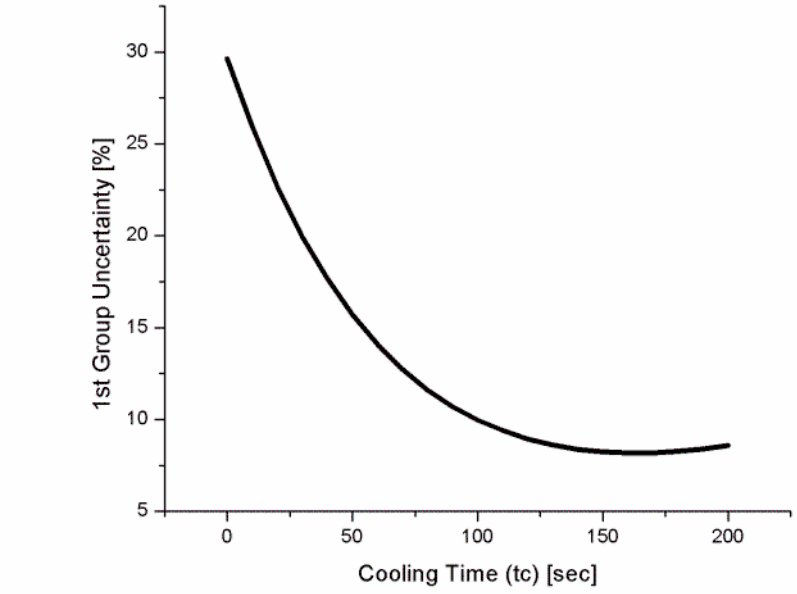

Figure 7-1. The relative uncertainty of the longest-lived group abundance vs. the cooling time, showing that 170 sec is the optimal cooling time to minimize uncertainty of the longest-lived delayed neutron group.

Figure 7-1 shows that the optimal cooling time to minimize the uncertainty of the delayed neutron group yield of the longest-lived group is 170 sec after the end of the irradiation.

Nuclear Data Library Selection for Delayed Gamma Parameters, b_γ, T_γ, and A_γ

Based on the criteria for a gamma line described in Chapter 3, and in combination with the optimized irradiation, cooling and acquisition times, the 1032 keV gamma line of ^{89}Rb was chosen as the fission rate estimator. Its activity and uncertainty were calculated, using Equation 3-11. This line is well suited due to the involved half-lives in the decay chain being similar to the irradiation and acquisition times. The calculated total gamma activity of ^{89}Rb at a certain time depends on the nuclear cross section library that is being used. Thus, the correlation between cooling time and the relative uncertainty of the longest-lived group with different libraries was calculated [Figure 7-2].

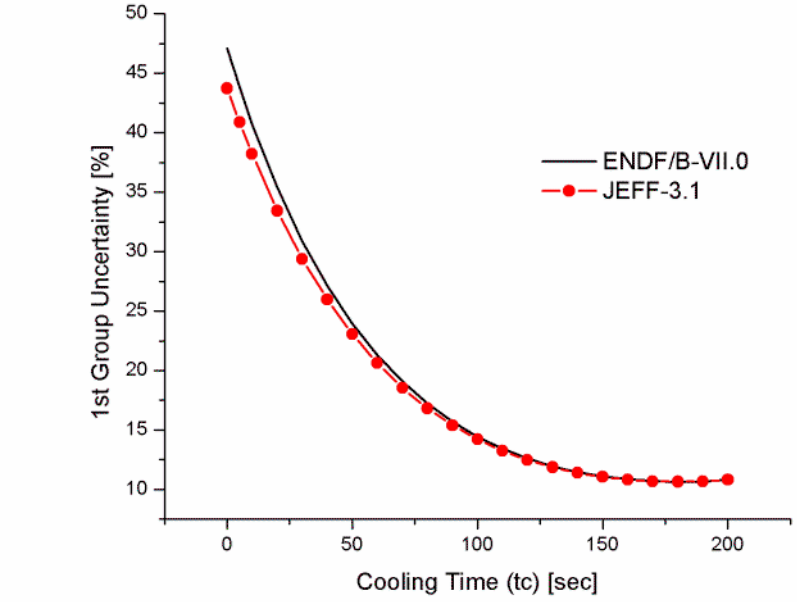

Figure 7-2. The relative uncertainty of the longest-lived group of ^{238}U with different libraries (ENDF vs. JEFF). Both libraries agree that 170 sec is the optimal cooling time to minimize uncertainty of the longest-lived delayed neutron group.

The difference is caused by the different decay data, fission yields and uncertainties in the JEFF-3.1 [29] and ENDF/B-VII.0 [9] libraries. However, the optimal cooling time, with regards to the relative uncertainty of the longest-lived group, remains 170 sec. With regards to the optimized cooling time, the calculated uncertainty of ^{89}Rb was 3.11 %.

Gamma-ray Attenuation and Detector Efficiency, μ_γ and ε_γ

The relative uncertainty of detector efficiency (ε_γ) and self-attenuation (μ_γ) for delayed gamma-rays were estimated via MCNP simulations.

The efficiency can be defined as the probability of measurement for each quantum of radiation which interacts within the active volume of a radiation detector, and two types of efficiency are generally referred as an absolute and intrinsic efficiency [27]:

$$\varepsilon_{abs} = \frac{number\ of\ pulses\ recorded}{number\ of\ radiation\ quanta\ emitted\ by\ source}, \quad (7\text{-}4)$$

$$\varepsilon_{int} = \frac{number\ of\ pulses\ recorded}{number\ of\ radiation\ quanta\ incident\ on\ detector}. \quad (7\text{-}5)$$

Efficiencies are also classified by the fraction of the energy deposited: full and partial energy deposition from the incident radiation. The energy deposition within a detector is depending on types of interactions involved with each radiation particle. Mostly, isotopes can be identified by their full energy deposition peak if the fraction of the full energy deposition is well-known. If the fraction of the full energy deposition is unknown then all peaks on a detector should be considered. Based on the fraction of the energy deposited, the detector efficiency can also be referred to as the total (all pulses) or full energy peak efficiency [27].

The full energy peak efficiency and uncertainty of the chosen gamma line at 1031.92 keV from ^{89}Rb were simulated via MCNP. The gamma spectrum from ^{89}Rb is shown in Figure 7-3.

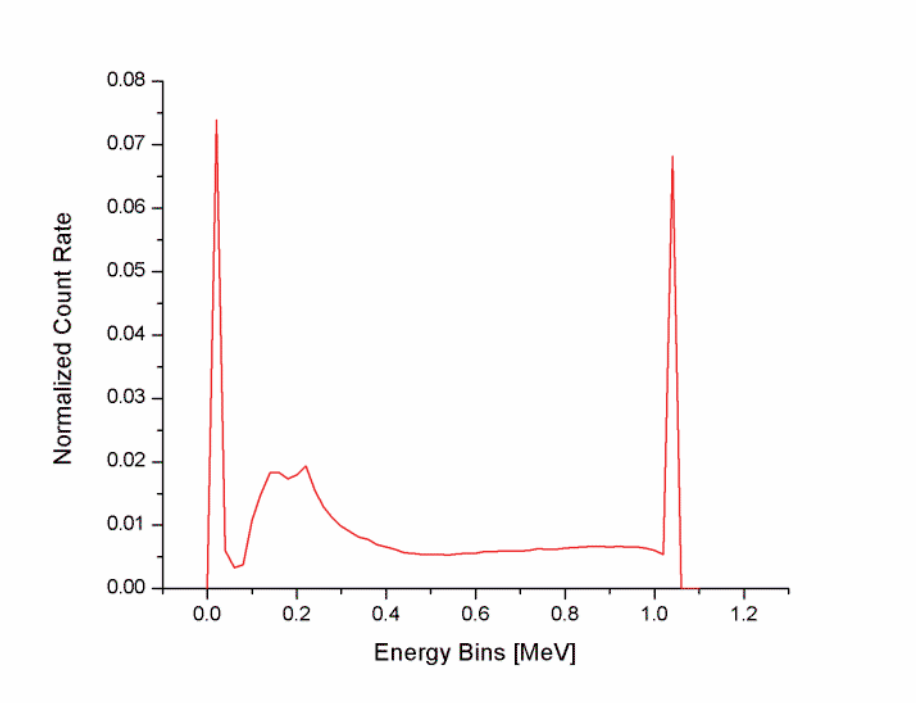

Figure 7-3. The expected gamma spectrum from ^{89}Rb via MCNP.

Figure 7-3 is drawn by the normalized count rate in number of interactions per a unit source. Therefore, the actual count rate can be estimated by multiplying the actual source intensity. Based on the MCNP results, the uncertainty of the full energy peak of ^{89}Rb at 1031.92 keV resulted in 0.01 % at 1.02 to 1.04 MeV.

Photons are attenuated through a sample based on sample size, shape, density, and chemical composition. The attenuation rate and its uncertainty through a pelletized UO_2 sample were calculated by using mesh tallies of MCNP. For this, two MCNP models were written. The first one was to find exact fission positions in the sample since fission rates are directly related to number density of the target precursor ^{89}Rb.

In the second simulation, the gamma energy distribution of ^{89}Rb in a sample, found in the first simulation, was considered as a source term. A sample was meshed by ten coarse mesh

points in z-direction (height) and four coarse mesh points in theta-direction (90 degree) [Figure 7-4].The uncertainty of gamma self-attenuation was then calculated and was less than 0.01 %.

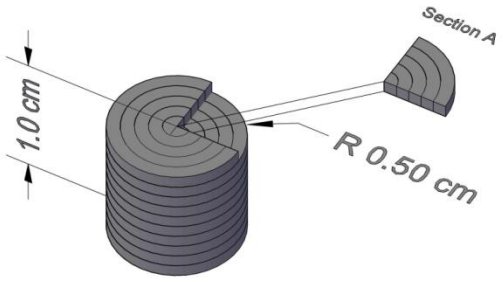

Figure 7-4. The geometry for attenuation and its uncertainty calculations via MCNP. This simulation was used to estimate the self-attenuation of gamma-rays in the sample.

In both cases for the chosen gamma lines, the calculated uncertainties (about or less than 0.01 %) would be negligible. The efficiency of neutron detectors (D_j) was also not considered in the uncertainty equation since they can be canceled out with the same experimental geometry.

Total Number of Delayed Fission Neutrons, ν_{d8}

For the total number of delayed fission neutrons ν_{d8}, many different sources of data are available [11, 21, 54-60]. Interestingly, the values for the yields of delayed neutron emissions are very similar, but the values for their uncertainties differ significantly [Table 7-3].

Table 7-3. Available references for delayed neutron yields from ^{238}U.

Reference (Year)	Yield	Relative Uncertainty (%)
Tuttle (1979)	0.0439	2.28
Piksaikin et al. (2002)	0.0457	3.50
Fort at al. (2002)	0.0471	3.99
Keepin et al. (1965)	0.0412	4.13
James at al. (1990)	0.0406	4.91
JEFF 3.1 (2006)	0.0465	5.16
Blachot at al. (1990)	0.0416	5.77
Blachot (1997)	0.0431	5.80
JEFF 2.2 (2000)	0.0468	6.41
Brady et al. (1989)	0.0405	7.16
England et al. (1983)	0.0354	7.69
Rudstam (1982)	0.0324	8.33
Manevich et al. (1983)	0.0425	12.0

For this study, Keepin data (1965) and Tuttle data (1979) were chosen and compared since they have been widely used in the nuclear industry [61], and give the best agreement with integral reactor experimental data. Furthermore, it is close to the recommended value from A. D'angelo, published in 2002 [59].

Based on the above analyses, values for the various parameters in the uncertainty equation were chosen for the calculation of the relative uncertainty of the longest-lived delayed neutron group from fast fission of ^{238}U, and listed in Table 7-4.

Table 7-4. The chosen uncertainty values of parameters from the optimized measurements and simulation. These values were used to calculate the relative uncertainty of the longest-lived delayed neutron group from fast fissions of ^{238}U.

Parameters	Value	Reference
T_c	170 (sec)	MCNP Results
$\sigma_{\upsilon d}$	2.28 (%) and 4.13 (%)	Tuttle (79) and Keepin (65) Data
$\sigma_{SUM\ (b\gamma,\ T\gamma,\ and\ A\gamma)}$	3.11 (%)	JEFF-3.1 Nuclear Library
$\sigma_{\varepsilon\gamma}$	Negligible, ~ 0.01 (%)	MCNP Results
$\sigma_{\mu\gamma}$	Negligible, > 0.01 (%)	MCNP Results

Result: Uncertainty Calculation for Longest-lived Delayed Neutron Group for ^{238}U

The fabricated UO_2 samples were initially irradiated by a D-D generator and delayed neutrons and gamma-rays (^{89}Rb at 1031.92 keV) were simultaneously measured. The measured photopeak of ^{89}Rb via the GINIE 2000 Gamma analysis software is shown in Figure 7-5.

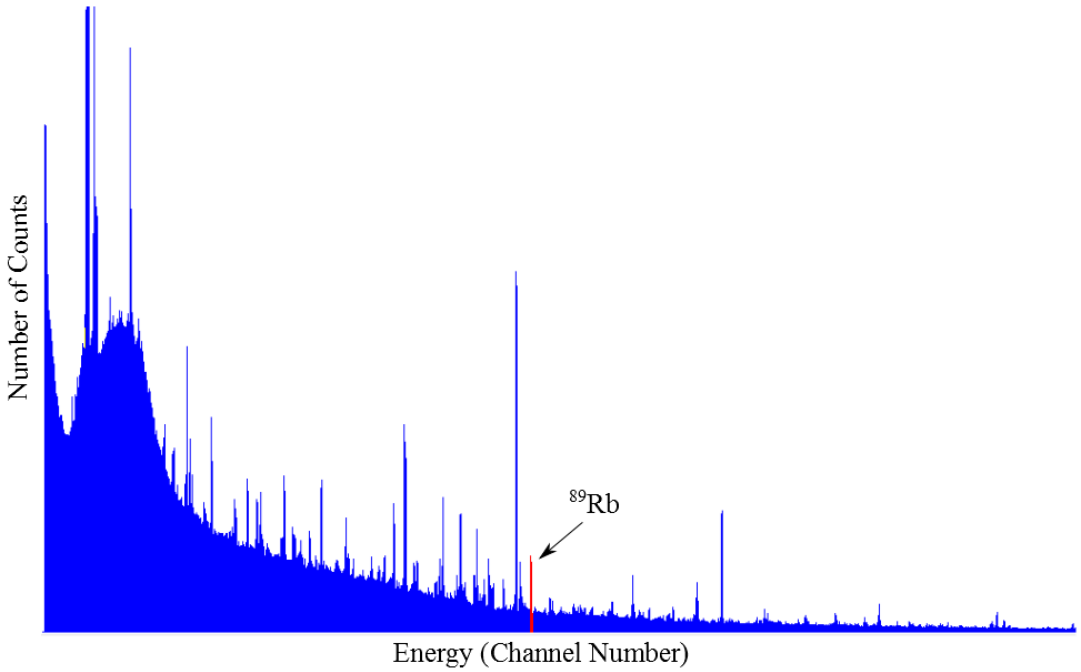

Figure 7-5. The measured photo peak of ^{89}Rb at 1032 keV, measured from a UO_2 sample irradiated by the neutron generator.

Times were chosen as 20 min, 170 sec, and 360 sec for irradiation, cooling, and acquisition, respectively. The neutron generator yield during the experiment was 1.1×10^9 neutrons per sec at 115 kV.

The chosen uncertainty values of relative parameters from the optimized measurements and simulation [Table 7-3] were applied for the uncertainty calculation of the longest-lived delayed neutron group for fast fission of ^{238}U. The estimated uncertainty was initially about 11 %.

More than 100 measurements had been performed but some measured data sets had shown unacceptable output arising from radiation induced electronics issues. Measurements were accepted or rejected based on the stability and lack of arcing in the D-D generator. Arcing interrupts neutron production, so estimates of total output and precursor saturation in the sample become unreliable.

In total, 43 data sets were obtained under these criteria and the estimated uncertainty was about 9.8 %. Further measurement trials will reduce the uncertainty, as we are not yet near the asymptotic limit. The correlation of measurement trials between the number of experiments and the relative uncertainty of the longest-lived delayed neutron group for fast fission of ^{238}U is shown in Table 7-5.

Table 7-5. The correlation between the number of experiments and the relative uncertainty of the longest-lived delayed neutron group for fast fission of ^{238}U.

No. of Experiment	1st Group Uncertainty with Tuttle's υ_d Data (%)	1st Group Uncertainty with Keepin's υ_d Data (%)
25	10.8	11.8
50	8.52	9.78
75	7.63	9.01
100	7.14	8.60

Repeatedly taking other samples into the experimental system, the relative uncertainty of the longest-lived delayed neutron group for fast fission of ^{238}U can be reduced by a factor of two lower than the Spriggs and Campbell recommended data set (16 % [1]).

For convenience, this uncertainty calculation was performed using MATLAB scripts, shown in Appendix A. The count rates of delayed neutrons and gamma-rays, experimental time setups in sec, ^{238}U enrichment in %, and sample dimensions in cm are the input parameters to the code [Figure 7-6].

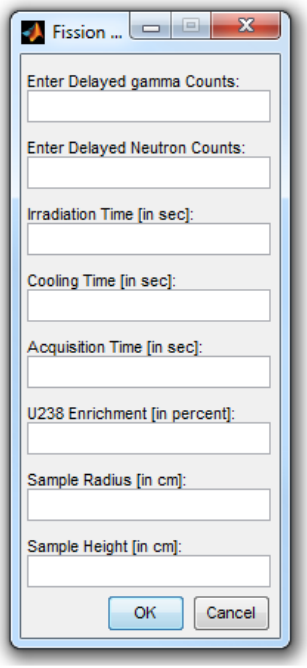

Figure 7-6. The MATLAB input deck for uncertainty calculation.

The output contains fission rates and uncertainties via the delayed gamma technique, and the calculated the longest-lived group abundance and its uncertainty via the combined technique.

In conclusion, the final improved value for the relative abundance and its uncertainty of the longest-lived delayed neutron groups for ^{238}U was resulted in 0.0082 ± 8.60 % with Keepin's delayed neutron yield data (1965) or alternatively 0.0075 ± 7.14 % with Tuttle data set (1979) in this study. The experimental agreement with the Keepin parameters combined with the lower

assessed uncertainty values indicates that there is an unidentified systematic error in the original Tuttle data.

Verification of the experimental data

A larger sample volume will result in a greater quantity of delayed neutrons and gamma-rays. Using the Mark I slug, the experimental result in the previous subchapter was verified. Considering its larger volume (104.144 cm^3), an irradiation time of 1 hour was chosen. The cooling and acquisition times were 170 sec and 20 min, respectively.

Assuming all values of the relative parameters are the same as the previous calculation, the relative uncertainty of the longest-lived delayed neutron group for fast fission of ^{238}U was calculated to be 6.6 %.

Even though the Mark I is surrounded by an aluminum cladding, the assumption for using exactly the same parameters was a good approximation since the thickness of the aluminum cladding is only 0.096 cm [Table 6-4].

To better understand the effects of the aluminum slug cladding on the attenuation of gamma-rays, two MCNP models were simulated: one with cladding and one without. The simulation geometry with cladding and the expected gamma spectrum from ^{89}Rb were drawn in Figure 7-7.

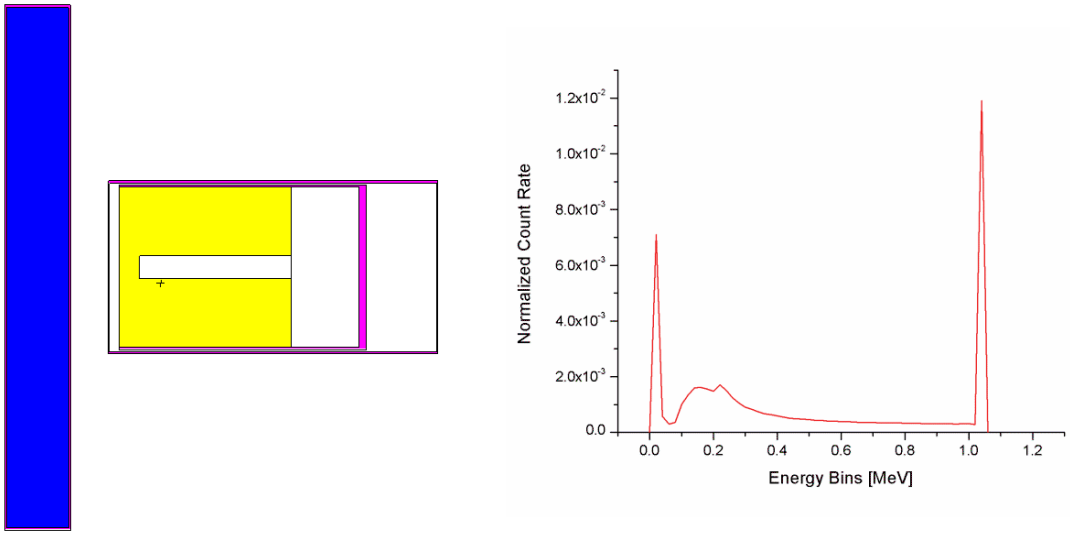

Figure 7-7. The MCNP geometry with aluminum slug cladding and the expected gamma spectrum from ^{89}Rb.

Since Figure 7-3 and 7-7 were drawn by the normalized count rate, two spectra can be directly compared in order to know the material attenuation of the aluminum cladding. Comparing those two figures, only low energy gamma-rays are significantly attenuated, and the full energy peak of ^{89}Rb at 1031.92 keV still shows good agreement between the two figures.

This effectiveness from the material attenuation can be easily verified by the simple attenuation equation [4]:

$$\frac{I}{I_0} = e^{-\mu \cdot t}, \qquad (7\text{-}7)$$

where I denotes the intensity of a gamma-ray, μ is the attenuation coefficient, and t is a material thickness.

The value of the attenuation coefficient for an aluminum cladding of 6.049x10^{-2} cm^2/g was found [62]. The density of aluminum is 2.7 g/cm^3 and the cladding thickness is 0.096 cm. Inserting these values into Equation 7-7, the uncollided fraction was calculated to be almost 98 %. This means the material attenuation of aluminum cladding can be neglected.

In the same manner as the previous attenuation calculation, the uncertainty of gamma self-attenuation was also simulated and resulted in less than 0.01 %.

The relative uncertainty of the longest-lived delayed neutron group for fast fission of ^{238}U (6.6 %) in the Mark I natural uranium slug is lower than the measurement value in a pelletized UO_2 sample (8.60 % with the Keepin's delayed neutron yield data or alternatively 7.14 % with Tuttle data set). However, the relative parameters in the uncertainty calculation were assumed to be the same as the chosen values of relative parameters for a pelletized UO_2 sample. Additionally, the Mark I slug was manually handled since the experimental apparatus was optimized for only a pelletized sample. Therefore, the parametric optimization study and modification of the experimental apparatus is required for the Mark I slug.

This verification study implies that another mostly sensitive factor in the uncertainty calculation is the sample size. With the parametric optimization study and modification of the experimental apparatus for the Mark I slug, better results in the uncertainty calculation can be expected.

CHAPTER 8
FUTURE WORK

Future Work in Nuclear Data Measurement

This study showed that the system designed, employing a D-D neutron generator and the combined delayed neutron and gamma ray method, has considerable potential to reduce the large uncertainties of the longest-lived delayed neutron group abundances. Further steps will be to try to reduce the uncertainties of the shorter-lived delayed neutron groups and for the different fissile materials. The limitations of the existing measurement methods lead to a search for improved ways of analyzing nuclear fuel. The details of a promising new technique using prompt neutrons and a new kind of detector are outlined in this chapter.

Prompt Neutron Fission Rate Measurement with Gas Scintillators

Delayed neutrons represent less than 1 % of the total neutron emission from fission. To measure delayed neutrons, the precursors must be saturated through an ~15 min irradiation before measurement. In this way we are blind to both the 99 % of neutrons that are promptly emitted, as well as the irradiation time. If there were a method to measure prompt neutrons during irradiation, we could improve the available signal by more than a factor of 1000.

A ^{4}He fast-neutron scintillation detector has recently been developed by Arktis Radiation Detectors. The ^{4}He scintillation detector is characterized by its low electron density, leading to excellent gamma rejection. This detector also has a fast response time on the order of nanoseconds and most importantly, preserves some neutron energy information. [63].

The ^{4}He scintillation detector consists of a cylindrical high-pressure vessel, filled with 150 bar of ^{4}He, and two photomultiplier tubes (PMTs) with associated electronics for recording data [63].

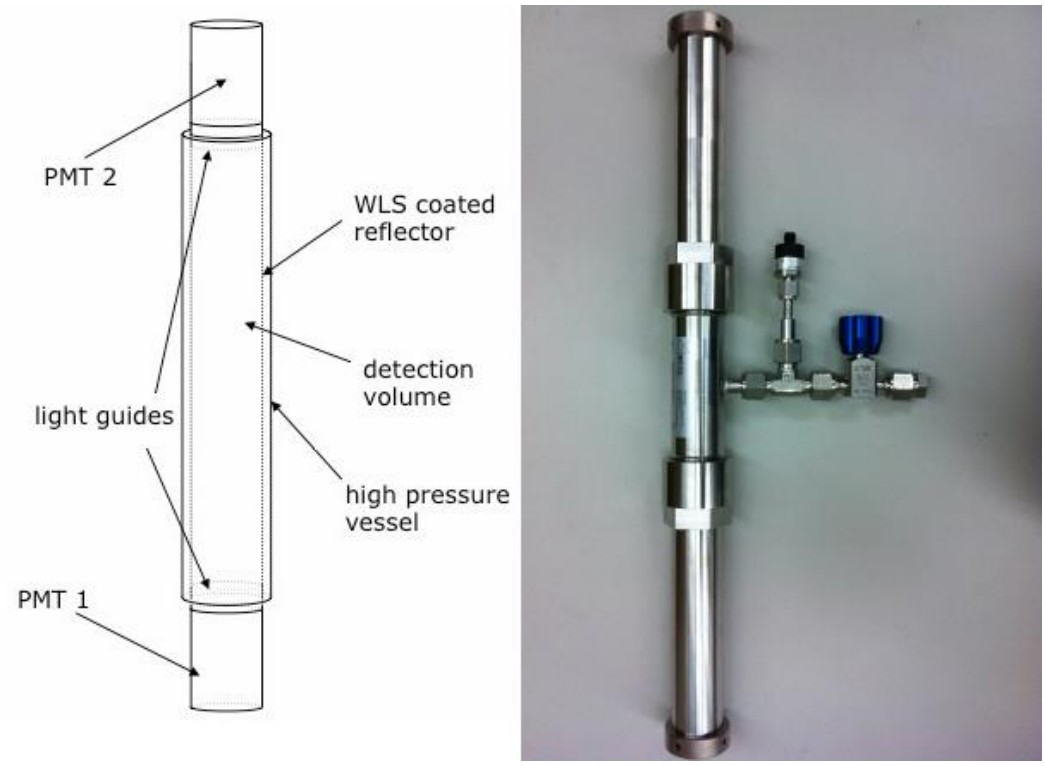

Figure 8-1. The schematic drawing (left, Arktis Radiation Detector Ltd.) and actual photo of a ^{4}He scintillation detector (right, Photo: Author, Heejun Chung). Incoming fast fission neutrons elastically scatter with the ^{4}He fill gas, producing scintillation photons that are counted by PMTs at either end.

A ^{4}He scintillation detector can be placed in a high intensity radiation area due to its excellent gamma rejection; fast fission neutrons can be directly measured without any moderation processes, unlike the general proportional neutron counters (^{3}He and BF_3).

In a few previous studies, the detector has been used for fission rate measurements to determine the plutonium content in Mixed Oxide (MOX) reactor fuel [64]. However, the feasibility of active neutron interrogation of a fissile sample has been not proved, so a new, prompt-neutron measurement technique, using a D-D neutron generator for active interrogation, was developed to try and leverage the increased signal availability.

The primary challenge is to differentiate between the prompt fission neutrons and the irradiation source. In a delayed neutron measurement, the time-emission behavior of delayed

neutrons is used as a separation criterion. For prompt neutrons, we can use energy separation between source and fission neutrons as provided by the elastic scatter signal in the ^{4}He detector.

Neutron elastic scattering is typically notated by (n, n). This physical process in a ^{4}He scintillation detector can be explained as a neutron collides and transfers some energy to the ^{4}He nucleus and finally is reflected in a different direction. The collided (recoiling) ^{4}He nucleus gains the energy from the incident neutron, depending on the angle of impact, and then increases speed. The recoiling ^{4}He nucleus loses energy through excitation or ionization in proportion to its initial energy, providing a (somewhat) proportional signal.

To distinguish the fission neutron signal, an energy threshold method using these detectors is proposed. The interrogation neutrons are mono-energetic and the energy distribution of prompt fission neutrons is according to the Watt fission spectrum, typically distributed from 0.1 MeV to 10 MeV [Figure 2-2]. From basic kinetics, an incident neutron can transfer up to 64 % of its energy to ^{4}He nucleus by elastic scattering, so the maximum energy deposited by a 2.45 MeV interrogation neutron will be 1.6 MeV. Therefore, any energy deposition greater than 1.6 MeV in the detector must be from a fission neutron rather than an interrogating neutron [65].

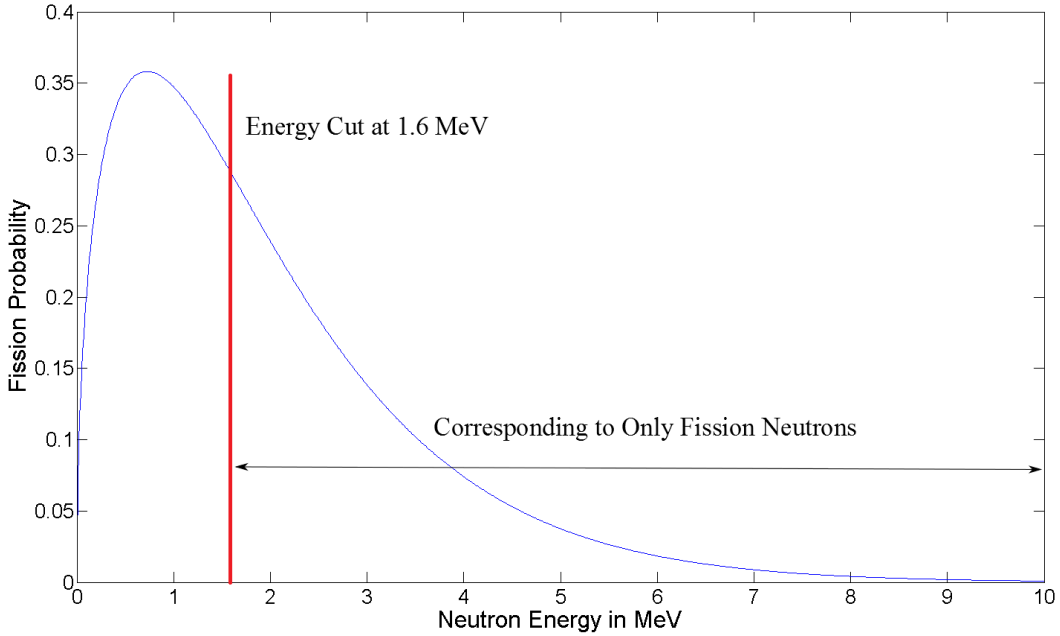

Figure 8-2. Energy cut-off for integrated counts of fission neutrons, 1.6 MeV is the maximum energy that can be deposited by an incident 2.45 MeV neutron from the D-D neutron generator.

Prompt Neutron Fission Rate Measurement Technique

Applying the energy threshold, the total counts from only prompt fission neutrons detected by a ^{4}He scintillation detector (M_P) can be written as:

$$M_P = F \cdot \alpha_P = F \cdot \sum_i S_i \cdot \varepsilon_P \cdot T \cdot V \cdot e^{-\Sigma_t \cdot d}, \tag{8-1}$$

where α_P is the proportionality factor, ε_P is the detector efficiency, T is the acquisition time, and V is the sample volume. The exponential term accounts for the attenuation in a sample, Σ_t is the macroscopic total cross section, and d is the distance between a fission position and the end of a sample. S_i is the normalized neutron source and can be defined as:

$$S_i = \frac{f_i}{F} \cdot \upsilon_{Pi}, \tag{8-2}$$

where f_i/F are the proportion of fission due to the fissioning isotopes i, and υ_P accounts for prompt fission neutron yields.

Since the fission proportion relates the amount of fissile material in a sample and its fission cross section, it can be written as:

$$\frac{f_i}{F} = \frac{N_i \cdot \sigma_i}{(N_1 \cdot \sigma_1 + \cdots + N_i \cdot \sigma_i)}. \quad (8\text{-}3)$$

Equation 8-1 can be simplified and approximated by:

$$M_P = F \cdot \alpha_P = F \cdot \sum_i S_i \cdot \varepsilon_P \cdot T \cdot V. \quad (8\text{-}4)$$

The approximation of Equation 8-4 is reasonable if the sample size is relatively small since the macroscopic total cross section is defined as multiplying the number density of a fissile material by the microscopic total cross section in the unit of barn (1 barn is equal to 10^{-24} cm^2).

If the fission yields of the isotopes are known, the most sensitive parameter in Equation 8-4 is the normalized source term, depending on nuclear data of the prompt neutron yield per fission υ_P, since other parameters can be precisely measured.

The prompt neutron yield per fission υ_P can be calculated in Equation 2-8 if the total fission neutron yield υ is known. A few sources of data for the total fission neutron yield υ are available, but mostly values and uncertainties are based on ENDF nuclear data. The current ENDF nuclear data for the total number of fission neutrons υ were evaluated by T. R. England and B. F. Rider, and shown in Table 8-1 [66].

Table 8-1. The total fission neutron yields from major radioactive nuclides

Nuclide	Type	Yield	Relative Uncertainty (%)
^{235}U	Thermal	2.42	4.96
^{235}U	Fast	2.47	4.86
^{235}U	High	4.38	5.02
^{238}U	Fast	2.79	5.02
^{238}U	High	4.42	4.98
^{239}Pu	Thermal	2.88	4.86
^{239}Pu	Fast	2.94	5.10
^{239}Pu	High	4.90	5.10

Three different fission rate measurement techniques have been introduced so far, and can be rewritten in terms of fission rate. Currently, the new proposed study for fission rate estimates from the same uranium sample via three techniques is ongoing, a better estimation of fission rate or an accurate assessment of a fissile material can be obtained.

CHAPTER 9
CONCLUSIONS

The uncertainties of the longest-lived delayed neutron groups for important fissile isotopes such as ^{235}U, ^{238}U, ^{239}Pu or ^{232}Th are large. These high uncertainties are caused by systematic uncertainties in measurements and mathematical instabilities in the parameters fitting methods.

Prior experiments and studies have laid the groundwork for a new measurement approach of the delayed neutron group yields. This is achieved through the combination of the widely used delayed gamma technique and a recently developed delayed neutron technique to measure fission rates in nuclear fuel. However, the combined method for data measurements had not been previously implemented.

The work presents the design, optimization, and measurement results from a newly built system for simultaneous measurement of the delayed neutron and the delayed gamma signals emitted by an irradiated sample of fissile material. Design studies were made with the objective to maximize the delayed neutron and the delayed gamma signals in the detectors. Based on the design studies, the actual system was built, tested, and compared with the simulation results.

The most important result associated with the originating purpose – the improvement of the relative uncertainties of the longest-lived delayed neutron groups – was the newly developed D-D neutron generator (DD-109X) in collaboration with Adelphi Technology Inc. This neutron generator uses an optimized plasma source and a unique target and chamber design, allowing for increased neutron production and for a higher aspect ratio for irradiation samples. With the chamber design, samples may be placed extremely close to the neutron target, thereby drastically increasing the neutron flux incident on the sample. University of Florida and Adelphi Technology Inc. have received the 2013 R&D 100 award for their development of this DD-109X model.

Various parametric studies have been conducted to find the optimal combination of experimental and calculative settings to reduce the uncertainty of the first delayed neutron group as much as possible. Irradiation, cooling, and acquisition times have been optimized. The nuclear data library in general (ENDF/B and JEFF were tested) does not have a large effect with the optimized time setups. However, the data set that is chosen for the total number of delayed neutrons - ν_{d8} - can change the results considerably. The data from Keepin (1965) and Tuttle (1979) were selected since they have been widely used in the nuclear industry.

The relative value of the longest-lived delayed neutron group for fast fission of ^{238}U using the previously used values for relative parameters in the uncertainty equation, taken from the optimized measurement and simulation, has been reevaluated and shown consistent with the Spriggs assessed value of 0.008, and the uncertainty has been reduced in this new evaluation from 16 % to 8.6 %. Similar improvements of the uncertainty of the first delayed neutron group are expected for the other relevant fissile isotopes.

A second reevaluation, using data obtained from Tuttle resulted in 0.0075 ± 7.14 %, which is inconsistent with the new experimental measurement, indicating an unidentified systematic error in the Tuttle measurements.

Finally, a prompt neutron fission rate measurement technique was proposed for fast neutron interrogation using a D-D neutron generator with ^{4}He gas scintillation fast neutron detectors, newly developed by Arktis Radiation Detectors.

APPENDIX A
COMPUTER CODE INPUT FILES

This appendix contains all of the MCNP and MATLAB input files used to calculate the fission rates, detector efficiency, and relative uncertainties.

MCNP Input File for Fission Rates

```
Neutron Irradiation via Generator (UO2 3.5%)

C ------ Cell Card ------------------------------------------------------------
1    1   -11.34     1 -2 3 -4 5 -6 7 8 9 10 11       IMP:N=1  $Lead
2    1   -11.34     -8                               IMP:N=1  $Lead
3    1   -11.34     -9                               IMP:N=1  $Lead
4    0              -7 11                            IMP:N=1  $Void
5    0              7 -10                            IMP:N=1  $Void
6    2   -10.46     -11                              IMP:N=1  $UO2
7    0              -1:2:-3:4:-5:6                   IMP:N=0  $Outside

C ------ Surface Card ----------------------------------------------------------
1    PZ -15
2    PZ 15
3    PY -15
4    PY 15
5    PX -15
6    PX 15
7    RCC 0 0 0.1 0 0 3.9 1
8    RCC 0 0 4 0 0 9 1
9    RCC 0 0 13 0 0 2 2
10   RCC 0 -15 0 0 16.5 0 2
11   RCC 0 0 2 0 0 1 0.41

C ------ Material Card ---------------------------------------------------------
C 3.5 w/o Converted to a/o
M1   82000 1                                        $Lead
M2   8016  2                                        $UO2
     92238 0.964566
     92235 0.0354323
C ------- Mode Card -------------------------------------------------------------
MODE N
C ------ Source Definition -----------------------------------------------------
SDEF par=1 POS=0 0 0 ERG=2.45
C ------ Tally Card ------------------------------------------------------------
M235 92235 1.0
M238 92238 1.0
C
FC4 Flux in the UO2
F4: N 6
C
FC14 Total Fission reaction rates in the UO2
F14: N 6
FM14 (-1 2 -6)
C
FC24 Fission reaction rates in U-235
F24: N 6
FM24 (8.26797E-04 235 -6)
C
FC34 Fission reaction rates in U-238
F34: N 6
C
```

```
FM34 (2.25077E-02 238 -6)
E0 0 0.0025E-6 1E-6 0.1 0.2 0.3 0.4 0.5 0.6 0.7 0.8 0.9 1 2 3 4 5 6 7 8 9 10
C ------ CutOff Card ------------------------------------------------------------
NPS 1E8
```

MCNP Input File for Efficiency of Detector Bundle

```
New Design for Detector Bundle
C Detector Angles: 15, 40, 65, 90, 115, 140, 165
C ------ Cell Card ------------------------------------------------------------------
1    1   -0.92      1 -2 (-3:-4) 12 13 14 15 16 17 18      IMP:N=1  $Poly
2    2   -0.00054   -5                                     IMP:N=1  $He3
3    2   -0.00054   -6                                     IMP:N=1  $He3
4    2   -0.00054   -7                                     IMP:N=1  $He3
5    2   -0.00054   -8                                     IMP:N=1  $He3
6    2   -0.00054   -9                                     IMP:N=1  $He3
7    2   -0.00054   -10                                    IMP:N=1  $He3
8    2   -0.00054   -11                                    IMP:N=1  $He3
9    3   -2.70      5 -12                                  IMP:N=1  $Al
10   3   -2.70      6 -13                                  IMP:N=1  $Al
11   3   -2.70      7 -14                                  IMP:N=1  $Al
12   3   -2.70      8 -15                                  IMP:N=1  $Al
13   3   -2.70      9 -16                                  IMP:N=1  $Al
14   3   -2.70      10 -17                                 IMP:N=1  $Al
15   3   -2.70      11 -18                                 IMP:N=1  $Al
16   3   -2.70      -19 20                                 IMP:N=1  $Al Case (out)
17   0              -20 21 22                              IMP:N=1  $Void
18   4   -1.848     -21                                    IMP:N=1  $Be Window
19   3   -2.7       -22 23                                 IMP:N=1  $Al Case (in)
20   5   -5.323     -24 25                                 IMP:N=1  $Ge
21   0              -23 24                                 IMP:N=1  $Void
22   0              -25                                    IMP:N=1  $Void
23   0              (-1:2:3) (-1:2:4) 19 -26               IMP:N=1  $Void
24   0              26                                     IMP:N=0  $Outside

C ------ Surface Card ------------------------------------------------------------------
C POLY
1    RCC 0 0 -1 0 0 21.32 1
2    RCC 0 0 -1 0 0 21.32 15.54
3    P   -0.188654 1 0 -0.188654
4    P   0.188654 1 0 -0.188654
C Detectors (Effective Length)
5    RCC -7.022 -1.882 0 0 0 20.32 1.181
6    RCC -5.569 -4.673 0 0 0 20.32 1.181
7    RCC -3.072 -6.589 0 0 0 20.32 1.181
8    RCC 0 -7.27 0 0 0 20.32 1.181
9    RCC 3.072 -6.589 0 0 0 20.32 1.181
10   RCC 5.569 -4.673 0 0 0 20.32 1.181
11   RCC 7.022 -1.882 0 0 0 20.32 1.181
C Detector Cases
12   RCC -7.022 -1.882 0 0 0 20.32 1.27
13   RCC -5.569 -4.673 0 0 0 20.32 1.27
14   RCC -3.072 -6.589 0 0 0 20.32 1.27
15   RCC 0 -7.27 0 0 0 20.32 1.27
16   RCC 3.072 -6.589 0 0 0 20.32 1.27
17   RCC 5.569 -4.673 0 0 0 20.32 1.27
18   RCC 7.022 -1.882 0 0 0 20.32 1.27
C HPGe
19   RCC 0 1 10.16 0 13.4 0 3.5                           $Ortec GEM-70 (Poptop)
```

```
20   RCC 0 1.05 10.16 0 13.3 0 3.4
21   RCC 0 1.45 10.16 0 0.005 0 3.326                    $Be Window
22   RCC 0 1.455 10.16 0 10.045 0 3.326                  $Al Can (in)
23   RCC 0 1.455 10.16 0 9.725 0 3.25                    $Al Can (in)
24   RCC 0 1.455 10.16 0 7 0 3.25                        $Ge
25   RCC 0 2.295 10.16 0 6.16 0 0.46                     $Hole in Ge
26   SO 100

C ------ Material Card ------------------------------------------------------------
M1   1001 2
     6000 1                                              $Poly
M2   2003 1                                              $He3
M3   13027 1                                             $AL (2.70 g/cc)
M4   4009 1                                              $Be
M5   32070 0.2123
     32072 0.2766
     32073 0.0773
     32074 0.3594
     32076 0.0744                                        $Ge
C ------- Mode Card ---------------------------------------------------------------
MODE N
C ------ Source Definition -------------------------------------------------------
SDEF par=1 POS=0 0 10.16 ERG=d1
SI1 L 0.25 0.56 0.43 0.62 0.42
SP1 D 0.00025 0.00166 0.00213 0.00241 0.00085
C ------ Tally Card --------------------------------------------------------------
FC4 Flux in the He3
F4: N 2 3 4 5 6 7 8 T
C24 Count rates in cubic cm in the He3
F24: N 2 3 4 5 6 7 8 T
FM24 (-1 2 -2)
C ------ CutOff Card -------------------------------------------------------------
NPS 1E8
```

MATLAB Input File for Uncertainty Calculation

```
clear all
clc

% Notice: This program was written based on:
% 1. Rb-89 at 1032 keV
% JEFF Nuclear Data

%% Input Prompt
prompt={'Enter Delayed gamma Counts:','Enter Delayed Neutron Counts:','Irradiation
Time [in sec]:','Cooling Time [in sec]:','Acquisition Time [in sec]:','Fractional
Fission Rate [No unit]:','Sample Radius [in cm]:','Sample Height [in cm]:'};
% Create all your text fields with the questions specified by the variable prompt.
title='Fission Rate Estimator';
% The main title of your input dialog interface.
answer=inputdlg(prompt,title);
Mr = str2num(answer{1});
Mn = str2num(answer{2});
TS1 = str2num(answer{3});
TS2 = str2num(answer{4});
TS3 = str2num(answer{5});
FFR = str2num(answer{6});
SR = str2num(answer{7});
SH = str2num(answer{8});

%% Estimated Fission Rate via the Delayed Gamma Technique

% EAG = Efficiency and Attenuation for Gamma-rays
EAG = 0.002;
% IG = Intensity of Gamma-rays
IG = 0.636;
% CYKr = Cumulative Yield of Parent, Kr89
CYKr = 0.03008;
% BrKr = Braching Ratio of Parent, Kr89
BRKr = 1;
% HFKr = Halflife of Parent, Kr89 [in sec]
HFKr= 189;
% RKr = Lamda of Kr89
LKr = log(2)./HFKr;

% IYRb = Individual Yield of Rb89
IYRb = 0.00026848;
% CYRb = Cumulative Yield of Rb89
CYRb = 0.030349;
% HFRb = Halflife of Rb89 [in sec]
HFRb = 924;
% RKr = Lamda of Rb89
LRb = log(2)./HFRb;

% TKr = Time accounts for the build-up and decay of Kr89
TKr = 1./LKr.*(1-exp(-LKr.*TS1)).*exp(-LKr.*TS2).*(1-exp(-LKr.*TS3));
% TRb = Time accounts for the build-up and decay of Rb89
TRb = 1./LRb.*(1-exp(-LRb.*TS1)).*exp(-LRb.*TS2).*(1-exp(-LRb.*TS3));
```

```
% AKr = Activity of Kr, corresponding to TKr
AKr = (BRKr.*LRb.*CYKr)./(LRb-LKr);
% AKr = Activity of Rb, corresponding to TRb
ARb = IYRb+(BRKr.*LKr.*CYRb)./(LKr-LRb);

% CF = Total Activity
CF = ARb.*TRb+AKr.*TKr;

% V = Sample Volume
V = pi.*SR^2.*SH;

% FR = Estimated Fission Rate via the Delayed Gamma Technique
FR= (Mr./(V.*CF.*EAG.*IG))

%% Evaluate a New Relative Abundance Ddata via the Combined Method

% A2 = Relative Abundance of 2nd Group (Spriggs)
A2 = 0.104;
% D = The correctional Factor for the Solid Angle and Attenuation
D=0.152;
% vd = The Total Delayed Neutron Yield (Keepin, 65)
vd = 0.0412;
% vd2 = The Total Delayed Neutron Yield (Tuttle, 79)
vd2 = 0.0439;

% LG1 = Lamda of Group 1
LG1 = log(2)/55.6;
% LG2 = Lamda of Group 2
LG2 = log(2)/24.5;

% TG1 and TG2 = Time accounts for Delayed Neutron Group 1 and 2
TG1=1./LG1.*(1-exp(-LG1.*TS1)).*exp(-LG1.*TS2).*(1-exp(-LG1.*TS3));
TG2=1./LG2.*(1-exp(-LG2.*TS1)).*exp(-LG2.*TS2).*(1-exp(-LG2.*TS3));

A1 = (Mn-FR.*vd.*D.*TG2.*A2.*V)/(F.*vd.*D.*TG1.*V)          % Keepin
A1_1 = (Mn-FR.*vd2.*D.*TG2.*A2.*V)/(F.*vd2.*D.*TG1.*V)      % Tuttle

%% Uncertainty Evaluation for the 1st Group (A1)

% RU2 = Relative Uncertain of 2nd Group                     % Spriggs
RU2 = 0.02;
% Relative Uncertainty on the Total Counts
RUMn = sqrt(Mn)/(Mn);
RUMr = sqrt(Mr)./(Mr);
% Relative Uncertainty on the Gamma Activity (JEFF)
RUA = 0.0313;
% Relative Uncertainty on Keepin (RUKvd) and Tuttle (RUTvd)
RUKvd = 0.0413;
RUTvd = 0.0228;

% Uncertainty for 1st group (A1) with Keepin
RUA1_sq =
(1+A2/A1.*TS2/TS1)^2*(RUMn.^2+RUA.^2+RUMr.^2+RUKvd.^2)+(A2/A1.*TS2/TS1)^2*A2.^2;
RUA1 = sqrt(RUA1_sq)
```

```
% Uncertainty for 1st group (A1) with Keepin
RUA1_sq_1 =
(1+A2/A1_1.*TS2/TS1)^2*(RUMn.^2+RUA.^2+RUMr.^2+RUTvd.^2)+(A2/A1_1.*TS2/TS1)^2*A2.^2;
RUA1_1 = sqrt(RUA1_sq_1)
```

APPENDIX B
MEASURED RADIATION DOSES

This appendix contains results of radiation survey of a neutron generator in nuclear science building. The D-D neutron generator was operated at 30 mA beam current and 100 kV potential. Neutron production yield was 2.0×10^9 neutrons/sec.

1) Neutron Survey Instrument:

Eberline neutron REM counter model PNR-4 (serial number 2750), Ludlum neutron survey meter Model 12-4 (serial number 38389)

2) X-ray and Gamma-ray Survey Instrument:

Bieron microRem survey meter (serial number B791W)

3) Survey Location:

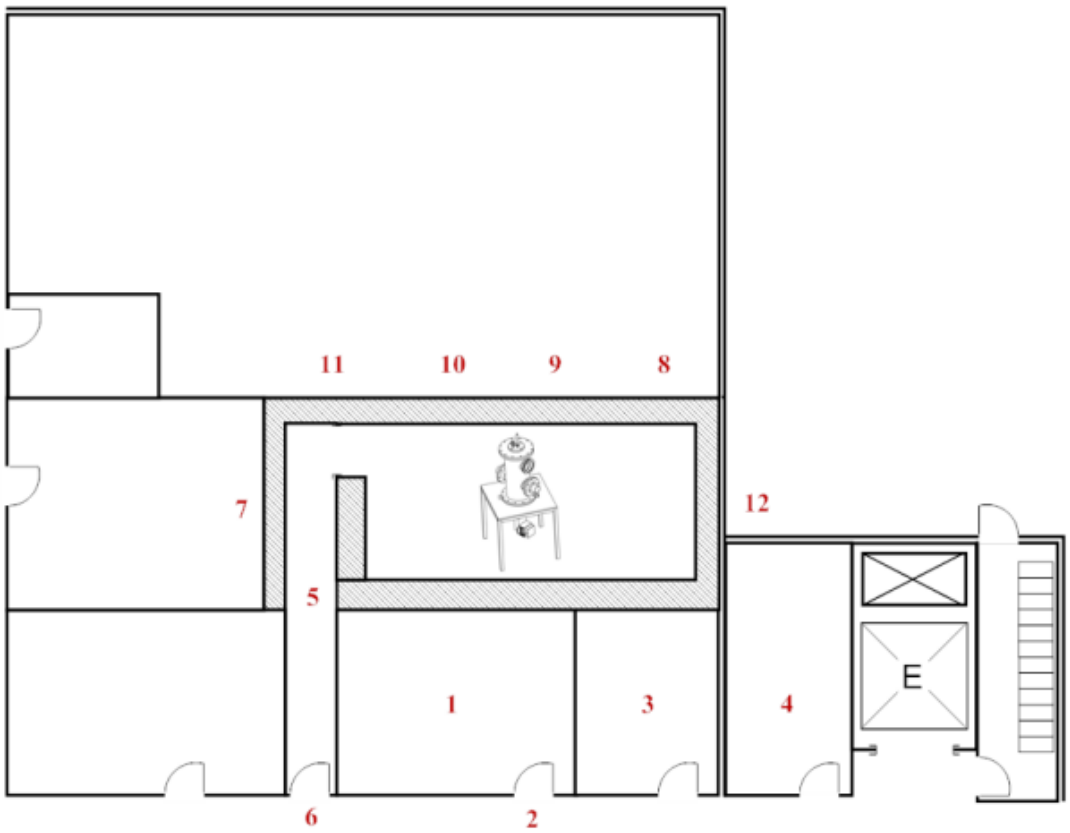

Nuclear Science Building First Floor

Nuclear Science Building Second Floor

4) Survey Results:

	Location	Neutron Dose (mrem/hr)	X-ray/Gamma Dose (μrem/hr)
First Floor	1. Control Room*	0.4	1600
	2. Hallway	0.4	50
	3. Shop*	1	200
	4. Drop Tower	< 0.2	20
	5. End of Shielded Maze*	1.25	420
	6. Hallway	0.5	70
	7. Office	< 0.2	3
	8. General Area	0.4	75
	9. General Area	0.6	160
	10. General Area	0.4	75
	11. General Area	< 0.2	20
	12. Outdoors	< 0.2	30
Second Floor	1. Computer Lab	< 0.2	20
	2. Computer Lab	< 0.2	25
	3. Computer Lab	< 0.2	25
	4. Office	< 0.2	20
	5. Office	< 0.2	25
	6. Hallway	< 0.2	10
	7. Hallway	< 0.2	10

* indicates the radiation restricted area.

LIST OF REFERENCES

[1] G. D. Spriggs and J. M. Campbell, “An 8-group Delayed Neutron Model Based on a Consistent Set of Half-Lives,” Progress in Nuclear Energy, vol. 41 (2002) 223-251

[2] J. Wang and W. D. Reece, “Comparison of Different Numerical Methods used in Delayed Neutron Decay Parameters Estimation,” Nuclear Science and Engineering, vol. 167 (2011) 154-164

[3] G. Perret and K. A. Jordan, “On the Combination of Delayed Neutron and Delayed Gamma Measurement Techniques for Nuclear Fuel and Its Application to Nuclear Data Uncertainty Reduction,” IEEE Transactions on Nuclear Science, vol. 59 (2012) 3166-3172

[4] J. R. Lamarsh, Introduction to Nuclear Engineering, 2rd ed., Addison-Wesley Publishing Company, Inc., MA, ISBN 0-201-14200-7, 1983, pp. 70-76, 102-104, 191-254, 276-285, 472-481

[5] H. Kröhnert, G. Perret, M. F. Murphy, and R. W. Mills, “Freshly induced short-lived gamma-ray activity as a measure of fission rates in lightly re-irradiated spent fuel,” Nuclear Instruments and Methods in Physics Research Section A, vol. 624 (2010) 101-108

[6] K. A. Jordan and G. Perret, “A Delayed Neutron Technique for Measuring Induced Fission Rates in Fresh and Burnt LWR Fuel,” Nuclear Instruments and Methods in Physics Research Section A, vol. 634 (2011) 91-100

[7] J. E. Turner, Atoms, Radiation, and Radiation Protection, 3rd ed., John Wiley and Sons, Inc., NY, ISBN 978-3-527-40606-7, 2007, pp. 83, 230-233

[8] K. S. Krane, Introductory Nuclear Physics, John Wiley and Sons, Inc., NY, ISBN 978-0-471-80553-3, 1988, pp. 272-277, 532

[9] M. B. Chadwick, P. Oblozinsky, M. Herman, N. M. Greene, and et al., “ENDF/B-VII.0: Next Generation Evaluated Nuclear Data Library for Nuclear Science and Technology”, Nuclear Data Sheets, vol 107 (2006) 2931-3060

[10] U.S. Department of Energy, DOE Fundamentals Handbook, Nuclear Physics and Reactor Theory, DOE-HDBK-1019/1-93, 1993

[11] A. L. Nichols, D. L. Aldama, and M. Verpelli, Handbook of Nuclear Data for Safeguards: Database Extensions, International Atomic Energy Agency, INDC (NDS)-0534, 2008

[12] R. B. Roberts, R. C. Meyer, and P. Wang, "Further Observations on the Splitting of Thorium and Uranium," Phys. Rev. 55 (1939) 510-511

[13] D. J. Hughes, J. Dabbs, A. Chan, and D. Hall, “Delayed Neutrons from Fission of ^{235}U,” Physics Review, vol. 73, (1948) 111-125

[14] G. R. Keepin, T. F. Wimett, and R. K. Zeigler, "Delayed Neutron Fissionable Isotopes of Uranium, Plutonium, and Thorium," Physical Review, vol. 107 (1957) 1044-1049

[15] G. R. Keepin, Physics of Nuclear Kinetics, 1st ed., Addison Wesley Publishing Company, MA, 1965, pp. 187

[16] G. Rudstam, Ph. Finck, A. Filip, A. D'Angelo, and R.D. McKnight, "Delayed Neutron Data for the Major Actinides," vol. 6, NEA/WPEC-6, NEA/OECD, Paris, France (2002)

[17] E. E. Lewis and W. F. Miller Jr., Computational Methods of Neutron Transport, American Nuclear Society Inc., IL, ISBN 0-89448-452-4, 1993, pp. 22-25

[18] M. H. Kim, Nuclear Physics [Lecture Notes], Kyunghee University, Republic of Korea

[19] J. J. Duderstadt and L. J. Hamilton, Nuclear Reactor Analysis, John Wiley and Sons, Inc., NY, ISBN 978-0-471-22363-4, 1976, pp. 272-277

[20] G. D. Spriggs, In-core Measurement of Delayed-neutron Parameters, University Microfilms International, Ann Arbor, MI: Department of Nuclear and Energy Engineering, The University of Arizona, 1982, Thesis

[21] V. M. Piksaikin, S. G. Isaev, and A. A. Goverdovski, "Characteristics of Delayed Neutrons: Systematics and Correlative Properties," Nuclear Energy, vol. 41, No. 1-4 (2002) 316-384

[22] M. Burger and J. Repisky, "Problems of Linear Least Square Regression," International Virtual Conference on Advanced Research in Scientific Areas 2012, Slovakia, Dec. 3-7, 2012

[23] W. Navidi, Statistics for Engineers and Scientists, 2nd ed., McGraw-Hill Companies, Inc., NY, ISBN 978-0-07-312779-8, 2008, pp. 163-191, 289-298, 533-636

[24] J. Gu, Feature Relational Mapping for Remote Sensing Images using Directional Edge Analytical Models, University Microfilms International, Ann Arbor, MI: School of Computing, University of Southern Mississippi, 2007, Thesis

[25] J. Wang, Uncertainty Evaluation of Delayed Neutron Decay Parameters, Nuclear Engineering, University of Texas A&M, 2008, Thesis

[26] N. Tsoulfanidis, Measurement and Detection of Radiation, 2nd ed., Taylor and Francis, WA, ISBN 1-56032-317-5, 1983, pp. 1-6

[27] G. F. Knoll, Radiation Detection and Measurement, 3rd ed., John Wiley and Sons, Inc., NY, ISBN 978-0-471-07338-3, 1999, pp. 86-92, 116-119, 505-520

[28] G. W. McKinney, J. W. Durkee, J. S. Hendricks, M. R. James, and et al., MCNPX User's Manual, Version 2.5.0, Los Alamos National Laboratory Report, LA-CP-05-0369, 2005

[29] A. Koning, R. Forrest, M. Kellett, R. Mills, and et al., The JEFF-3.1 Nuclear Data Library, JEFF Report 21, NEA No.6190, ISBN 92-64-02314-3, 2006

[30] J. C. Philippot, "Automatic Processing of Diode Spectrometry Results," IEEE Transactions on Nuclear Science, NS-173 (1970) 449

[31] Canberra, Genie 2000 Tutorial Manual, Canberra Industries, Inc., 2006

[32] A. N. Garg and R. J. Batra, "Isotopic Sources in Neutron Activation Analysis," Journal of Radioanalytical and Nuclear Chemistry, vol. 98 (1986) 167-194

[33] E. M. Hussein, Handbook on Radiation Probing, Gauging, Imaging and Analysis, Volume I: Basics and Techniques, Kluwer Academic Publichers, NY, ISBN 1-4020-1294-2, 2004, pp 55-58

[34] A. Letouneau, J. Galin, F. Goldenbaum, B. Lott, and et al., "Neutron Production in Bombardments of Thin and Thick W, Hg, Pb Targets by 0.4, 0.8, 1.2, 1.8 and 2.5 GeV Protons," Nuclear Instruments and Methods in Physics Research Section B, vol. 170 (2000) 299-322

[35] J. Cugnon, C. Volant, and S. Vuillier, "Nucleon and Deuteron Induced Spallation Reactions," Journal of Nuclear Physics A, vol. 625 (1997) 729-757

[36] D. Reilly, N. Ensslin, H. Smith, and S. Kreiner, Passive Nondestructive Assay of Nuclear Materials, Los Alamos National Laboratory, NUREG/CR-5550, 1991

[37] S. J. Tobin, H. O. Menlove, M. T. Swinhoe, P. Blanc, and et al., "Technical Cross-cutting Issues for the Next Generation Safeguards Initiative's Spent Fuel Nondestructive Assay Project," Journal of Nuclear Materials Management, vol. XI, No. 3 (2012) pp. 18-24

[38] IAEA, Use of Accelerator Based Neutron Sources, IAEA Radiation Technology Reports, IAEA-TECDOC-1153, 2000

[39] Kaman Instrumentation Co., Manual: A-711 Sealed Tube Neutron Generators, MF Physics, 1990

[40] IAEA, Neutron Generators for Analytical Purposes, IAEA Radiation Technology Reports Series No. 1, ISBN 978-92-0-125110-7, 2012

[41] K. A. Van Riper, Moritz User's Guide, Version 1.16-Demo, White Rock Science, 2008

[42] B. R. Doe and M. F. Newell, "Isotopic Composition of Uranium in Zircon, the American Mineralogist," vol. 50, (1965) 613-618

[43] G. Jia, M. Belli, U. Sansone, S. Rosamilia, R. Ocene, and S. Gaudino, "Determination of Uranium Isotopes in Environmental Samples by Alpha-spectrometry," Journal of Radioanalytical and Nuclear Chemistry, vol. 253, No. 3 (2002) 395-406

[44] M.H. Nassef, W. El Mowafi, and M.S. El Tahawy, "Non Destructive Assay for 235U Determination in Reference Materials of Uranium Oxide," Journal of Nuclear and Radiation Physics, vol. 4, No. 2 (2009) 9965-9973

[45] Y.Y. Ebaid, "Use of Gamma-ray Spectrometry for Uranium Isotopic Analysis in Environmental Samples," Romanian Journal of Physics, vol. 55, Nos. 1-2 (2010) 69-74

[46] A. R. Strganov, F. F. Gavrilov, and S. P. Efremov, "Quantitaive Spectral Analysis of the Isotopic Composition of Enriched Uranium," Soviet Journal of Atomic Energy, vol. 2 (1957) 337-344

[47] H. O. Denschalg and A. A. Gordus, "Gas-chromatographic Technique for Rapid Isolation of Uranium Fission Products," Fresenius' Zeitschrift für Analytische Chemie, vol. 226, No. 1 (1967) 62-71

[48] M. Wallenius, A. Morgenstern, and C. Apostolidis, "Determination of the Age of High Enriched Uranium, Anal Bioanal Chem," vol. 374 (2002) 379-384

[49] H. Assmann and H. Bairiot, Process and Product Control of Oxide Power and pellets for Reactor Fuel Application, Guidebook on Quality Control of Water Reactor Fuel, Tech., Report Series No. 221, IAEA, Vienna, 1983

[50] S. Yeo, E. Mckenna, R. Baney, G. Subhash, and J. Tulenko, "Enhanced Thermal Conductivity of Uranium Dioxide-silicon Carbide Composite Fuel Pellets Prepared by Spark Plasma Sintering (SPS)," Journal of Nuclear Materials, vol. 433 (2013) 66-73

[51] L. Ge, G. Subhash, J. Tulenko, R. Baney, and E. McKinna, "Densification of uranium dioxide fuel pellets prepared by spark plasma sintering (SPS)," Journal of Nuclear Materials, vol. 435, Issues 1–3 (2013) 1-9

[52] T. Plower, M. Rowe, G. Sjoden, R. Detwiler, and J. Baciak, "Assessment of Mark I rod Irradiations in the UF Subcritical Water Tank Experiment Using Transport Methods," International Conference on Mathematics, Computational Methods and Reactor Physics (M&C 2009), Saratoga Springs, NY, May 3-7, 2009

[53] T. Shiratori and K. Fukuda, "Fabrication of Very High Density Fuel Pellets of Thorium Dioxide," Journal of Nuclear Materials, vol. 202 (1993) 98-103

[54] J. Blachot, M. C. Brady, A. Filip, R. W. Mills, and D. R. Weaver, Status of Delayed Neutron Data, OECD Nuclear Energy Agency, NEACRP-L-323, 1990

[55] J. Blachot, C. Chung, and F. Storrer, "JEFF-2 Delayed Neutron Yields for 39 Fissioning systems," Nuclear Energy, vol. 24, No. 6 (1997) 489-504

[56] A. Zukeran, H. Hanaki, S. Sawada, and T. Suzuki, "Uncertainty Evaluation of Effective Delayed Neutron Fraction β_{eff} of Typical Proto-type Fast Reactor," Nuclear Science and Engineering, vol. 36 (1999) 61-80.

[57] E. Fort, V. Zammit-Averlant, M. Salvatores, A. Filip, and J-F Lebrat, "Recommended Values of the Delayed Neutron Yield for: U-235; U-238 and Pu-239," Nuclear Energy, vol. 41, No. 1-4 (2002) 317-359

[58] W. B. Wilson and T. R. England, "Delayed Neutron Study using ENDF/B-VI Basic Nuclear Data," Nuclear Energy, vol. 41, No. 1-4 (2002) 71-107

[59] A. D'angelo and J. L. Rowlands, "Conclusions Concerning the Delayed Neutron Data for the Major Actinides," Nuclear Energy, vol. 41, No. 1-4 (2002) 391-412

[60] V. M. Piksaikin and S. G. Isaev, Correlation Properties of Delayed Neutrons from Fast Neutron Induced Fission, International Nuclear Data Committee, INDC(CCP)-415, 1998

[61] T. Sakurai and S. Okajima, "Adjustment of Total Delayed Neutron Yields of 235U, 238U and 239Pu in JENDL-3.2 using Benchmark Experiments on Effective Delayed Neutron Fraction β_{eff}," Nuclear Science and Technology, vol. 39, N0. 1 (2002) 19-30

[62] J. K. Shultis and R. E. Faw, Radiation Shielding, American Nuclear Society, Inc., IL, ISBN 0-89448-456-7, 2000, pp. 459

[63] R. Chandra, G. Davatz, H. Friederich, U. Gendotti, and D. Murer, "Fast Neutron Detection with Pressurized ^{4}He Scintillation Detectors," Journal of Instrumentation, vol. 7, No. 03 (2012) C03035

[64] D. Murer, R. Chandra, G. Davatz, H. Friederich, and et al., "^{4}He Detectors for Mixed Oxide (MOX) Fuel Measurement," IEEE Nuclear Science Symposium and Medical Imaging Conference (NSS/MIC), 2011 IEEE Conference Record, Valencia, Spain, Oct. 23-29, 2011

[65] J. M. Lewis, D. Raetz, D. Murer, and K. A. Jordan, "Analysis for In-site Fission Rate Measurements using ^{4}He Gas Scintillation Detectors," Advancements in Nuclear Instrumentation Measurement Methods and their Applications (ANIMMA), 2013 3rd International Conference Record, Marseille, France, June 23-27, 2013

[66] T. R. England and B. F. Rider, Evaluation and Compilation of Fission Product Yields, Los Alamos National Laboratory Report LA-UR-94-3106, 1994

BIOGRAPHICAL SKETCH

Heejun Chung was born in Seoul, Republic of Korea (S. Korea) on April 4, 1977. He received the Bachelor and Master of Engineering degrees in Nuclear Engineering from the Kyunghee University in S. Korea in 2004 and 2006 respectively, and enrolled in Ph. D. Program of the Nuclear and Radiological Engineering at the University of Florida in August of 2009.

While pursuing his Ph. D. degree, He has served as a research assistant for developing a new micro-pocket sized fission detector, designing a neutron generator laboratory, and improving high uncertainties on the delayed neutron nuclear data. He has also served as a teaching assistant for reactor analysis and radiation detection classes.

With his achievements at the University of Florida, he was awarded the R&D 100 Award (the Oscars of Innovation) with his supervisor, Dr. Kelly A. Jordan, in 2013. He is scheduled to graduate with a Doctor of Philosophy degree in May, 2014.